Simulation of surface heat budget by RegCM3 model in South Asian region

A thesis submitted

to the Department of Physics

Bangladesh University of Engineering and Technology (BUET) for the partial fulfillment of the degree of Master of Philosophy (M. Phil) in Physics

Submitted by

Romee Afroz

Roll No. 040414037 P

Reg. No. 0404575

Bangladesh University of Engineering and Technology (BUET)

December 2006

BANGLADESH UNIVERSITY OF ENGINEERING AND TECHNOLOGY

DEPARTMENT OF PHYSICS

Certification of Thesis Work

The thesis titled **"Simulation of surface heat budget by RegCM3 model in South Asian region"** submitted by Romee Afroz, Roll No. 040414037 P, Registration No. 0404575, Session: April 2004 has been accepted as satisfactory in partial fulfillment of the requirement for the degree of Master of Philosophy in Physics on 23 December, 2006.

Board of Examiners

1. _____ Chairman
Dr. Md. Nazrul Islam (Supervisor)
Associate Professor
Department of Physics, BUET, Dhaka

2. _____ Member (Ex-officio)
Dr. Joan Podder
Professor and Head
Department of Physics, BUET, Dhaka

3. _____ Member
Fahima Khanam
Associate Professor
Department of Physics, BUET, Dhaka

4. _____ Member (External)
Dr. Samarendra Karmakar
Director,
Bangladesh Meteorological Department
Agargaon, Dhaka

DECLARATION

It is hereby declared that this thesis or any part of it has not been submitted elsewhere for the award of any degree or diploma.

Romee Afroz

(Romee Afroz)

Candidate

Roll No. 040414037 P

Session: April 2004

Acknowledgements:

I would like to express my sincere admiration and gratitude to my supervisor Dr. Md. Nazrul Islam, Associate Professor, Department of Physics, BUET for providing me incessant supervision of this research work. He has continuously kept an eye on the progress of the work. I am unambiguous that it would not be possible on my part to complete the dissertation without his strong support. I am deeply grateful to Dr. Kanti Prasad, Head, Theoretical Division, SAARC Meteorological Research Centre (SMRC), Dhaka for his constant encouragement and for giving me the software modules to process the ECMWF Reanalysis (ERA-40) data sets which were downloaded from their ftp site.

The acknowledgement is due to the authorities of the Bangladesh University of Engineering and Technology (BUET) for providing me the opportunities to do the M. Phil. studies and complete the research work on the topic "Simulation of surface heat budget by RegCM3 model in South Asian region".

I extend my sincere thanks to the SMRC authority for giving me the permission to do M. Phil. and allowing me to use the computer of this organization.

The acknowledgement is due to Md. Mizanur Rahman, who has extended help to make a good discussion about the subject matter of my thesis. I could not accomplish the work timely without these potential supports and opportunity.

Table of Contents

List of Figures

Abstract

Regional Climate Model (RegCM3) developed by ICTP, Trieste, Italy is used for simulation of different meteorological parameters including net absorbed solar energy flux, net infrared energy flux, sensible heat, evaporation to define Surface heat budget (SHB) over South Asian domain including Bangladesh. The model domain is selected to cover the South Asia region (65^0E-117^0E, 5^0N-35^0N) on a rotated mercator projection (ROTMER) at a 60 km horizontal resolution and 16 sigma levels in the vertical. The centre of the domain is 20^0N, 90^0E. Daily 6-hour interval Lateral Boundary Conditions (LBCs) data from NCEP is used as the input to run RegCM model in different options which are i) Grell scheme with Arakawa-Schubert (GAS) assumptions for the year 1995-2000 (6-year), ii) Grell scheme with Fritch-Chappell (GFC) assumptions for 1983, 1996, iii) Betts-Miller Scheme with Fritch-Chappell (BFC) for 1983. iv), MIT-Emanuel scheme with Fritch-Chappell (EFC) for 1983 and v) Kuo Scheme with Fritch-Chappell (KFC) assumptions for 1983. It is important to do some validation of the RegCM model outputs to adopt the RegCM for this region. Due to the lack of surface observational data of SHB over this region, the European Centre for Medium-Range Weather Forecasts (ECMWF) data at 0.5^0 x 0.5^0 lat /long (~55 km) horizontal grid resolution is used to calibrate RegCM output. Comparison between model and ECMWF data for SHB has been made in 7 selected windows over South Asian region and at the central points of these selected windows for monthly and 6-hourly, respectively. For the year 1995 the four parameters such as net absorbed solar energy flux, net infrared energy flux, sensible heat, latent heat of SHB are analysed for the selected domains.

The variations of SHB along latitude and longitude have been observed using RegCM model and ECMWF data for the Pre-monsoon (March-May), Monsoon (June-September) and Post-

monsoon (October-November) periods. The same is also performed for July and December. Different schemes data of RegCM model are used for sensitivity test in the year 1983.

In general model underestimates SHB from March to May and overestimates from June to September. Over ocean the value of SHB is high from March to September and low from November to December. On the other hand, over land the same condition is occurred except low in magnitude. SHB at different latitudes along longitudes (70^0E-94^0E) is high over ocean and low over land during summer and opposite condition is observed in winter. The difference of SHB between RegCM and ECMWF data are also more over ocean compared to over land. For SHB the role of latent heat is important for water surface and sensible heat for land surface. According to the diurnal variation of SHB for both RegCM and ECMWF data it has been observed that the peak hour is at 12LST (local standard time) for GAS. Same phase is observed for both data at 00, 12 and 18LST. Some discrepancy is seen at 06LST. The BFC option is found better for the calculation of SHB for monsoon season in 1983. However, more research work is necessary on SHB using different schemes of RegCM model for more years and the other parameters of SHB.

Abbreviations

RegCM: Regional Climate Model

SHB: Surface Heat Budget

GAS: Grell Arakawa and Schubert

GFC: Grell Fritsch and Chappell

BFC: Betts-Miller Fritsch and Chappell

KFC: Kuo Fritsch and Chappell

EFC: MIT-Emanuel Fritsch and Chappell

BUET: Bangladesh University of Engineering and Technology

LAM: Limited Area Model

GCM: General Circulation Model

LBC: Lateral Boundary Conditions

BATS: Biosphere-Atmosphere Transfer Scheme

MM5: Mesoscale Model

NCAR-PSU: National Center for Atmospheric Research-Pennsylvania State University

CCM: Community Climate Model

IPCC: Intergovernmental Panel on Climate Change

PBL: Planetary Boundary Layer

GLCC: Global Land Cover Characterization

AVHRR: Advanced Very High Resolution Radiometer

USGS: United States Geological Survey

OISST: Optimum Interpolation Sea Surface Temperature

ECMWF: European Centre for Medium-Range Weather Forecasts

NCEP: National Centre for Environmental Prediction

ICBC: Initial Concentrations and Boundary Condition

CHAPTER 1: INTRODUCTION

1.1 Introduction

The heat budget describes what happens to the sun's radiation (heat, light) received by the Earth. The balance between the energy received and energy lost maintains the Earth's constant average temperature.

Energy from the sun drives the circulation of the atmosphere and ocean: winds, ocean surface currents, and thermohaline circulation. Sun's energy and the response of the atmosphere and land drive the Earth's weather and climate.

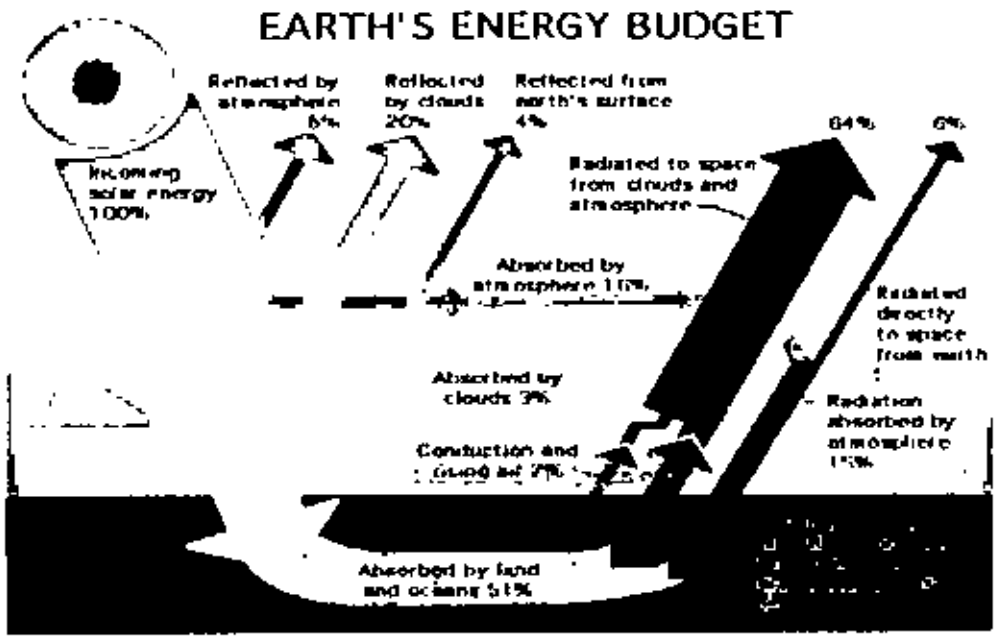

Fig. 1: Transfers of Energy among the Sun, Atmosphere and Earth's Surface (land and Ocean). As the diagram above shows, a variety of factors condition the Earth's radiation budget.

Transfers of energy:

Radiation (solar energy = shorter wavelengths; terrestrial emissions = longer wavelengths)

Nonradiative processes: convection, advection, conduction, latent heat.

Energy exchanges at the Earth's surface:

Shortwave: incoming (insolation); outgoing (reflected insolation)

Longwave: outgoing (terrestrial radiation); incoming (longwave energy reflected and emitted by atmospheric components)

Earth's energy (radiation) balance: inputs, outputs

Earth's radiation balance (note: %'s vary according to different estimates) of incoming solar radiation, about 30% is reflected (by gases in Atmosphere 6%, water vapor 20%, and the surface 4%) back to space as shortwave radiation and 70% leaves as longer wave radiation (heat) of incoming solar radiation, 19% is absorbed by atmospheric gases, dust and clouds of incoming solar radiation, 51% is absorbed by the Earth's surface Globally, the Earth's temperature stays the same when inputs = outputs; it changes if one (or more of the components are changed)

The net radiation budget differs by latitude and season because of the amount of insulation which is affected by angle of incoming solar rays (direct vs. oblique rays) and proximity of the sub solar point (axial tilt, parallelism, sphericity, revolution, rotation). The transformations of energy in the Earth system occur through atmosphere to hydrosphere and lithosphere and back again through the atmosphere. The Earth is in equilibrium with its surroundings, which means that the budget has to balance: energy going into the system must equal the amount exiting it. All life on Earth ultimately depends on that energy, even though the Earth receives only a very small percentage of the Sun's total energy output. Many interactions drive the exchange of heat between the atmosphere and the Earth's surface features. One factor is that different surface features will have different abilities to absorb, reflect, and radiate energy. Earth's reflectivity or albedo accounts for around 30% of the energy that approaches the top of Earth's atmosphere. Another factor, that single-handedly accounts for almost a quarter of the energy that enters the Earth system is due to the latent heat of water's transformation in the troposphere. Wind is a factor that further tunes the engine of the Earth's atmosphere and conditions the flow of energy through it.

The global surface heat budget is made up of the simultaneous interactions of local surface heat budgets. Usually, the single most important factor that conditions a local energy budget is latitude, because this single factor limits the maximum and minimum amount of solar energy available to that location. The resulting variation in temperature from the Equator to the poles affects the patterns of heating and cooling around the Earth. These patterns drive atmospheric winds, ocean currents, and their interactions with weather and climate. It is important to keep track of the Earth's radiation budget because the production of greenhouse gases seems to be affecting the natural balance. This creates concerns about rising sea levels, changing precipitation patterns, and an array of other possible effects. With the use of polar orbiting satellites, scientists hope to monitor changes in tropospheric and stratospheric temperatures to look for ways in which we are altering the Earth's radiation balance. Therefore, the impact of the radiative properties on the Earth's surface may play an important role on the Earth's radiation balance.

The research work on surface heat budget over South Asia which is in subtropical zone will be helpful in understanding the radiative impacts on the development mechanism of tropical convections. The 7 topographical regions are chosen to do these activity represent 7 distinctly different terrains. Each region has a predominant feature: land, coastal area, sea, Deep Ocean or desert. Each has a unique albedo (reflectance), absorbance ability and heat capacity. These factors, among others, determine how the Earth's surface interacts with the input of solar radiation. Using the predicted range of surface heat budget over land and ocean, the indication of the development of precipitation systems may be predicted. The lead-time information about the development of precipitation systems may useful to formulate future planning for agriculture, water management, health, infrastructure and so on. Due to the lack of observational data, RegCM3 model data and ECMWF data are used for measuring surface

heat budget over South Asia. In support of this analysis RegCM3 model is installed in the Atmospheric laboratory of the Department of Physics, BUET.

1.2 Geographical Description and Climate of South Asia:

The highest mountains in the world, lush jungles and the tenth-largest desert on Earth, deep river valleys and high mountain plateaus, all of these features and many others decorate the countries that make up South Asia. It boasts one of the most diverse assortments of geographic features of any region on Earth. Contrasting with the low, flat desert are the glorious Himalayas, the highest mountain range in the world. These mountains are so high that they cause some of the worst storms on Earth: monsoons. Monsoons wreak terrible havoc, but without them South Asia would be dry and almost uninhabitable.

South Asia comprises the countries of India, Pakistan, Bangladesh, Nepal, and Bhutan, as well as the island nations of Sri Lanka and the Maldives. About 1.73 million square miles make up South Asia.

India is, by area, the seventh largest country in the world with the Indian mainland covering an area of 3,287,782 sq.km. From north to south, the country measures 3,214 km and from east to west 2,933 km. India's land frontiers are approximately 15,200 km long and its coastline is about 6,100 km. India's puzzle board of 26 states holds virtually every kind of landscape imaginable.

Fig.2: Map of South Asia

North India is the country's largest region. It begins with the panhandle of Jammu and Kashmir, a dynamic area with terrain varying from arid mountains in the far north to the lake country and forests near Srinagar and Jammu. The mountain region, which stretches along almost the entire northernmost part of the country, comprises three almost parallel ranges extending over a distance of around 2,400 km. In these mountain ranges are found some of the highest peaks in the world. Falling south along the Indus river valley, (the river valleys of the Indus, Ganga and Brambaputra merge to form the Indo-Gangetic Plain, which extends across Northern India for about 2,400 km, with a width

varying from 260 to 350 km. This almost flat plain is amongst the most densely populated areas on earth. The desert region of India comprises the 'great desert' and the 'little desert'.) the North becomes flatter and more hospitable, widening into the fertile plains of Punjab to the west and the Himalayan foothills of Uttar Pradesh and the Ganges river valley to the East. Cramped between these two states is the capital city, Delhi. The southwestern extremity of the North is the large state of Rajastan, whose principal features are the Thar Desert and the stunning "pink city" of Jaipur. To the southeast is southern Uttar Pradesh and Agra, home of the famous Taj Mahal.

West India contains the states of Gujarat, Maharashtra, Goa, and part of the massive, central state of Madhya Pradesh. The west coast extends from the Gujarat peninsula down to Goa, and it is lined with some of India's best beaches. The land along the coast is typically lush, with rainforests reaching southward from Bombay all the way to into Goa. A long mountain chain, the **Western Ghats**, separates the verdant coast from the Vindya mountains and the dry Deccan plateau further inland.

Home of the Ganges river and the majority of Himalayan foothills, **East India** begins with the states of Madhya Pradesh, Bihar, Orissa, which comprise the westernmost part of the region. East India also contains an area known as the eastern triangle, which is entirely distinct. This is the last gulp of land that extends beyond Bangladesh, culminating in the Naga Hills along the Burmese border. A forested region east of Bangladesh boasts the town of CHERRAPUNUJI, the second-wettest place on Earth. During the monsoon season, the town can receive more than 1,143 centimeters (450 inches) of rainfall.

India reaches its peninsular tip with **South India**, which begins with the Deccan in the north and ends with Cape Comorin, where Hindus believe that bathing in the waters of the three oceans will wash away their sins. The states in South India are Karnataka, Andhra Pradesh,

Tamil Nadu, and Kerala, a favorite leisure destination. The southeast coast, mirroring the west, also rests snugly beneath a mountain range the Eastern Ghats.

Climate: Because of India's size, its climate depends not only on the time of year, but also the location. India's climate is strongly influenced by the Himalayas and the Thar Desert. The Himalayas, along with the Hindu Kush mountains in Pakistan, provide a barrier to the cold winds from Central Asia. This keeps most of the Indian subcontinent warmer than most locations in similar latitudes. The Thar Desert is responsible for attracting the moisture laden southwest monsoon winds that provide most of India's rainfall between June and September. The climate varies as much as the scenery, with cold winters and hot summers in the north and a mild climate in the south, moderated by the influence of the ocean. The central parts have extremely hot summers with temperatures rising to 45C (113F), followed by very cold winters, often falling below freezing. There is very little rainfall ranging from less than 250 mm to more than 1,250 mm (9.8–49.2 inch), mostly brought by the unreliable south-westerly monsoon winds during the late summer.

In general, temperatures tend to be cooler in the north, especially between September and March. The south is coolest between November to January. In June, winds and warm surface currents begin to move northwards and westwards, heading out of the Indian Ocean and into the Arabian Gulf. This creates a phenomenon known as the south-west monsoon, and it brings heavy rains to the west coast. Between October and December, a similar climatic pattern called the north-east monsoon appears in the Bay of Bengal, bringing rains to the east coast. In addition to the two monsoons, there are two other seasons, spring and autumn.

Though the word "monsoon" often brings to mind images of torrential floods and landslides, the monsoon seasons are not bad times to come to India. Though it rains nearly every day, the downpour tends to come and go quickly, leaving behind a clean, glistening landscape.

Bangladesh is located in the low-lying Ganges-Brahmaputra River Delta or Ganges Delta. This delta is formed by the confluence of the Ganges (local name Padma or Pôdda), Brahmaputra (Jamuna or Jomuna), and Meghna rivers and their respective tributaries. The alluvial soil deposited by these rivers has created some of the most highly fertile plains of the world.

Most parts of Bangladesh are within 10 metres above the sea level, and it is believed that about 10% of the land would be flooded if the sea level were to rise by 1 metre. The highest point in Bangladesh is in Mowdok range at 1,052 m (3,451 ft) in the Chittagong Hill Tracts to the southeast of the country. Cox's Bazar, south of the city of Chittagong, has a beach that stretches uninterrupted over 120 kilometres (75 miles); it is one of the longest unbroken natural sea beaches of the world. A major part of the coastline comprises a marshy jungle, the Sundarbans, one of the largest mangrove forests in the world and home to diverse flora and fauna, including the Royal Bengal Tiger.

Climate: Straddling the Tropic of Cancer, Bangladeshi climate is tropical with a mild winter from October to March, a hot, humid summer from March to June. A warm and humid monsoon season lasts from June to October and supplies most of the country's rainfall. Natural calamities, such as floods, tropical cyclones, tornadoes, and tidal bores occur almost every year, combined with the effects of deforestation, soil degradation and erosion. In Bangladesh, the mean annual temperature is about 25C while the highest and lowest through the year ranges between 43C and 4C. The humidity is over 80% during the monsoon months and about 58% in other months. The wind direction is mainly from NW and SW during pre-monsoon and monsoon periods and from SE and NE during post-monsoon and winter periods. Annual rainfall is about 2200 mm. About 20%, 65%, 13% and 2% of the annual rain falls during pre-monsoon, monsoon, post-monsoon and winter periods respectively.

Pakistan covers 880,254 square kilometres (339,867 sq mi.), with its eastern regions located on the Indian tectonic plate and the western and northern regions on the Iranian plateau and Eurasian landplate. Apart from the 1,046 kilometre (650 mi) Arabian Sea coastline, Pakistan's land borders total 6,774 kilometres—2,430 kilometres (1,509 mi) with Afghanistan to the northwest, 523kilometres (325 mi) with China to the northeast, 2,912kilometres (1,809 mi) with India to the east and 909 kilometres (565 miles) with Iran to the southwest.

Pakistan is a land of many splendours. The different types of natural features range from the sandy beaches, lagoons, and mangrove swamps of the southern coast to preserved moist temperate forests and the icy peaks of the Himalaya, Karakoram and Hindu Kush mountains in the north. There are an estimated 108 peaks above 7,000 metres (23,000 ft) high that are covered in snow and glaciers. Five of the mountains in Pakistan (including K2 and Nanga Parbat) are over 8,000 metres (26,000 ft). Linking Indian-controlled Kashmir to the Northern Areas of Pakistan and running the length of the country is the Indus River with its many tributaries. To the west of the Indus are the dry, hilly deserts of Balochistan; to the east are the rolling sand dunes of the Thar Desert. Most areas of Punjab and parts of Sindh are fertile plains where agriculture is of great importance. Thus, the variety of landscape divides Pakistan into six major regions: the North High Mountainous Region, the Western Low Mountainous Region, the Balochistan Plateau, the Potohar Uplands, the Punjab and the Sindh Plains.

Climate: Although the country is in the monsoon region, it is arid; except for the southern slopes of the Himalayas and the sub-Mountainous tracts which have a rainfall from 76 to 127 cm. Balochistan is the driest part of the country with an average rainfall of 21 cm. On the southern ranges of the Himalayas, 127 cm. of precipitation takes place, while under the lee of these mountains (Gilgit and Baltistan) rainfall is hardly 16 cm. Rainfall also occurs from western cyclonic distrubances originating in the Mediterrancan.

It is appreciable in the western mountains and the immediate fore lying area; here the rainfall average ranges from 27 to 76 cm. The contribution of these western disturbances to rainfall over the plains is about 4 cm. A large part of the precipitation in the northern mountain system is in the form of snow which feeds the rivers. The four well-marked seasons in Pakistan are:-

(i) Cold season (December to March).

(ii) Hot season (April to June).

(iii) Monsoon season (July to September).

(iv) Post-Monsoon season (October and November).

The cold season sets in by the middle of December. This period is characterized by fine weather, bracing air-low humidity and large diurnal range of temperature. Winter disturbances in this season accordingly cause fairly widespread rain. Average minimum and maximum temperatures are 4C and 18C, though on occasions the mercury falls well below freezing point. The winter sun is glorious. The hot season is usually dry. Relative humidity in May and June varies from 50 per cent in the morning to 25 per cent or less in the afternoon. The temperature soars to 40C and beyond. The highest recorded temperature at Jaccobabad in June is 53C. While the interior is blazing hot, the temperature along the sea Coast Ranges between 25C to 35C, but the humidity persists around 70 to 80 per cent. The strength of the south-west monsoon current increases from June to July; it then remains steady, and starts retreating towards the end of August, though occasionally, it continues to be active even in September when some of the highest floods of the Indus Basin have been recorded. In October, the maximum temperature is of the order of 34C to 37C all over Pakistan, while the nights are fairly cool with the minimum temperature around 16C. In the month of November, both the maximum and the minimum temperatures fall by about 6C and the weather becomes pleasant. October and November are by far the driest months all over the plains of Pakistan.

Nepal is of roughly rectangular shape, 650 km wide and 200 km broad, with an area of 147,181 km². Nepal is commonly divided into three physiographic areas: the Mountain, Hill, and Terai Regions. These ecological belts run east-west and are bisected by Nepal's major river systems.

The **Terai Plains** bordering India are part of the northern rim of the Indo-Gangetic plains. They were formed and are fed by three major rivers: the Kosi, the Narayani (India's Gandak River), and the Karnali. This region has a hot, humid climate.

The **Hill Region** (Pahar in Nepali) abuts the mountains and varies from 1,000 to 4,000 metres in altitude. Two low mountain ranges, the Mahabharat Lekh and Shiwalik Range (also called the Churia Range) dominate the region. The hilly belt includes the Kathmandu Valley, the country's most fertile and urbanised area. Despite its geographical isolation and limited economic potential, the region always has been the political and cultural centre of Nepal. Unlike the valleys, elevations above 2,500 m are sparsely populated.

The **Mountain Region** contains the highest region in the world. The world's highest mountain, Mount Everest (Sagarmatha in Nepali) at 8,850 m is located on the border with Tibet. Eight of the world's ten highest mountains are located in Nepal. Kanchenjunga, the world's third highest peak, is also located on its eastern border with Sikkim. Deforestation is a major problem in all regions, with resulting erosion and degradation of ecosystems.

Climate: Nepal has five climatic zones, broadly corresponding to altitude. The tropical and subtropical zones lie below 1,200 m, the temperate zone 1,200 to 2,400 m, the cold zone 2,400 to 3,600 m, the subarctic zone 3,600 to 4,400 m, and the arctic zone above 4,400 m. Nepal experiences five seasons: summer, monsoon, autumn, winter and spring. The Himalaya blocks cold winds from Central Asia in winter, and forms the northern limit of the monsoon wind patterns.

The Kingdom of Bhutan is a landlocked South Asian nation situated between India and Tibet, People's Republic of China. The entire country is mountainous except for an 8-10 mile (13-16 km) wide strip of subtropical plains in the extreme south which is intersected by valleys known as the Duars. The elevation gain from the subtropical plains to the glacier-covered Himalayan heights exceeds 23,000 feet (7,000 m).

The northern region consists of an arc of glaciated mountain peaks with an extremely cold climate at the highest elevations. Most peaks in the north are over 23,000 feet (7,000 m) above sea level. The Black Mountains in central Bhutan form a watershed between two major river systems: the Mo Chhu and the Drangme Chhu. The Black Mountains in central Bhutan form a watershed between two major river systems: the Mo Chhu and the Drangme Chhu. The Torsa, Raidak, Sankosh, and Manas are the main rivers of Bhutan, flowing through this region. Most of the population lives in the central highlands. In the south, the Shiwalik Hills are covered with dense, deciduous forests, alluvial lowland river valleys, and mountains up to around 4,900 feet (1,500 m) above sea level. The foothills descend into the subtropical Duars plain. Most of the Duars is located in India, although a 6–9 mile (10–15 km) wide strip extends into Bhutan. The Bhutan Duars is divided into two parts: the northern and the southern Duars. The northern Duars, which abuts the Himalayan foothills, has rugged, sloping terrain and dry, porous soil with dense vegetation and abundant wildlife. The southern Duars has moderately fertile soil, heavy savannah grass, dense, mixed jungle, and freshwater springs. Mountain rivers, fed by either the melting snow or the monsoon rains, empty into the Brahmaputra river in India.

Climate: The climate in Bhutan varies with altitude, from subtropical in the south to temperate in the highlands and polar-type climate, with year-round snow, in the north. Bhutan experiences five distinct seasons: summer, monsoon, autumn, winter and spring. Western

Bhutan has the heavier monsoon rains; southern Bhutan has hot humid summers and cool winters; central and eastern Bhutan is temperate and drier than the west with warm summers and cool winters.

The island of Sri Lanka lies in the Indian Ocean, southwest of the Bay of Bengal. It is separated from the Indian subcontinent by the Gulf of Mannar and the Palk Strait.
The pear-shaped island consists mostly of flat-to-rolling coastal plains, with mountains rising only in the south-central part. Amongst these are Sri Pada and the highest point Pidurutalagala (also known as Mt Pedro), at 2,524 meters (8,281 ft). The 334 km (207 mile) long Mahaweli ganga (Mahaweli river), the longest river in Sri Lanka, along with other major rivers and numerous reservoirs provide fresh water to the population.At its maximum, Sri Lanka is 435km (235 miles) long (North to South) and 225km (140 miles) wide (East to West).

The **climate** is tropical, characterized by monsoons: the northeast monsoon lasts from December to March, the southwest monsoon from June to October. The lowest gravitational field on Earth lies just off the coast of Sri Lanka.

Maldives is situated in the South West of Sri Lanka, on the equator. About 1190 islands (the actual number varies as islands are continuously being washed away and new ones formed) are spread over 26 atolls, ring like coral formations enclosing a lagoon, which gives the Maldives its unique paradise-like appearance. They stretch for about 820 km from North to South, 130 km at the widest point and do not exceed a length of 4.5 miles or an altitude of 6 feet above sea level. Out of the incredibly large number of islands only 200 islands are inhabited, with 88 islands adapted as exclusive resort islands. The sea forms over 99 percent of the Maldives. Only 0.331 percent, 298 km2 (115 square miles), of its 298 km2 (34, 750 square miles) is land.

Climate: It has a tropical climate with warm temperatures all year round and a great deal of sunshine. The weather is determined largely by the monsoons. Maldives has two distinct seasons; dry season (northeast monsoon) and wet season (southwest monsoon). In these two seasons the temperature varies hardly. Northeast monsoon extends from Jannary to March. Since Maldives consists of small islands and are snrronnded by seas, hot days are often tempered by cooling sea breezes and balmy evening temperatures. Thronghout the year, temperature remains almost same in the Maldives. However, daily temperature ranges from around 31 degrees Celsius in daytime to 23 degrees Celsius in nighttime. The hottest month on average is April and the coolest, December. The wet season- sonthwest monsoon runs from mid-May to November. In this season Maldives experiences torrential rain. Central, Southern and Northern parts of the Maldives receive annnal average rainfall of 1924.7mm, 2277.8mm, and 1786.4mm, respectively. May and October records the highest average monthly rainfall. The severe storms and cyclones are extremely rare events. However the country is affected whenever cyclones form in the Bay of Bengal or the Arabian Sea. 'Faru' or ring-shaped reef structures form the atolls and these reefs provide natural defense against wind and wave action, on these delicate islands.

1.3 Objectives and scope of the present work

RegCM3 will be adopted to calculate surface heat budget in South Asian region. The model calculated surface heat budget will be calibrated with 40-year re-analysis data of ECMWF (European Centre for Medium Range Weather Forecasting) called ERA-40 [6, 7]. The variation of surface heat budget for monthly, inter-seasonal, seasonal and yearly over land and water, along latitude-longitude differences, diurnal variation at the centre point of different selected zones, will be obtained. The relationship between the variations of surface heat budget and precipitation will be obtained. The parameters Net absorbed solar energy flux, Net infrared energy flux, Sensible heat and latent heat will be used in calculation of surface heat budget over South Asian region. Among these parameters which one is more effective on surface heat budget will also be pointed out.

The outcome of the research will be helpful in understanding the radiative impacts on the development mechanism of tropical convections. Using the predicted range of surface heat budget over land and ocean, the indication of the development of precipitation systems may be predicted. The lead-time information about the development of precipitation systems may useful to formulate future planning for agriculture, water management, health, infrastructure and so on.

CHAPTER 2: RegCM MODEL AND ECMWF DATA DESCRIPTION

2.1 Introduction of RegCM Model

The idea that limited area models (LAMs) could be used for regional studies was originally proposed by Dickinson et al., (1989) and Giorgi, (1990b). This idea was based on the concept of one way nesting, in which large scale meteorological fields from general circulation model (GCM) runs provide initial and time-dependent meteorological lateral boundary conditions (LBC) for high resolution regional climate model (RCM) simulations, with no feedback from the RCM to the driving GCM.

The first generation NCAR RegCM was built upon the National Center for Atmospheric Research-Pennsylvania State University (NCAR-PSU) Mesoscale Model version MM4 in the late 1980s (Dickinson et al., 1989; Giorgi, 1989). The dynamical component of the model originated from that of the MM4, which is a compressible, finite difference model with hydrostatic balance and vertical σ-coordinates. Later the use of a split-explicit time integration scheme was added along with an algorithm for reducing horizontal diffusion in the presence of steep topographical gradients (Giorgi et al., 1993a; Giorgi et al., 1993b). As a result the dynamical core of the RegCM is similar to that of the hydrostatic version of MM5 (Grell et al., 1994a).

For application of the MM4 to climate studies, a number of physics parameterizations were replaced, mostly in the areas of radiative transfer and land surface physics, which led to the first generation RegCM (Dickinson et al., 1989; Giorgi, 1990b). The first generation RegCM included the Biosphere-Atmosphere Transfer Scheme (BATS), (Dickinson et al., 1986) for surface process representation, the radiative transfer scheme of the NCAR Community Climate Model (CCM) version CCM1, a medium resolution local planetary boundary layer

scheme, the Kuo-type cumulus convection scheme of Anthes (1977) and the explicit moisture scheme of Hsie et al. (1984).

A first major upgrade of the model physics and numerical schemes was documented by (Giorgi et al., 1993a; Giorgi et al., 1993b), and resulted in a second generation RegCM, hereafter referred to as RegCM2. The physics of RegCM2 was based on that of the NCAR CCM2 (Hack et al., 1993), and the mesoscale model MM5 (Grell et al., 1994a). In particular, the CCM2 radiative transfer package (Briegleb, 1992) was used for radiation calculations, the non local boundary layer scheme of (Holtslag et al., 1990) replaced the older local scheme, the mass flux cumulus cloud scheme of (Grell, 1993) was added as an option, and the latest version of BATS1E (Dickinson et al., 1993) was included in the model.

In the last few years, some new physics schemes have become available for use in the RegCM, mostly based on physics schemes of the latest version of the CCM, CCM3 (Kiehl et al., 1996). First, the CCM2 radiative transfer package has been replaced by that of the CCM3. In the CCM2 package, the effects of H_2O, O_3, O_2, CO_2 and clouds were accounted for solar radiative transfer was treated with a δ-Eddington approach and cloud radiation depended on three cloud parameters, the cloud fractional cover, the cloud liquid water content, and the cloud effective droplet radius. The CCM3 scheme retains the same structure as that of the CCM2, but it includes new features such as the effect of additional greenhouse gases (NO_2, CH_4, CFCs), atmospheric aerosols, and cloud ice.

The other primary changes are in the areas of cloud and precipitation processes. The original explicit moisture scheme (Hsie et al., 1984) has been substituted with a simplified version of it. This is because the original scheme was computationally too expensive to be run in climate mode. In the simplified scheme only a prognostic equation for cloud water is included, which accounts for cloud water formation, advection and mixing by turbulence, re-evaporation in

sub-saturated conditions, and conversion into rain via a bulk autoconversion term. The main novelty of this scheme does not reside of course in the simplistic microphysics, but in the fact that the prognosed cloud water variable is directly used in the cloud radiation calculations. In the previous versions of the model, cloud water variables for radiation calculations were diagnosed in terms of the local relative humidity. This new feature adds a very important and far reaching element of interaction between the simulated hydrologic cycle and energy budget calculations.

Finally, an important aspect of model development was the inclusion of a stretched grid model configuration, by which the model horizontal resolution is relatively coarse in the lateral buffer zone and increases towards the interior of the domain. Preliminary experiments using an adiabatic version of the model in stretched grid mode are presented by (Qian et al., 1999). However, the stretched grid option is not available with the new RegCM3 version. Other new features in the RegCM include improvements in the coupled lake model (Small et al., 1999) and the incorporation of a tracer model with capability of radiative interactions (Qian et al.. 1999).

Other improvements in RegCM3 involve the input data. The USGS Global Land Cover Characterization and Global 30 Arc-Second Elevation datasets are now used to create the terrain files. In addition, NCEP and ECMWF global reanalysis datasets are used for the initial and boundary conditions.

The whole released RegCM modeling system is composed by four components: Terrain, ICBC, RegCM, and Postprocessor.

Terrain and ICBC are the two components of RegCM preprocessor. Terrestrial variables (include elevation, land use and sea surface temperature) and three-dimensional isobaric

meteorological data are horizontally interpolated from a latitude-longitude mesh to a high-resolution domain on either a Rotated (and Normal) Mercator, Lambert Conformal, or Polar Stereographic projection. Vertical interpolation from pressure levels to the σ-coordinate system of RegCM is also performed. σ Surfaces near the ground closely follow the terrain, and the higher-level σ-surfaces tend to approximate isobaric surfaces.

Since the vertical and horizontal resolution and domain size can vary, the modeling package programs employ parameterized dimensions requiring a variable amount of core memory, and the requisite hard-disk storage amount is varied accordingly.

Seasonal variations in observed precipitation over the South Asia region as a consequence of summer monsoon activity are poorly simulated by most of the models (IPCC 2001). An interannual mode of monsoon variability has been identified which is closely related to the observed seasonal mean Bangladesh Rainfall (BR). A counterpart of this mode has also been identified at subseasonal time-scales which projects strongly on to the daily BR, confirming that a common mode of monsoon variability exists on sub-seasonal and interannual time-scales.

Advances are limited by the lack of data in the region and an inability to identify the fundamental processes that create the variability. Little is known about the state of the upper Indian Ocean than its surface temperature and its surface height. In fact, satellite estimates indicate that the northern Bay of Bengal receives the largest mean precipitation in south Asia during the summer monsoon.

The development mechanism of summer monsoon convections, which is one of the key points to understand the water cycle as well as the global circulation of the atmosphere, will be obtained. Climate change is important issues to know and can be possible using the model simulation.

Considering the above, the seasonal and annual variability of precipitation and surface air temperature have been studied for the region in and around Bangladesh.

2.2 The Frame Work of RegCM Model

The modeling system usually uses its data on surface pressure, the pressure have to be interpolated to the model's vertical coordinate before it introduce as model input. The vertical coordinate is the terrain following σ coordinate system. The lower grid levels follow the terrain while the upper surface is flatter. Intermediate levels progressively flatten as the pressure decreases toward the top of the model. A dimensionless σ coordinate is used to define the model levels where p is the pressure, p_t is a specified constant top pressure, p_s is the surface pressure.

$$\sigma = \frac{p - p_t}{p_s - p_t}$$

Numerical experiments driven by analyses of observations are used to limit systematic biases due to driving data used at lateral boundary conditions. To validate the model performance of the RegCM, in this study, a 7-year simulation, which is driven by NCEP re-analysis data, is performed for the 1983, 1995-2000 periods. The model domain is selected to cover the South Asia region 65^0E-117^0E, 5^0N-35^0N on a rotated mercator projection at a 60 km horizontal resolution and 16 levels in the vertical.

2.3 Model Description

2.3.1 Dynamics

The model dynamic equations and numerical discretization are described by (Grell et al., 1994a).

Horizontal Momentum Equations

$$\frac{\partial p^* u}{\partial t} = -m^2\left(\frac{\partial p^* uu/m}{\partial x} + \frac{\partial p^* vu/m}{\partial y}\right) - \frac{\partial p^* u\dot{\sigma}}{\partial \sigma}$$

$$-mp^*\left[\frac{RT_v}{(p^* + p_t/\sigma)}\frac{\partial p^*}{\partial x} + \frac{\partial \phi}{\partial x}\right] + fp^* v + F_H u + F_v u \qquad \ldots\ldots (1)$$

$$\frac{\partial p^* v}{\partial t} = -m^2\left(\frac{\partial p^* uv/m}{\partial x} + \frac{\partial p^* vv/m}{\partial y}\right) - \frac{\partial p^* v\dot{\sigma}}{\partial \sigma}$$

$$-mp^*\left[\frac{RT_v}{(p^* + p_t/\sigma)}\frac{\partial p^*}{\partial y} + \frac{\partial \phi}{\partial y}\right] + fp^* u + F_H v + F_v v \qquad \ldots\ldots\ldots (2)$$

where u and v are the eastward and northward components of velocity, T_v is virtual temperature, ϕ is geopotential height, f is the coriolis parameter, R is the gas constant for dry air, m is the map scale factor for either the Polar Stereographic, Lambert Conformal,or Mercator map projections, $\dot{\sigma} = \frac{d\sigma}{dt}$ and F_H and F_V represent the effects of horizontal and vertical diffusion, and $p^* = p_s - p_t$.

Continuity and Sigmadot $(\dot{\sigma})$ Equations

$$\frac{\partial p^*}{\partial t} = -m^2\left(\frac{\partial p^* u/m}{\partial x} + \frac{\partial p^* v/m}{\partial y}\right) - \frac{\partial p^* \dot{\sigma}}{\partial \sigma} \qquad \ldots\ldots\ldots\ldots\ldots (3)$$

The vertical integral of Equation (3) is used to compute the temporal variation of the surface pressure in the model,

$$\frac{\partial p^*}{\partial t} = -m^2 \int_0^1 \left(\frac{\partial p^* u/m}{\partial x} + \frac{\partial p^* v/m}{\partial y}\right) d\sigma \qquad \ldots\ldots\ldots\ldots\ldots (4)$$

After calculation of the surface-pressure tendency $\frac{\partial p^*}{\partial t}$, the vertical velocity in sigma coordinates $(\dot{\sigma})$ is computed at each level in the model from the vertical integral of Equation (3).

$$\dot{\sigma} = -\frac{1}{p^*}\int_0^{\sigma}\left[\frac{\partial p^*}{\partial t} + m^2\left(\frac{\partial p^* u/m}{\partial x} + \frac{\partial p^* v/m}{\partial y}\right)\right]d\sigma' \quad \ldots\ldots\ldots\ldots\ldots\ldots \quad (5)$$

Where σ' is a dummy variable of integration and $\dot{\sigma}(\sigma = 0) = 0$.

Thermodynamic Equation and Equation for Omega (ω)

The **thermodynamic equation** is

$$\frac{\partial p^* T}{\partial t} = -m^2\left(\frac{\partial p^* uT/m}{\partial x} + \frac{\partial p^* vT/m}{\partial y}\right) - \frac{\partial p^* T\dot{\sigma}}{\partial \sigma} +$$

$$\frac{RT_v\omega}{C_{pm}(\sigma + P_t/P_{ast})} + \frac{p^* Q}{C_{pm}} + F_H T + F_v T \quad \ldots\ldots\ldots \quad (6)$$

where C_{pm} is the specific heat for moist air at constant pressure, Q is the diabatic heating, $F_H T$ represents the effect of horizontal diffusion, $F_v T$ represents the effect of vertical mixing and dry convective adjustment, and ω is

$$\omega = p^*\dot{\sigma} + \sigma\frac{dp^*}{dt} \quad \ldots\ldots\ldots\ldots\ldots\ldots\ldots\ldots\ldots\ldots\ldots\ldots\ldots\ldots (7)$$

Where,

$$\frac{dp^*}{dt} = \frac{\partial p^*}{\partial t} + m\left(u\frac{\partial p^*}{\partial x} + v\frac{\partial p^*}{\partial y}\right)$$

The expression for $C_{pm} = C_p(1 + 0.8q_v)$,0

Where C_p is the specific heat at constant pressure for dry air and q_v is the mixing ratio of water vapor.

Hydrostatic Equation

The hydrostatic equation is used to compute the geopotential heights from the virtual temperature T_v,

$$\frac{\partial \sigma}{\partial \ln(\sigma + p_t / p^*)} = -RT_v \left[1 + \frac{q_c + q_r}{1 + q_v} \right]^{-1} \quad \ldots\ldots\ldots\ldots\ldots\ldots\ldots\ldots\ldots\ldots \quad (8)$$

Where $T_v = T(1 + 0.608 q_v)$, q_v, q_c, and q_r are the water vapor, cloud water or ice, and rain water or snow, mixing ratios.

2.3.2 Physics

RegCM3 uses the radiation scheme of the NCAR CCM3, which is described in (Kiehl et al., 1996). Briefly, the solar component, which accounts for the effect of O_3, H_2O, CO_2, and O_2, follows the δ-Eddington approximation of (Kiehl et al., 1996). It includes 18 spectral intervals from 0.2 to 5 μm. The cloud scattering and absorption parameterization follow that of Slingo (1989), whereby the optical properties of the cloud droplets (extinction optical depth, single scattering albedo, and asymmetry parameter) are expressed in terms of the cloud liquid water content and an effective droplet radius. When cumulus clouds are formed, the gridpoint fractional cloud cover is such that the total cover for the column extending from the model-computed cloud-base level to the cloud-top level (calculated assuming random overlap) is a function of horizontal grid point spacing. The thickness of the cloud layer is assumed to be equal to that of the model layer, and different cloud water content is specified for middle and low clouds.

2.3.3 Land Surface Model

The surface physics are performed using BATS1E (Biosphere-Atmosphere Transfer Scheme) which is described in detail by (Dickinson et al., 1993). BATS is a state of the art surface package designed to describe the role of vegetation and interactive soil moisture in modifying

the surface-atmosphere exchanges of momentum, energy, and water vapor. The model has a vegetation layer, a snow layer, a surface soil layer, 10 cm thick, or root zone layer, 1-2 m thick, and a third deep soil layer 3 m thick. Prognostic equations are solved for the soil layer temperatures using a generalization of the force-restore method of Deardoff (1978). The temperature of the canopy and canopy foliage is calculated diagnostically via an energy balance formulation including sensible, radiative, and latent heat fluxes.

The soil hydrology calculations include predictive equations for the water content of the soil layers. These equations account for precipitation, snowmelt, canopy foliage drip, evapotranspiration, surface runoff, infiltration below the root zone, and diffusive exchange of water between soil layers. The soil water movement formulation is obtained from a fit to results from a high-resolution soil model (Climate Processes and Climate Sensitivity, 1984) and the surface runoff rates are expressed as functions of the precipitation rates and the degree of soil water saturation. Snow depth is prognostically calculated from snowfall, snowmelt, and sublimation. Precipitation is assumed to fall in the form of snow if the temperature of the lowest model level is below 271 K.

Sensible heat, water vapor, and momentum fluxes at the surface are calculated using a standard surface drag coefficient formulation based on surface-layer similarity theory. The drag coefficient depends on the surface roughness length and on the atmospheric stability in the surface layer. The surface evapotranspiration rates depend on the availability of soil water.

2.3.4 Planetary Boundary Layer Scheme

The planetary boundary layer scheme, developed by (Holtslag et al., 1990), is based on a nonlocal diffusion concept that takes into account counter gradient fluxes resulting from large-scale eddies in an unstable, well-mixed atmosphere. The vertical eddy flux within the PBL is given by

$$F_c = -K_c(\frac{\partial C}{\partial z} - \gamma_c) \quad \text{..... (9)}$$

Where γ_c is a "countergradient" transport term describing nonlocal transport due to dry deep convection. The eddy diffusivity is given by the nonlocal formulation

$$K_c = k\omega_t z(1-\frac{z^2}{h}) \quad \text{..... (10)}$$

Where k is the von Karman constant; ω_t is a turbulent convective velocity that depends on the friction velocity, height, and the Monin-Obhukov length; and h is the PBL height. The countergradient term for temperature and water vapor is given by

$$\gamma_c = C\frac{\phi_c^0}{\omega_t h} \quad \text{..... (11)}$$

Where C is a constant equal to 8.5, and ϕ_c^0 is the surface temperature or water vapor flux. Equation (11) is applied between the top of the PBL and the top of the surface layer, which is assumed to be equal to 0.1h. Outside this region and for momentum, γ_c is assumed to be equal to 0.

For the calculation of the eddy diffusivity and countergradient terms, the PBL height is diagnostically computed from

$$h = \frac{Ri_c r\left[u(h)^2 + v(h)^2\right]}{(g/\theta_s)\left[\theta_v(h) - \theta_s\right]} \quad \text{..... (12)}$$

Where $u(h)$, $v(h)$, and θ_v are the wind components and the virtual potential temperature at the PBL height, g is gravity, $Ri_c r$ is the critical bulk Richardson number, and θ_s is an appropriate temperature of are near the surface.

2.3.5 Convective Precipitation Schemes

Convective precipitation is computed using one of three schemes: (1) Grell scheme (Grell, 1993); (2) Modified-Kuo scheme (Anthes, 1977); and (3) Betts-Miller Scheme (Accordind to RegCM Version 3.0) and MIT-Emanuel scheme (Emanuel, 1991; Emanuel and Zivkovic-Rothman, 1999) (Accordind to RegCM Version 3.1). In addition, the Grell parameterization is implemented using one of two closure assumptions: (1) the Arakawa and Schubert closure (Grell et al., 1994a) and (2) the Fritsch and Chappell closure (Fritsch and Chappell, 1980), hereafter referred to as AS74 and FC80, respectively.

2.3.5.1 Grell Scheme

The Grell scheme (Grell, 1993), similar to the AS74 parameterization, considers clouds as two steady-state circulations: an updraft and a downdraft. No direct mixing occurs between the cloudy air and the environmental air except at the top and bottom of the circulations. The mass flux is constant with height and no entrainment or detrainment occurs along the cloud edges. The originating levels of the updraft and down-draft are given by the levels of maximum and minimum moist static energy, respectively. The Grell scheme is activated when a lifted parcel attains moist convection. Condensation in the updraft is calculated by lifting a saturated parcel. The downdraft mass flux (m_0) depends on the updraft mass flux (m_b) according to the following relation:

$$m_0 = \frac{\beta I_1}{I_2} m_b \quad \text{..... (13)}$$

Where I_1 is the normalized updraft condensation, I_2 is the normalized downdraft evaporation, and β is the fraction of updraft condensation that re-evaporates in the

downdraft. β depends on the wind shear and typically varies between 0.3 and 0.5. Rainfall is given by

$$P^{CU} = I_t m_b (1-\beta) \quad \text{..... (14)}$$

Heating and moistening in the Grell scheme are determined both by the mass fluxes and the detrainment at the cloud top and bottom. In addition, the cooling effect of moist downdrafts is included.

Due to the simplistic nature of the Grell scheme, several closure assumptions can be adopted. RegCM3's default version directly implements the quasi-equilibrium assumption of AS74. It assumes that convective clouds stabilize the environment as fast as nonconvective processes destabilize it as follows:

$$m_b = \frac{ABE^{*} - ABE}{NA\Delta t} \quad \text{..... (15)}$$

Where ABE is the buoyant energy available for convection, ABE^{*} is the amount of buoyant energy available for convection in addition to the buoyant energy generated by some of the non-convective processes during the time interval Δt, and NA is the rate of change of ABE per unit m_b. The difference $ABE^{*}-ABE$ can be thought of as the rate of destabilization over time Δt. ABE^{*} is computed from the current fields plus the future tendencies resulting from the advection of heat and moisture and the dry adiabatic adjustment.

Another stability based closure assumption that is commonly implemented in GCMs and RCMs is the FC80 type closure assumption. In this closure, it is assumed that convection removes the ABE over a given time scale as follows:

$$m_b = \frac{ABE}{NA_\tau} \quad \text{..... (16)}$$

Where τ is the ABE removal time scale.

The fundamental difference between the two assumptions is that the AS74 closure assumption relates the convective fluxes and rainfall to the tendencies in the state of the atmosphere, while the FC80 closure assumption relates the convective fluxes to the degree of instability in the atmosphere. Both schemes achieve a statistical equilibrium between convection and the large-scale processes. However, this subtle distinction in the implementation of the closure will prove to be an important difference.

2.3.5.2 Kuo Scheme

Convective activity in the Kuo scheme is initiated when the moisture convergence M in a column exceeds a given threshold and the vertical sounding is convectively unstable. A fraction of the moisture convergence β moistens the column and the rest is converted into rainfall P^{CU} according to the following relation:

$$P^{CU} = M(1-\beta)$$

β is a function of the average relative humidity $\overline{RH}$ of the sounding as follows:

$$\beta = 2(1-\overline{RH}) \qquad \overline{RH} \geq 0.5$$

$$\beta = 1.0 \qquad \text{otherwise}$$

Note that the moisture convergence term includes only the advective tendencies for water vapor. However, evapotranspiration from the previous time step is indirectly included in M since it tends to moisten the lower atmosphere. Hence, as the evapotranspiration increases, more and more of it is converted into rainfall assuming the column is unstable. The latent heating resulting from condensation is distributed between the cloud top and bottom by a function that allocates the maximum heating to the upper portion of the cloud layer. To eliminate numerical point storms, a horizontal diffusion term and a time release constant are

included so that the redistributions of moisture and the latent heat release are not performed instantaneously (Giorgi and Bates, 1989; Giorgi and Marinucci, 1991).

2.3.5.3 Betts-Miller Scheme

In the Betts-Miller scheme, the sub-grid scale effects of convective clouds are represented by adjusting temperature and moisture profiles to the observed quasi-equilibrium structures for deep convection and to a mixing line structure for shallow convection. Quasi-equilibrium between the cloud field and the large-scale forcing forms the basis of representing deep convection in the BM scheme. Quasi-equilibrium means that the convective cloud field constrains the thermal and moisture structure of the atmosphere against the destabilizing influence of the large scale flow. The concept has been found to be valid on large spatial and temporal scales. The effects of shallow convection are viewed as a mixing process between the surface layer air and the free atmosphere.

Observational basis for deep convection: The thermodynamics of the BM scheme is based on the saturation point formulation as reported in (Betts, 1982). The saturation point (sp) is defined as the temperature and pressure (T^*, p^*) at the lifting condensation level (LCL). The subsaturation parameter P is the difference between air parcel saturation level pressure and the actual pressure level i.e. $P = p^* - p$. (Betts, 1986) observed that temperature profiles below the freezing level in deep convection is parallel to the θ_{ESV} isopleth, where θ_{ESV} is defined as a constant virtual equivalent potential temperature. This led to the proposal that the reference lapse rate in the lower-troposphere is moist virtual adiabatic rather than the widely accepted moist adiabat. Since the slope of the θ_{ESV} isopleth is 0.9 times that of the moist adiabat, the air parcel buoyancy reduction due to cloud water content is accounted for. This

reference structure in the presence of deep convection is universal as reported by (Betts, 1986) for the cases of hurricanes,

GATE slow and fast moving squall lines and Venezuela convective episodes. Thus, the reference structure below 600 hPa or the freezing level is the θ_{ESV} with θ_{ES} constrained to a minimum at 600 hPa. Above 600 hPa the observed thermal profile increases to cloud top θ_{ES} value. Considerable variability is associated with the observed moisture structure. Despite this a reference moisture profile is specified in the scheme.

Observational basis for shallow convection: A shallow cumulus cloud field is regarded as a mixing process between the surface layer air and the free atmosphere. This mixing is characterized by a mixing line. Thus when two air parcels mix in the vertical, the *sp* of every possible mixture lies on the mixing line joining the *sps* of the two parcels. This mixing line structure for shallow cumulus convection was highlighted by (Betts, 1982) by plotting *sps* between 900-700 hPa and the *sps* were found to lie close to the line joining the *sps*. This evidence was presented for the undisturbed trade wind region and tropical land stations.

2.3.5.4 MIT-Emanuel scheme:

The newest cumulus convection option to the Regional Climate Model version 3 (RegCM3) is the Massachusetts Institute of Technology (MIT) scheme. More detailed descriptions can be found in Emanuel (1991) and Emanuel and Zivkovic-Rothman (1999). The scheme assumes that the mixing in clouds is highly episodic and inhomogeneous (as opposed to a continuous entraining plume) and considers convective fluxes based on an idealized model of sub-cloud-scale updrafts and downdrafts. Convection is triggered when the level of neutral buoyancy is greater than the cloud base level. Between these two levels, air is lifted and a

fraction of the condensed moisture forms precipitation while the remaining fraction forms the cloud. The cloud is assumed to mix with the air from the environment according to a uniform spectrum of mixtures that ascend or descend to their respective levels of neutral buoyancy. The mixing entrainment and detrainment rates are functions of the vertical gradients of buoyancy in clouds. The fraction of the total cloud base mass flux that mixes with its environment at each level is proportional to the undiluted buoyancy rate of change with altitude. The cloud base upward mass flux is relaxed towards the sub-cloud layer quasi equilibrium. In addition to a more physical representation of convection, the MIT-Emanuel scheme offers several advantages compared to the other RegCM3 convection options. For instance, it includes a formulation of the auto-conversion of cloud water into precipitation inside cumulus clouds, and ice processes are accounted for by allowing the auto conversion threshold water content to be temperature dependent. Additionally, the precipitation is added to a single, hydrostatic, unsaturated downdraft that transports heat and water. Lastly, the MIT-Emanuel scheme considers the transport of passive tracers.

2.4 The European Centre for Medium-Range Weather Forecasts (ECMWF)

ECMWF is an international organization supported by 26 European States. The comprehensive earth-system model developed at ECMWF forms the basis for all the data assimilation and forecasting activities. All the main applications required are available through one integrated computer software system (a set of computer programs written in FORTRAN) called the Integrated Forecast System or IFS.

2.4.1 ECMWF 40 Year Re-analysis (ERA-40) Data Archive

The whole period from September 1957 to August 2002 is now available. The Level III-B archive is subdivided into four classes of data sets:

- Basic 2.5° atmospheric
- Full Resolution atmospheric
- Wave
- Atmospheric Monthly Means

The data sets are based on quantities analyzed or computed within the ERA-40 data assimilation scheme or from forecasts based on these analyses.

Basic 2.5° atmospheric: These Data Sets contain values in a compact form at a resolution of 2.5° x 2.5°. They are particularly suitable for users with limited data processing resources. Much of this data is available from the ECMWF Data Server at no charge for research usage. All the ERA-40 data from the Data Server can be supplied by ECMWF Data Services as described.

Full Resolution atmospheric: These Data Sets provide access to most of the data from the ERA-40 atmospheric model archived at ECMWF. They have a higher space resolution. They

should only be used where high resolution is essential; in this respect they are particularly suited for use in conjunction with case studies and as initial conditions for high resolution models. They include analysis, forecast accumulation and forecast data. Analysis data are available for surface, pressure, model, isentropic and potential vorticity levels. Daily forecast data are available for surface, pressure and model levels.

Wave: These Data Sets contain analysis and forecast data from the ERA-40 wave model.

Atmospheric Monthly Means: The Atmospheric Monthly Means Data Sets provide monthly means and monthly means of daily means of analysis and forecast data. Analysis data are available for surface, pressure, model, isentropic and potential vorticity levels. Daily forecast data are available for surface, pressure and model levels.

The ERA-40 archive is currently maintained using the WMO FM 92-IX Ext GRIB (grid in binary) form of data representation, with ECMWF local versions of GRIB Table 2. All fields of data are global within the archive except for Mediterranean wave model data. Data are stored in FM 92 GRIB using sufficient bits to ensure that the grid point values can be retrieved to accuracy consistent with the analysis methods used. A full extraction service is provided, enabling users to obtain sub-areas of data and data at various resolutions on regular Gaussian or latitude/longitude grids, or as spherical harmonics with selected triangular truncation. All extracted data are delivered using the GRIB representation.

2.4.2 The data assimilation system

General overview: A very large amount of observed data is available for use by the assimilation and forecast system. In a typical 12-hour period there is a total of 75 million pieces of data available, around 98% from satellites. Most of the available data are considered for use but the quality control, redundancy checks and thinning of locally dense data will

reduce the numbers. The observations can roughly be divided into conventional, in situ observations, and non-conventional, remote-sensing observations. The earth-atmosphere system can be measured directly by conventional in situ instruments, and indirectly by remote sensing instruments. The latter can be done in two different ways: passively and actively. The various data types have different characteristics in terms of geographical coverage, vertical structure and temporal distribution, which determine their ability to affect the analysis. With increased availability of non-conventional observations the analysis system has developed into higher sophistication to be able to cope with off-time data and, in particular, indirect measurements such as radiances from satellites instead of direct observations of temperature, humidity, pressure, ozone and wind.

2.4.3 Conventional observations

Since the conventional data report the values in the same units as the model variables, and on pressure or height levels, they can be used more or less directly by the analysis system after vertical interpolation. Reports of pressure and humidity are used from SYNOP (conventional surface weather station reports). 10 meter wind observations are not used, not even from marine locations such as coastal stations or minor islands. Pressure and winds are used from SHIP (conventional weather reports from moving ships) and DRIBU (drifting buoys).

Temperature, wind and humidity from TEMP (upper air observations from radio sonde stations) are used and their position defined according to the pressure at all reported levels. Temperatures in the stratosphere are corrected for estimated mean errors (bias correction). Humidity observations from drop sondes are not used. Winds from PILOT (wind measurements in the free atmosphere from stations launching balloons) are used, except when there is a duplicate with radio sonde data. PROFILERS (measuring winds with remote sensing) provide wind speed and direction at very high temporal resolution.

Temperature and wind reports are used from AIREP (manual air craft reports), AMDAR (Aircraft Meteorological Data Relay) and ACARS (automatic air craft reports). The traditional AIREP observations now only account for ~4% of all used aircraft data, as most commercial aircrafts operate the AMDAR or ACARS systems. During landing and take-off the latter provide data in quantity, quality and location comparable to radio sondes.

PAOB is a hybrid between conventional and satellite data. They are manually derived pseudo-observations of MSLP on the Southern Hemisphere, made by the Australian Bureau of Meteorology from satellite images.

Humidity observations reported as relative humidity or dew point, are transformed into specific humidity using the reported temperature. SYNOP dew points are used, together with the temperature to calculate the 2 m specific humidity.

Other data types are used to analyse snow, ice, SST, soil wetness and ocean waves. These are at present analyzed separately, but might in the future be incorporated in the full data assimilation system.

2.4.4 Satellite observations

During the last 5-10 years there has been a significant increase in the quantity, quality and diversity of satellite observations. At the time of writing (autumn 2003) ECMWF routinely receives data from more than 15 satellites, some of which are equipped with several instruments that provides in total 28 satellite data sources.

ECMWF has during the last 10-15 years developed new assimilation techniques to make use of this new information. Although satellite data is slightly less accurate than conventional observations such as radio sonde observations, their great advantage is their broad

geographical coverage. While the data assimilation system has to spread out the information in space of radio sonde observations, this is less of an undertaking with satellite observations.

Another advantage is that the use of satellite data ensures that the elusive small amplitude-large scale errors over the oceans are corrected for, something which isolated measurements would have difficulties to do. Although the amplitude of the analysis increments are weak, their large-scale nature becomes important after some days integration when they have "cascaded" into smaller scales, which might develop and affect synoptic scale weather systems.

Consequently there is now a strong benefit from satellite data in the ECMWF and the influences of other conventional data types are becoming less critical. In particular over the Southern Hemisphere, where there is a lack of conventional data, satellite data has had a large impact on the scores which are now almost as good as in the Northern Hemisphere. However there are limitations in the use of satellite data over land surfaces. Over desertic areas and frozen regions, at the state of the art, is particularly difficult to use tropospheric channels due to the inaccurate knowledge of the underlying surface emissivity. On global scale these are areas were overall we assimilate less data. To ensure that only good quality data are used for the analysis an intricate quality control is applied. There are several ways data can be prevented from affecting the analysis.

CHAPTER 3: DATA USED AND METHOLOGY

3.1 Data Used

A regional climate simulation there is two pre-processing steps. The first step involves defining the domain and grid interval and interpolating the landuse and elevation data to the model grid. The second step is to generate the files used for the initial and boundary conditions during the simulation. The input data necessary to run the model can be downloaded from the PWC website at the following URL:

http://www.ictp.trieste.it/_pubregcm/RegCM3

The terrain program horizontally interpolates the landuse and elevation data from a latitude-longitude grid to the Cartesian grid of the chosen domain. RegCM currently uses the Global Land Cover Characterization (GLCC) datasets for the vegetation/landuse data. The GLCC dataset is derived from 1 km Advanced Very High Resolution Radiometer (AVHRR) data and is based on the vegetation/land cover types defined by Biosphere Atmosphere Transfer Scheme (BATS). The 18 vegetation / land cover types and associated parameters are used. Each grid cell of the model is assigned one of the eighteen categories.

The elevation data used is from the United States Geological Survey (USGS). Both the landuse and elevation data files are available at 30 and 10 minute resolutions.

ICBC

The ICBC program interpolates sea surface temperature (SST) and global re-analysis data to the model grid. These files are used for the initial and boundary conditions during the simulation. (Eventually, interfaces will exist to allow GCM output to be used for initial and boundary conditions.)

Sea Surface Temperature

There are two options for Sea Surface Temperature (SST) data. One is the Global Sea Surface Temperature (GISST) one-degree monthly gridded data available from the Hadley Centre Met Office. And also available is the Optimum Interpolation Sea Surface Temperature (OISST) one-degree weekly analysis available from the National Ocean and Administration.

3.2 Initial and Boundary Conditions

There are some options to choose from for the global analysis datasets to use for the initial and boundary conditions.

ECMWF: The European Centre for Medium-Range Weather Forecasts Reanalysis datasets (T42, L15).

NNRP: The National Centre for Environmental Prediction (NCEP) Reanalysis datasets (2.5 degrees grid, L17).

The numerical treatment of the lateral boundaries is a difficult but very important aspect of the regional climate model. There are five types of boundary conditions that can be used in the model.

i. **Fixed:** This will not allow time variation at lateral boundaries. Not recommended for real-data applications.

ii. **Time-dependent:** Outer two rows and columns have specified values of all predicted fields. Recommended for nests where time-dependent values are supplied by the parent domain. Not recommended for coarse mesh where only one outer row and column would be specified.

iii. **Linear relaxation:** Outer row and column is specified by time-dependent value, next four points are relaxed towards the boundary values with a relaxation constant that decreases linearly away from the boundary.

iv **Sponge:** (Perkey and Kreitzberg, 1976)

v **Exponential relaxation:** (Davies and Turner, 1977) (default)

The (one-way) nested modeling technique has been increasingly applied to climate change studies in the last few years. This technique consists of using output from GCM simulations to provide initial and driving lateral meteorological boundary conditions for high-resolution Regional Climate Model (RegCM) simulations, with no feedback from the RegCM to the driving GCM. Hence, a regional increase in resolution can be attained through the use of nested RegCMs to account for sub-GCM grid-scale forcing.

Continuous month or season-long to multi-year experiments for present-day conditions with RegCMs driven either by analyses of observations or by GCMs was generated for regions in North America, Asia, Europe, Australia, and Africa. In the experiments mentioned above, the model horizontal grid point spacing 60 km and the length of runs from 1 month to 10 years. The choice of an appropriate domain is not trivial. The influence of the boundary forcing can reduce as region size increases (Jones et al., 1995; Jacob and Podzun, 1997) and may be dominated by the internal model physics for certain variables and seasons (Noguer et al., 1998). This can lead to the RegCM solution significantly departing from the driving data, which can make the interpretation of down-scaled regional climate changes more difficult (Jones et al., 1997). The domain size has to be large enough so that relevant local forcing and effects of enhanced resolution are not damped or contaminated by the application of the boundary conditions (Warner et al., 1997). The exact location of the lateral boundaries can influence the sensitivity to internal parameters (Seth and Giorgi, 1998) or may have no significant impact (Bhaskaran et al., 1996). Finally, location of boundaries over areas with significant topography may lead to inconsistencies and noise generation (e.g., Hong and Juang, 1998).

Surface forcing due to land, ocean and sea ice greatly affects regional climate simulation (e.g., Giorgi et al., 1996; Seth and Giorgi, 1998; Wei and Fu, 1998; Christensen, 1999; Pan et al., 1999; Pielke et al., 1999; Rinke and Dethloff, 1999; Chase et al., 2000; Maslanik et al., 2000, Rummukainen et al., 2000). In particular, RegCM experiments do not start with equilibrium conditions and therefore the initialisation of surface variables, such as soil moisture and temperature, is important. For example, to reach equilibrium it can require a few seasons for the rooting zone (about 1 m depth) and years for the deep soils (Christensen, 1999).

The choice of RegCM resolution can modulate the effects of physical forcings and parametrizations (Giorgi and Marinucci, 1996a; Laprise et al., 1998). The description of the hydrologic cycle generally improves with increasing resolution due to the better topographical representation (Christensen et al., 1998; Leung and Ghan, 1998). Resolving more of the spectrum of atmospheric motions at high resolution improves the representation of cyclonic systems and vertical velocities, but can sometimes worsen aspects of the model climatology (Machenhauer et al., 1998; Kato et al., 1999). Different resolutions may be required to capture relevant forcings in different sub-regions, which can be achieved via multiple one-way nesting (Christensen et al., 1998; McGregor et al., 1999), two-way nesting (Liston et al., 1999) or smoothly varying horizontal grids (Qian and Giorgi, 1999).

RegCM model physics configurations are derived either from a pre-existing (and well tested) limited area model system with modifications suitable for climate application (Pielke et al., 1992; Giorgi et al., 1993b,c; Leung and Ghan, 1995, 1998; Copeland et al., 1996; Miller and Kim, 1997; Liston and Pielke 2000; Rummukainen et al., 2000) or are implemented directly from a GCM (McGregor and Walsh, 1993; Jones et al., 1995; Christensen et al., 1996; Laprise et al., 1998). In the first approach, each set of parameterizations is developed and optimized for the respective model resolutions. However, this makes interpreting differences

between nested model and driving GCM more difficult, as these will not result only from changes in resolution. Also, the different model physics schemes may result in inconsistencies near the boundaries (Machenhauer et al., 1998; Rummukainen et al., 2000). The second approach maximizes compatibility between the models. However, physics schemes developed for coarse resolution GCMs may not be adequate for the high resolutions used in nested regional models and may be, at least, require recalibration (Giorgi and Marinucci, 1996a; Laprise et al., 1998). Overall, both strategies have shown performance of similar quality (e.g., IPCC, 1996), and either one may be preferable (Giorgi and Mearns, 1999). In the context of climate change simulations, if there is no resolution dependence, the second approach may be preferable to maximize consistency between RegCM and GCM responses to the radiative forcing.

3.3 ECMWF reanalysis (ERA-40) grid Data:

The data used for evaluate the model data (model output) are the ECMWF reanalysis (ERA-40) gridded data sets downloaded from their ftp site. The ERA data sets in GRIB coded form are available on a coarse resolution of 2.5^0 x 2.5^0 lat. /long. grid on constant pressure surfaces. The data: surface net solar radiation (SSR), surface net thermal radiation (STR), surface sensible heat flux (SSHF) and surface latent heat flux (SLHF) at 6 hourly map times 00, 06, 12 and 18 UTC in a day are downloaded for the analysis. These are first deGRIBed using an ECMWF GRIB decoding software package, also downloaded from their ftp site, and customized to satisfy our requirements. The gridded fields are then interpolated to the limited area model grid and transformed from pressure to the 16 model sigma levels at 0.5^0 x 0.5^0 lat. /long. horizontal grid resolution via a pressure to sigma converter.

3.4 Methodology

Regional Climate Model developed by ICTP Trieste, Italy (Giorgi and Marinucci, 1996a; Laprise et al., 1998) installed at the Department of Physics, BUET and ECMWF reanalysis (ERA-40) data sets downloaded from their ftp site have been used to simulate different meteorological parameters including Net absorbed solar energy flux, Net infrared energy flux, Sensible heat and Evapotranspiration. These parameters are used in calculation of surface heat budget over South Asian region. The following equation has been used for the calculation of surface heat budget:

*Net surface radiation balance (W/m*2) = Net absorbed solar energy flux+Net infrared energy flux+ Sensible heat flux÷ Latent heat flux*

*here, Latent heat flux =Evapotranspiration (2.51040e^6)/(60*60*24) in W/m^2*

In this work, 6-year (1995-2000) simulation model output has been driven using 6-hourly NCEP (Numerical Centre for Environmental Prediction) re-analysis data as model input. The model domain has been selected to cover the South Asia region (65^{0}E-117^{0}E, 5^{0}N-35^{0}N) on a rotated mercator projection (ROTMER) at a 60 km horizontal resolution and 16 sigma levels in the vertical. The centre point of the domain is 20^{0}N, 90^{0}E. The ROTMER projection is used in Grell convective precipitation schemes with Arakawa-Schubert, Fritsch and Chappell, Kuo, Betts-Miller and MIT-Emanuel assumptions. Daily 3-hour interval SRF (surface) data of RegCM3 model output and Daily 6-hour interval SRF (surface) data of ECMWF reanalysis (ERA-40) data are obtained and analyzed using Linux OS.

The RegCM model outputs are binary files which are analyzed and display on GrADs to create for data file and data file converted into ASCII file with the help of FORTARN programme.

CHAPTER 4: SURFACE HEAT BUDGET FOR SELECTED AREA VARIATION

The variation of Surface heat budget mostly depends on the reflectivity, absorbance ability and heat capacity of the Earth's surface. So, the condition of terrain has crucial role for surface heat budget. There are seven different selected zones over South Asia are chosen for analysis which are shown in fig. 3. Those areas are

i) Over Bangladesh (22^0N-27^0N latitude and 88^0E -93^0E longitude)

ii) Over Bay of Bengal adjacent of Bangladesh coastal region (17^0N-22^0N latitude and 88^0E -93^0E longitude)

iii) Over Bay of Bengal (deep Ocean) far from Bangladesh coastal region (9^0N-14^0N latitude and 87^0E -92^0E longitude)

iv) Over West coast of India (9^0N-14^0N latitude and 74^0E -79^0E longitude)

v) Over Thar Desert (23^0N-28^0N latitude and 70^0E -75^0E longitude)

vi) Near east coast of India (13^0N-18^0N latitude and 81^0E -86^0E longitude)

vii) Over Middle Zone of India (19^0N-24^0N latitude and 77^0E -82^0E longitude)

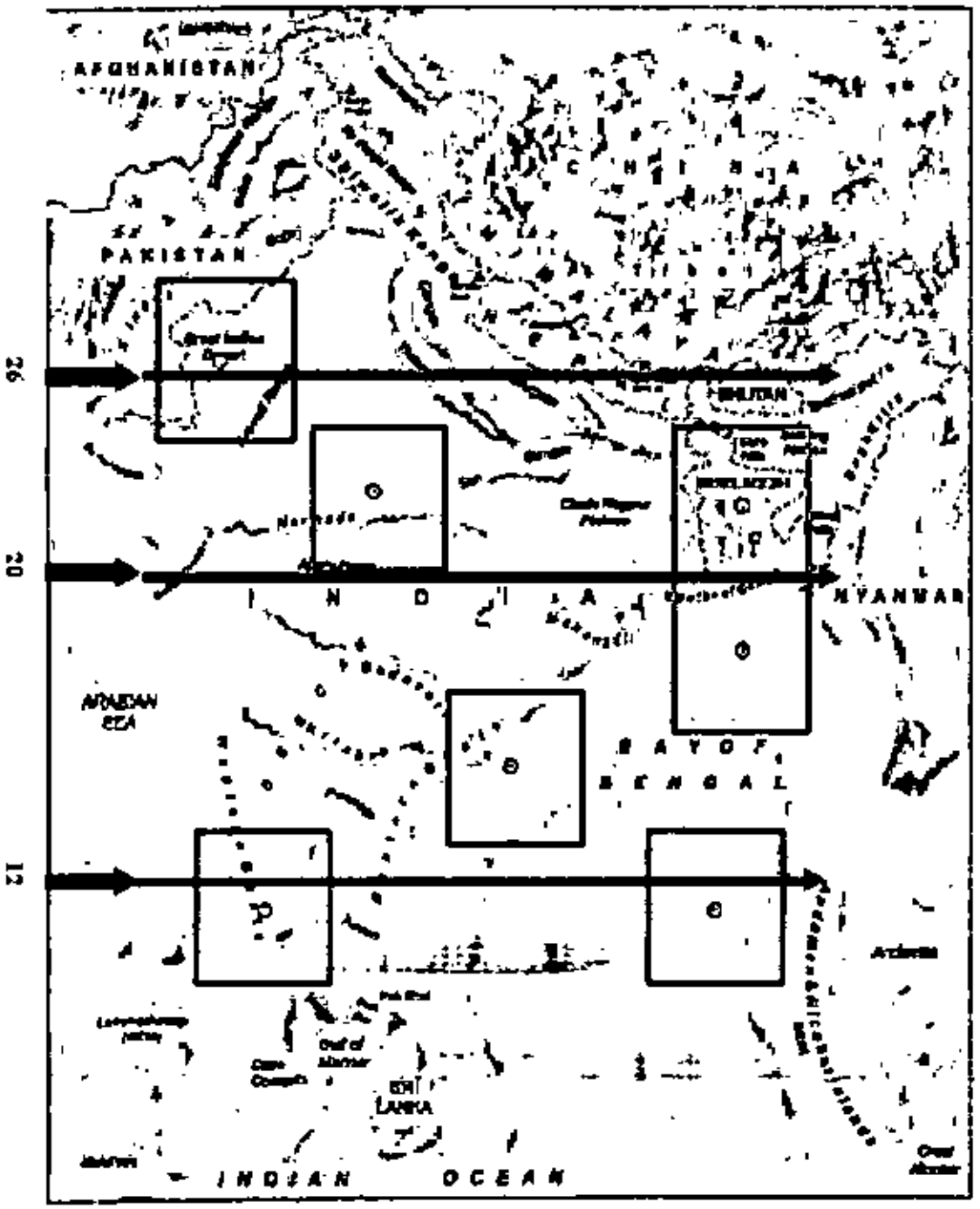

Fig.3: Map of South Asia with indicating 7 selected windows (areas) with center points and 12^0N, 20^0N, 26^0N Latitude along 70-94^0E Longitude

4.1 Surface heat budget at selected areas for GAS, GFC and ECMWF for 1996

The values of surface heat budget (SHB) for RegCM GAS and GFC Scheme for different selected areas have been analyzed and compared to the ECMWF data for 1996.

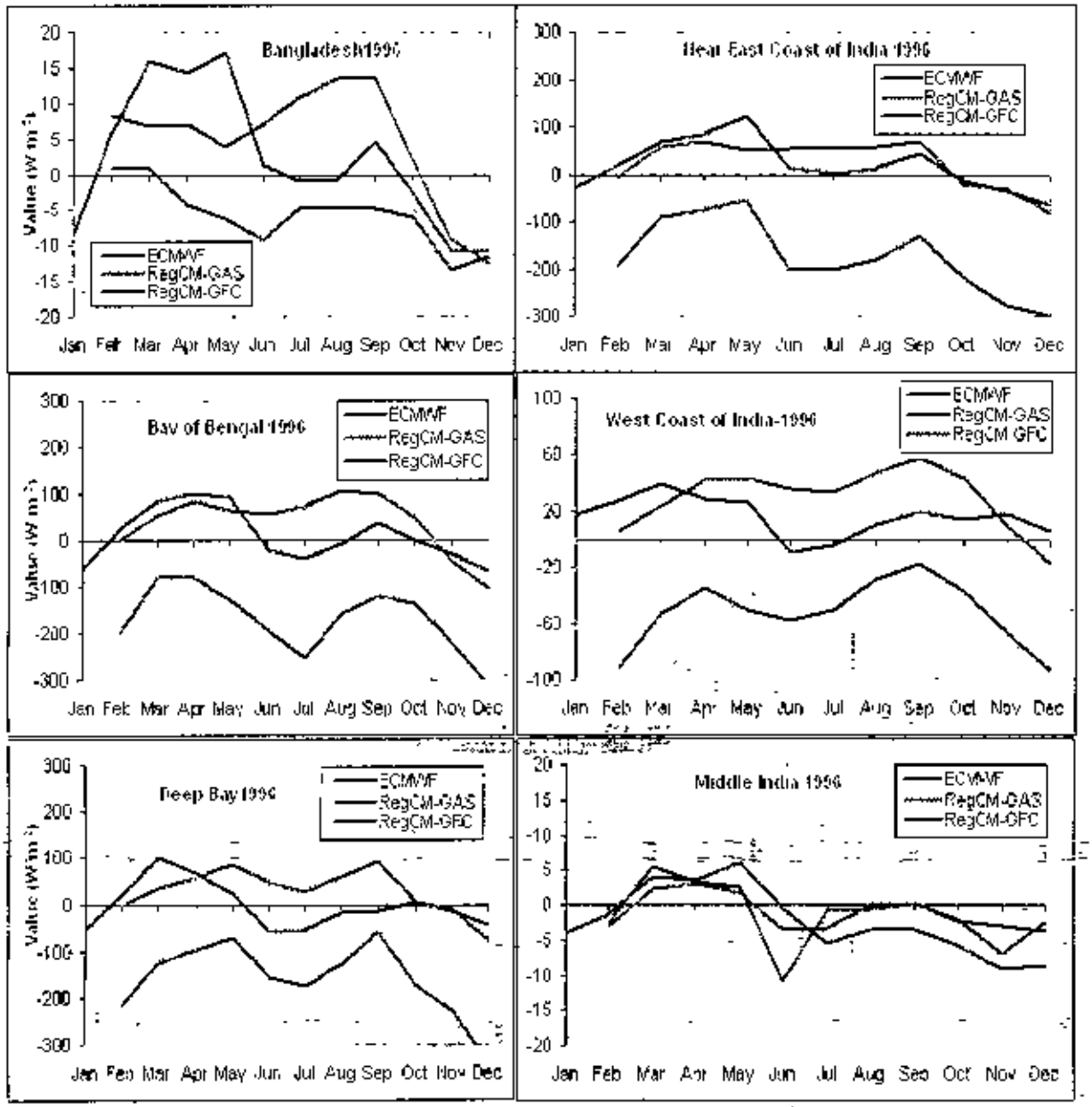

Fig.4: Monthly variation (for 1996) of surface heat budget at selected areas for GAS, GFC and ECMWF

It has been seen in fig. 4 for RegCM GAS, GFC and ECMWF data that over land the value of SHB is about within $20w/m^2$ to $-15w/m^2$; over ocean the value of SHB is about within

125w/m^2 to -350w/m^2; over west coast of India the value of SHB is within 59w/m^2 to -100w/m^2 for whole year. Hence it is seen that the variation of the value of SHB is high over ocean and low over land. According to ECMWF data value of SHB over Bangladesh, Bay of Bengal near coast, Near East coast of India, Thar Desert and Mid-India zone is highest in May; over Deep Bay of Bengal and West Coast of India is highest in May. The value of SHB is lowest in December for all selected areas.

It has been observed for comparing RegCM-GAS data to ECMWF data that the value of SHB is underestimated from March to May (Pre-monsoon) and in December; overestimated from June to September/October. For RegCM-GFC data compared to ECMWF data the value of SHB is underestimated for all selected areas except dry-zone (Mid India and Thar desert) for all months of 1996. So, for further analysis of SHB RegCM-GAS data and ECMWF re-analysis data have been taken for different years.

4.2 Validation (monthly) of SHB for RegCM-GAS data and ECMWF data (1995-2000)

It has been observed in fig. 5(a) for the year 1995-2000 (six years) that **over Bangladesh** the value of SHB is low (range from -9W/m^2 to -17W/m^2) in January, November and December and the value of SHB is high (range from 3W/m^2 to 18W/m^2) in February-May except in February 2000 (value -1.9W/m^2). The highest value observed in the month of April except in May 1997 (value 17W/m^2). In the months of June to September the value of SHB is about from -3W/m^2 to 3W/m^2. Comparing the value of RegCM GAS data to ECMWF reanalysis data it has been seen usually that the value of SHB during March-May are underestimate about 5 W/m^2 and during June-September are overestimate about 10 W/m^2.

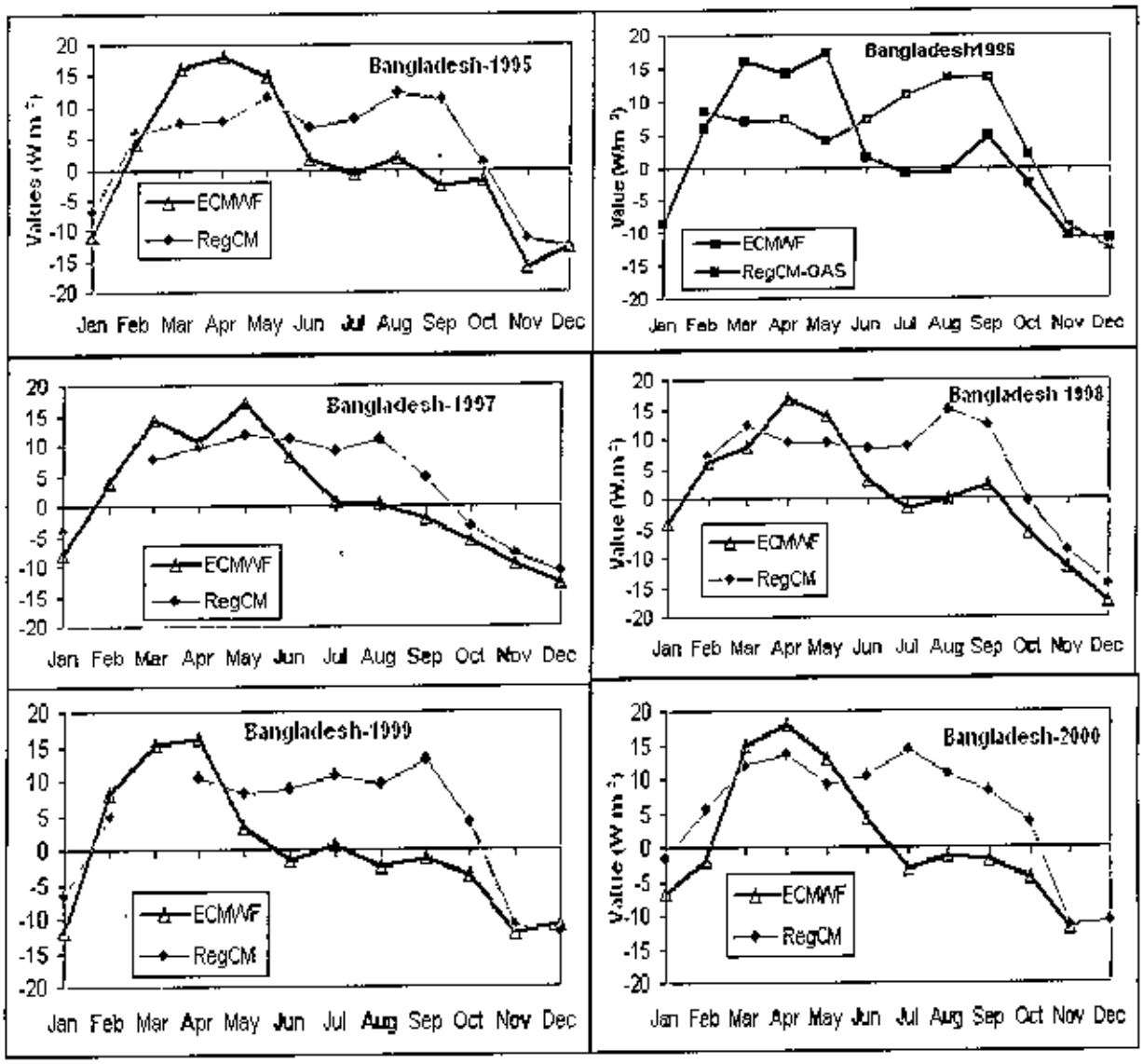

Fig.5(a): RegCM3 Model and ECMWF determined SHB (monthly) over Bangladesh for 1995-2000

According to the fig. 5(b), it has been observed that for both option (GAS and GFC) of RegCM over Bangladesh rainfall is overestimate in pre-monsoon season and underestimate in monsoon season compared to the observed data. But RegCM3 Model data in GAS option for SHB show underestimate and overestimate in pre-monsoon and monsoon season respectively compare to the ECMWF data. Hence opposite condition occurs for SHB compare to Rainfall over Bangladesh.

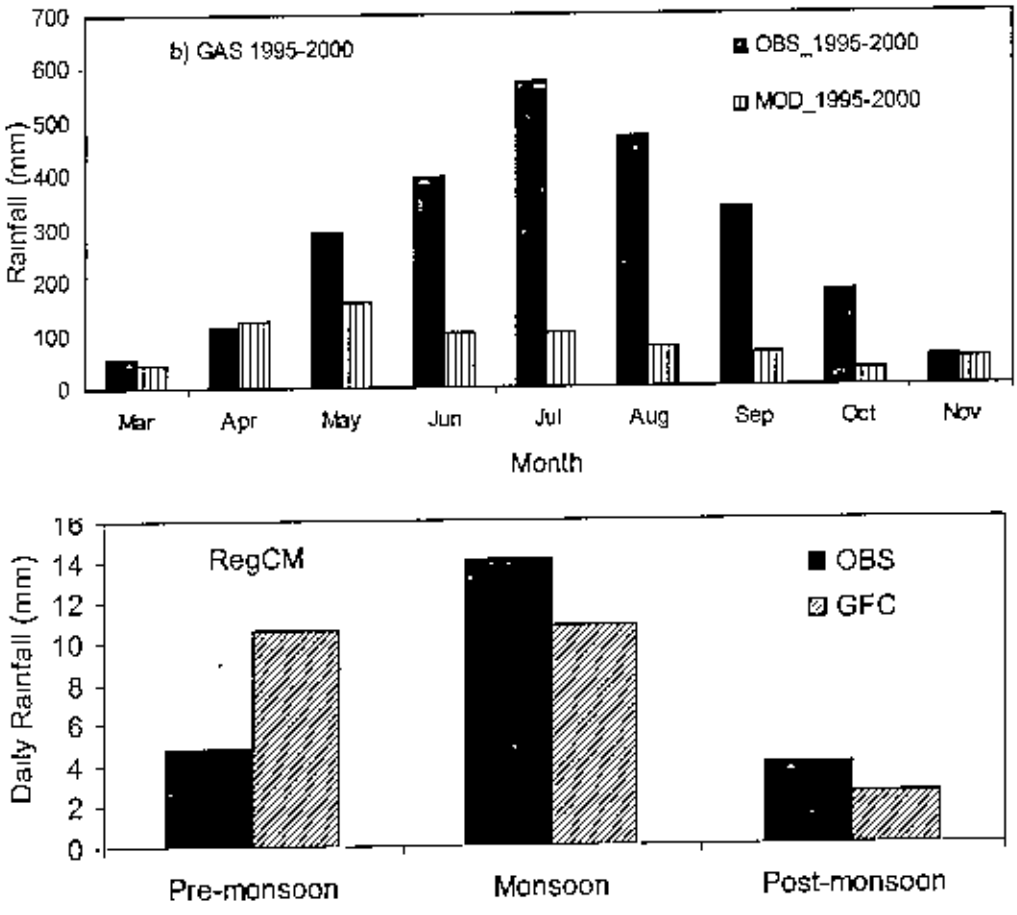

Fig. 5(b): Average Rainfall over Bangladesh for RegCM GAS and GFC option for 6-year (1995-2000)

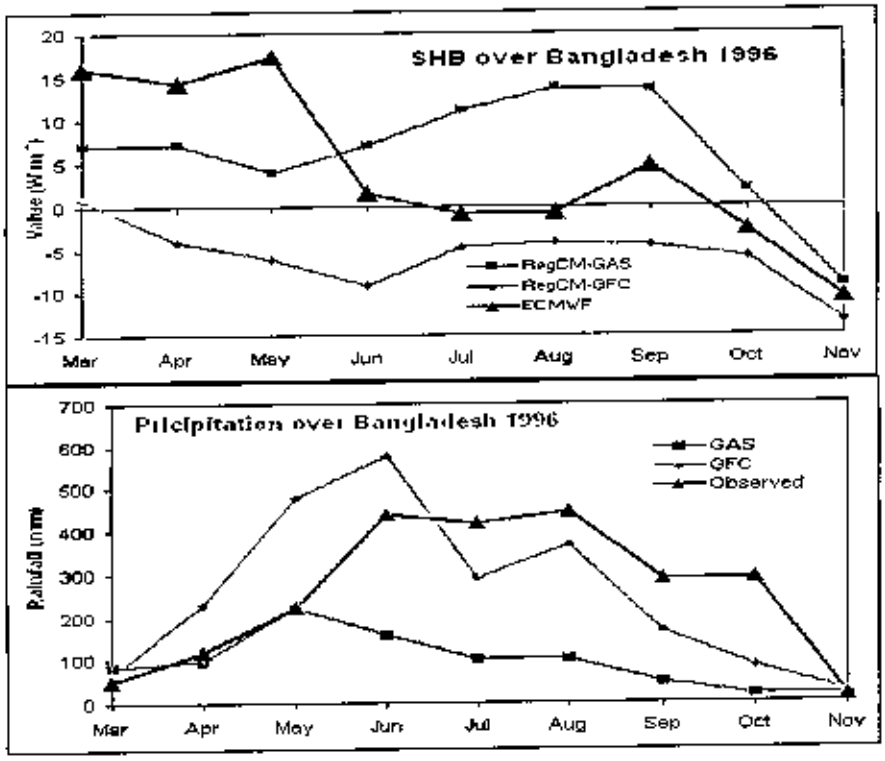

Fig. 5(c): SHB and precipitation over Bangladesh for 1996

The SHB is high when cloud cover is minimal and insulation of solar energy is high. In fig. 5(c) it has been seen that whether observed precipitation over Bangladesh is low, SHB for ECMWF data is high and when observed precipitation is high SHB is low in 1996. Accordingly, it can be said that SHB and precipitation is inversely related and there is radiative impact for development of convective system.

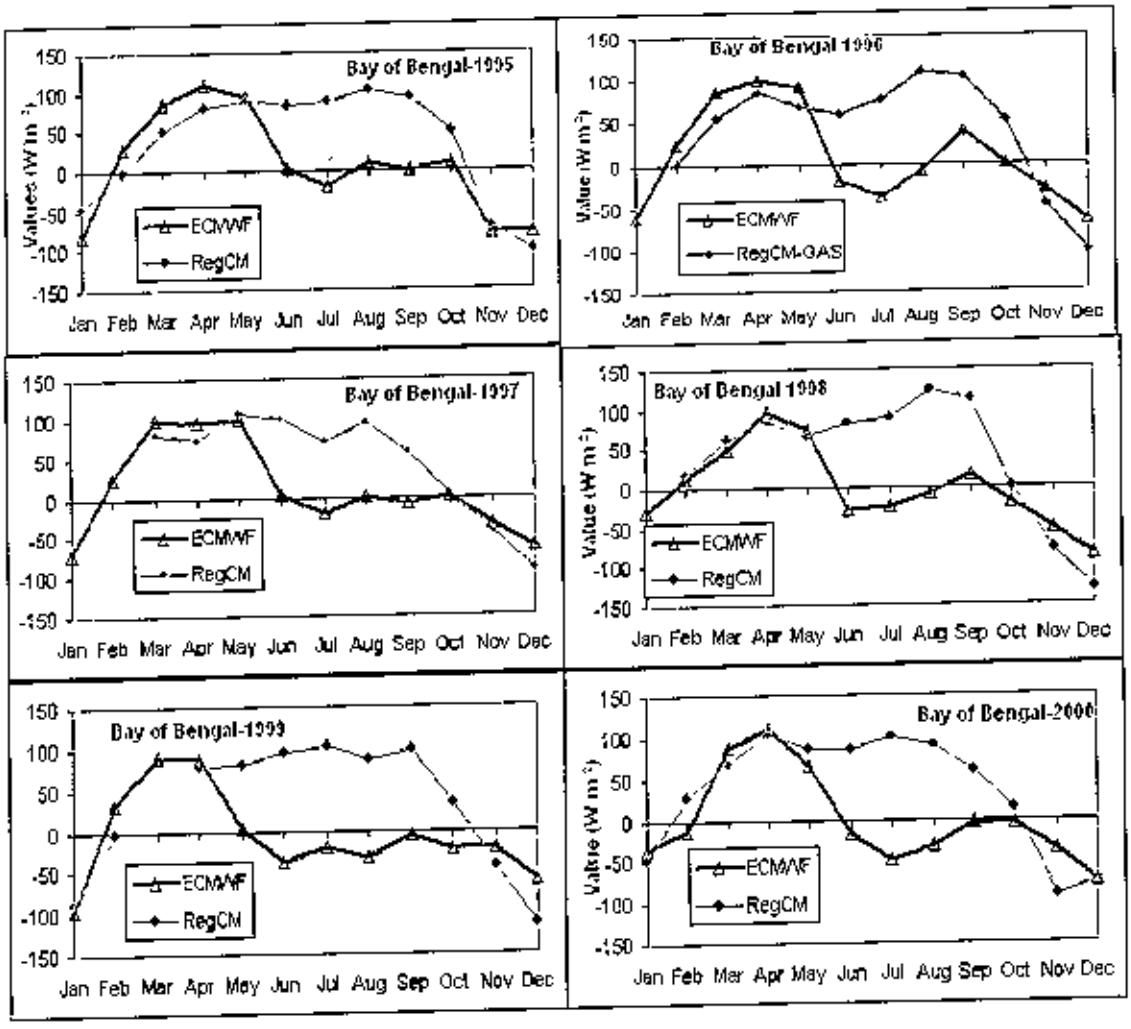

Fig. 6: RegCM3 Model and ECMWF determined SHB (monthly) over Bay of Bengal for 1995-2000

In fig. 6 **Over Bay of Bengal,** the value of SHB is low (range from -35W/m^2 to -90W/m^2) in January, November and December and the value of SHB is very high (range from 90W/m^2 to 110W/m^2) in March to May for the year 1995, 1997-2000 which is observed in figs. (5-7). In

February the value of SHB is also high (about value 30W/m^2) except in February 2000 (value -12W/m^2) as shown in fig. 7. In the months of June to September the value of SHB is about from -48W/m^2 to 15W/m^2. Comparing the value of RegCM GAS data to ECMWF reanalysis data it has been noticed generally that the values of SHB during February-May are underestimate about 30 W/m^2 and during June-September are overestimate about 100 W/m^2. The value of SHB is high over Bay of Bengal compare to Bangladesh because water surface has high heat capacity and the land has low heat capacity.

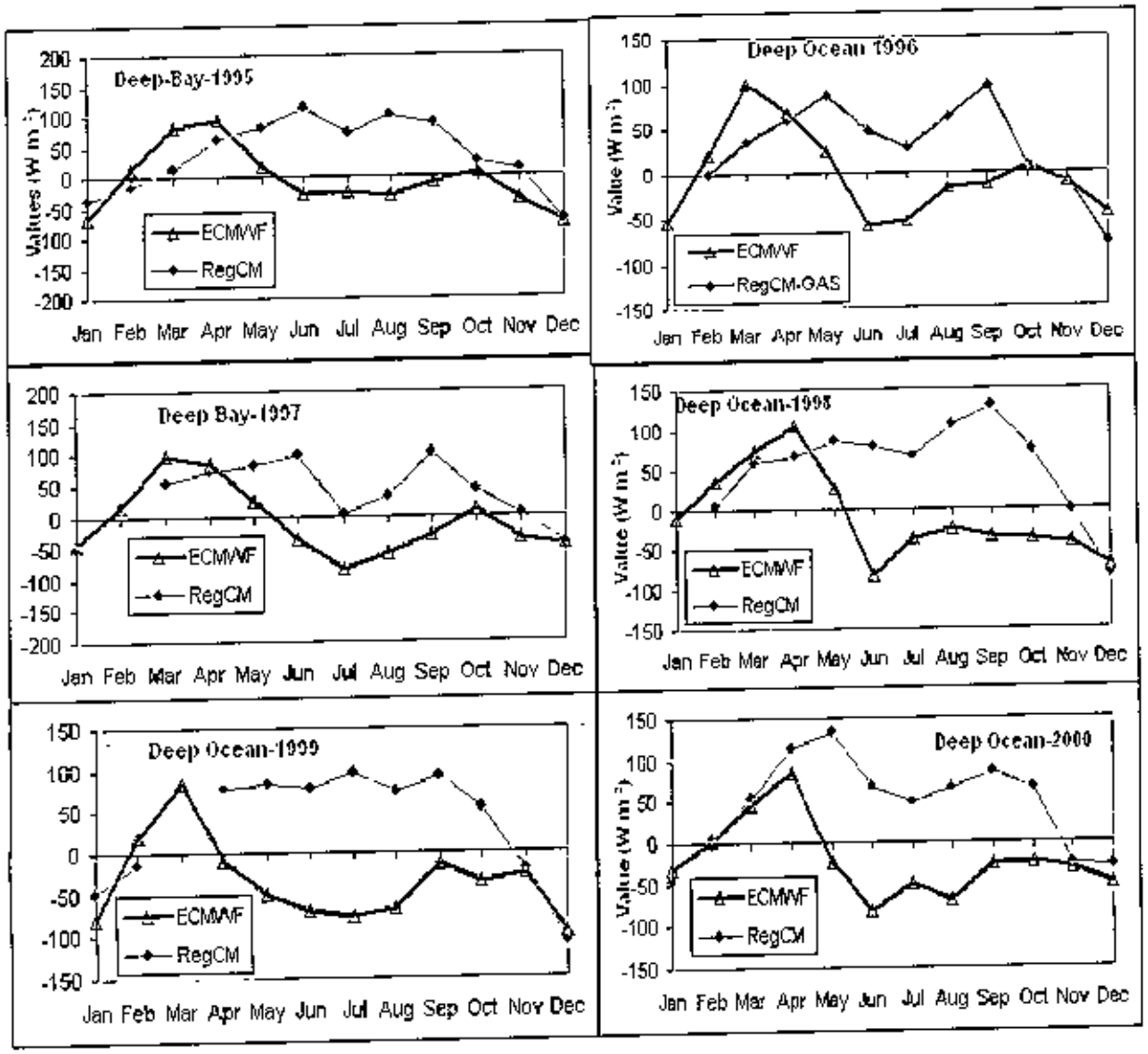

Fig. 7:RegCM3 Model and ECMWF determined SHB (monthly) over Deep Ocean for 1995-2000

In fig. 7 Over Deep Ocean (far from Bay of Bengal) the value of SHB is low in January, December, June-September sometimes May-November. The value of SHB is very high (range from 45 to 110W/m^2) in March and April. The value of SHB is fluctuating in different year. Comparing the value of RegCM GAS data to ECMWF reanalysis data it has been perceived generally that the values of SHB during January and May to December are overvalue and during February-April are undervalue.

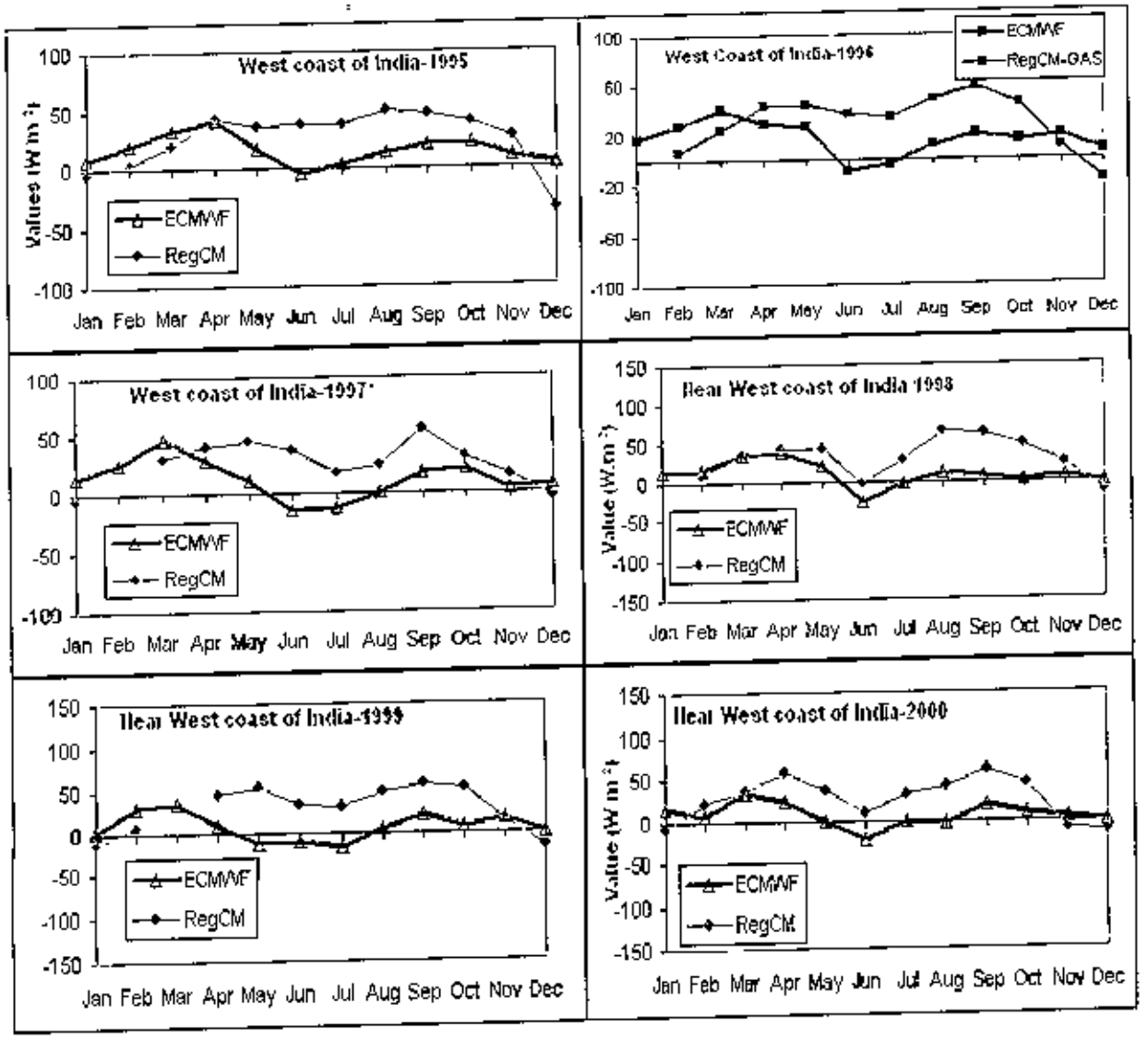

Fig. 8: RegCM3 and ECMWF determined SHB (monthly) over West Coast of India for 1995-2000

According to the fig.8, **Over West Coast of India** the value of SHB is low in June and July sometimes in May. The value of SHB is very high in March, April, September and October about 40W/m^2. Comparing the value of RegCM GAS data to ECMWF reanalysis data it has been apparent usually that the values of SHB is underestimate in January, February and December except 2000 and overestimate in April-November.

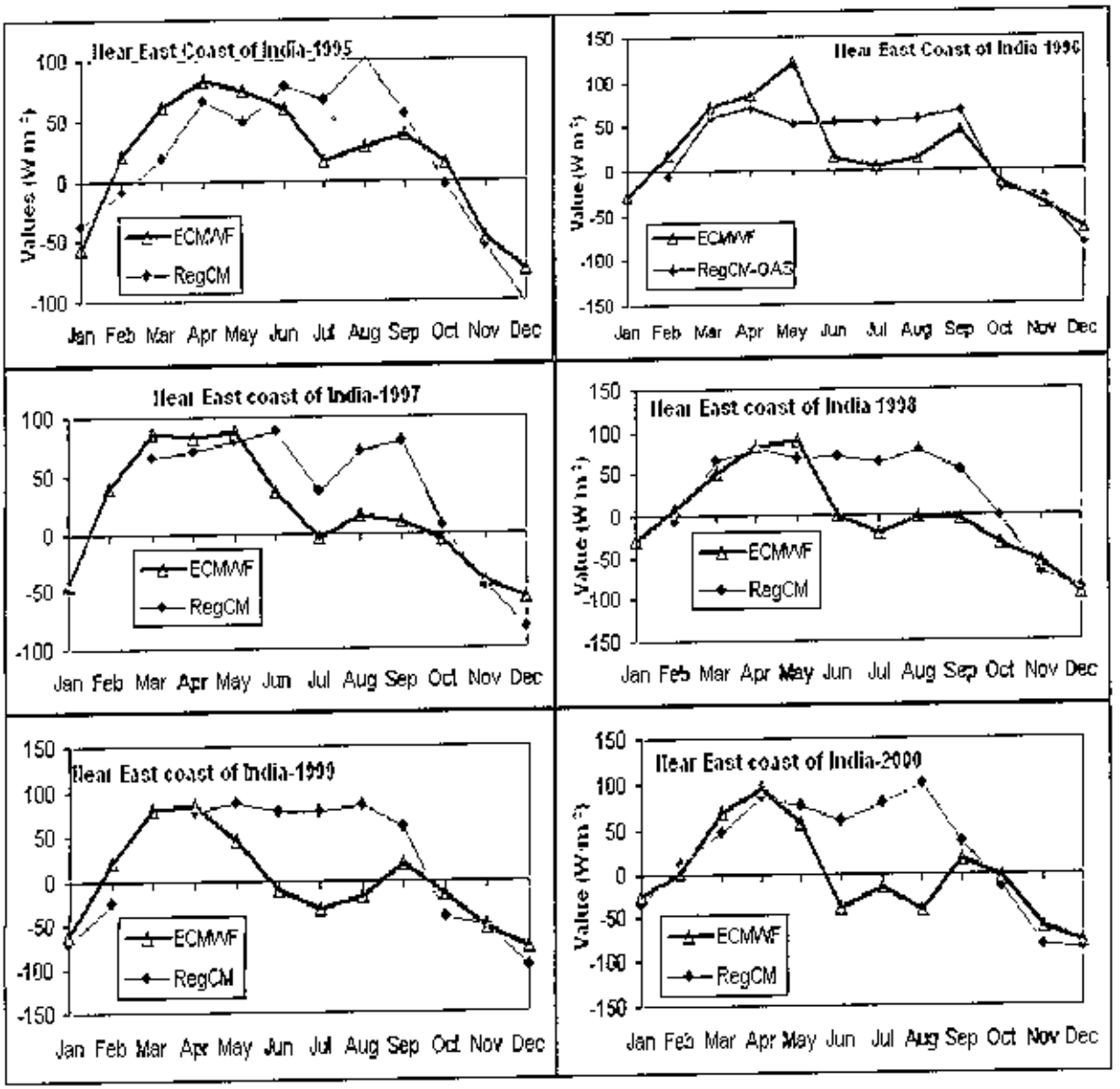

Fig. 9: RegCM3 and ECMWF determined SHB (monthly) over Near East Coast of India for 1995-2000

In fig. 9 **over near East Coast of India** the value of SHB for RegCM GAS data are similar to ECMWF data in June-April and October-December but overestimate in May-September for 1999, 2000. The values of SHB for RegCM GAS data are slightly underestimate in January-May and December to ECMWF data in June-September for 1995, 1997. For both data the values of SHB are low in January, June, July, November, December and are high in April, May for 1995-2000.

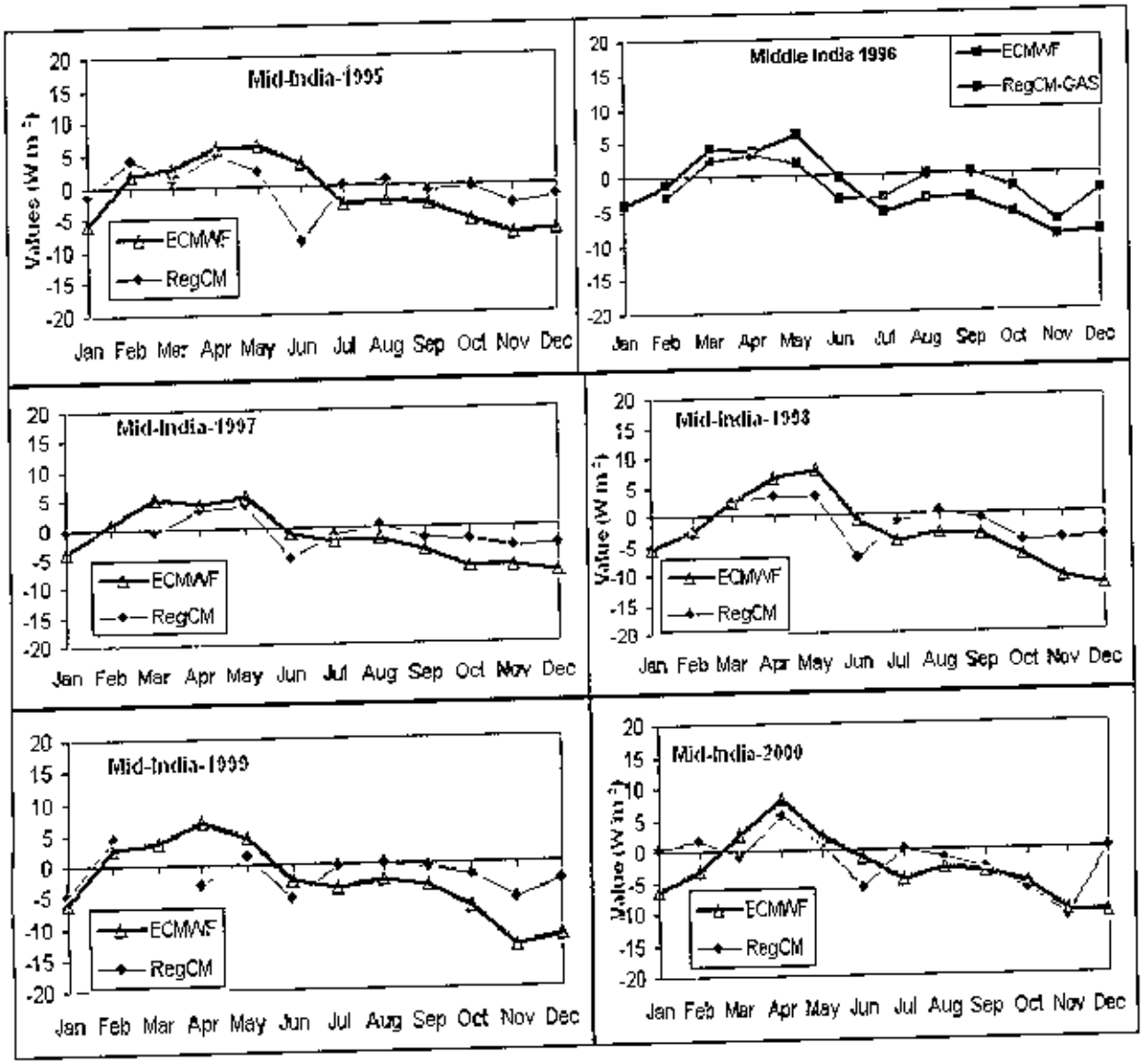

Fig. 10: RegCM3 Model and ECMWF determined SHB (monthly) over Mid-India for 1995-2000

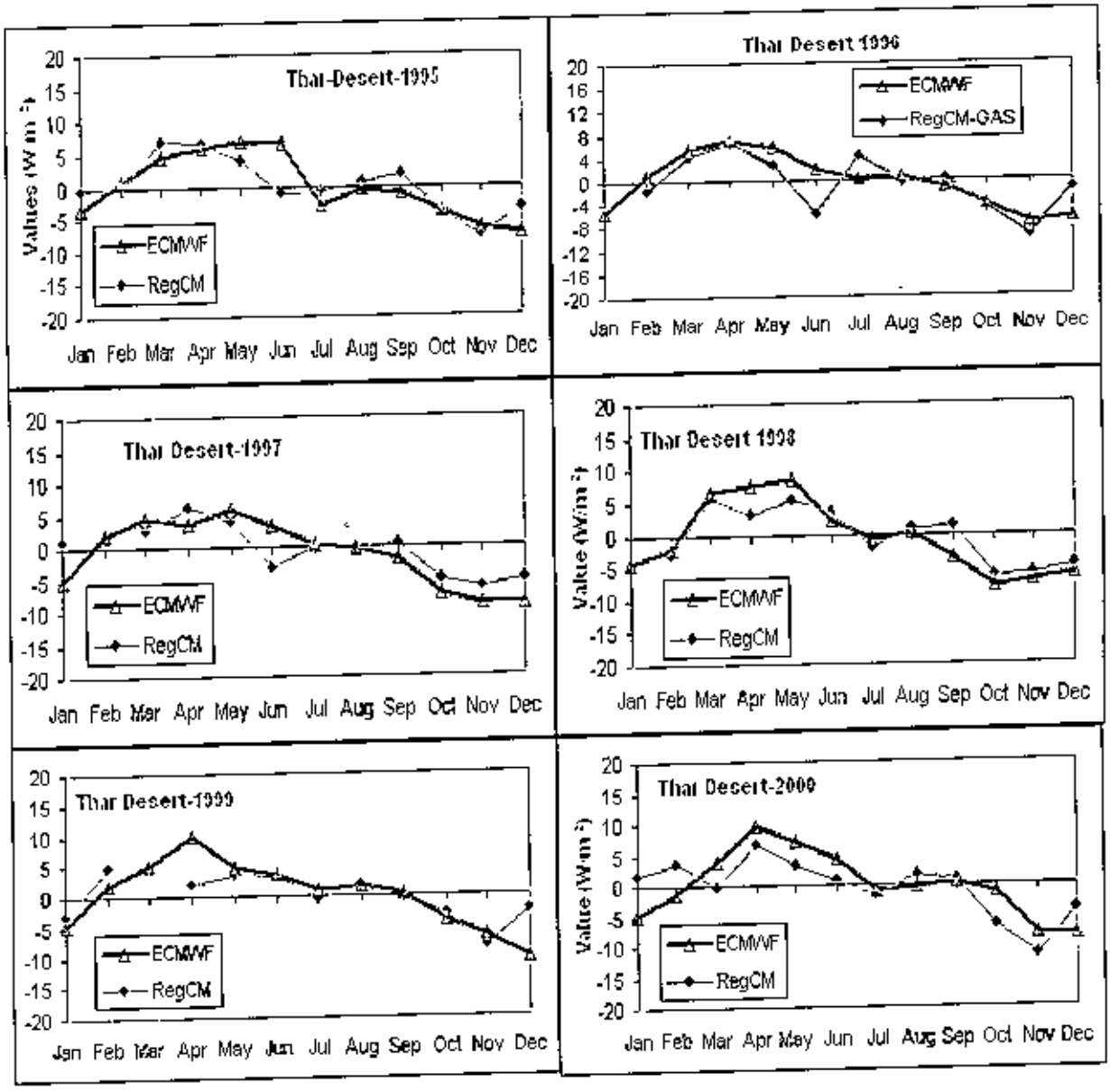

Fig. 11: RegCM3 Model and ECMWF determined SHB (monthly) over Thar Desert for 1995-2000

As fig 10 and 11 shows that **Over Desert Area (Thar Desert and Mid-India)** the value of SHB for RegCM GAS data are overestimate to ECMWF data in January, February and December but for other months the values of SHB are close for both data 1995-2000. The pattern of values of SHB for Thar Desert and Mid-India areas is same. The range of SHB is within $10W/m^2$ to $-10W/m^2$.

SHB is dominated by the shortwave portion. In July highest values occur along the subtropical oceans of the Northern Hemisphere. Lowest values occur over areas of low solar input such as the South Pole, and areas of high surface reflection such as the North Pole. So, over the selected analysis areas, it is observed that highest value occurs over ocean.

In January highest values occur along the subtropical oceans of the Southern Hemisphere. Lowest values occur over areas of low solar input such as the North Pole, and areas of high surface reflection such as the South Pole. In January solar insulation is low over Northern Hemisphere than over Southern Hemisphere. So, SHB is low over the selected analysis areas.

4.3 Hourly Variation of surface heat budget (SHB) for central point of 7 selected areas for the year of 2000

Hourly variation of SHB is determined by ECMWF reanalysis data and RegCM (GAS) model data at the center point of 7 selected areas for the year of 2000. 6-hourly (00, 06, 12 and 18 local standard time (LST)) observation is taken in a day for analysis. The solid bar in the figures[14-26] represents the ECMWF reanalysis data and the check bar represents RegCM (GAS) model data. The results show that the variability patterns are not uniform from region to region. This is because of heterogeneous characteristics of the orography and different capacity of absorbance and emission of radiation of land and ocean surface. Moreover the pattern of the value of SHB for the said LST for ECMWF reanalysis and RegCM (GAS) model data are not similar for all months except in July. Peak value occurs at 12LST for both data. As shown in fig. 12 and 13, both data maintain the diurnal variation.

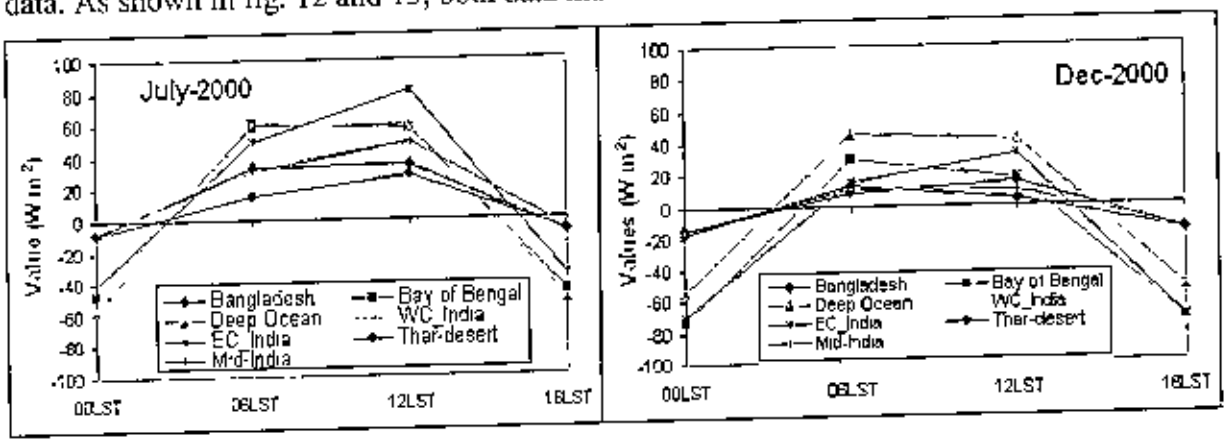

Fig.12 : Diurnal variations of SHB for ECMWF in July & December at the 7 selected central points of the 7 windows over South Asia

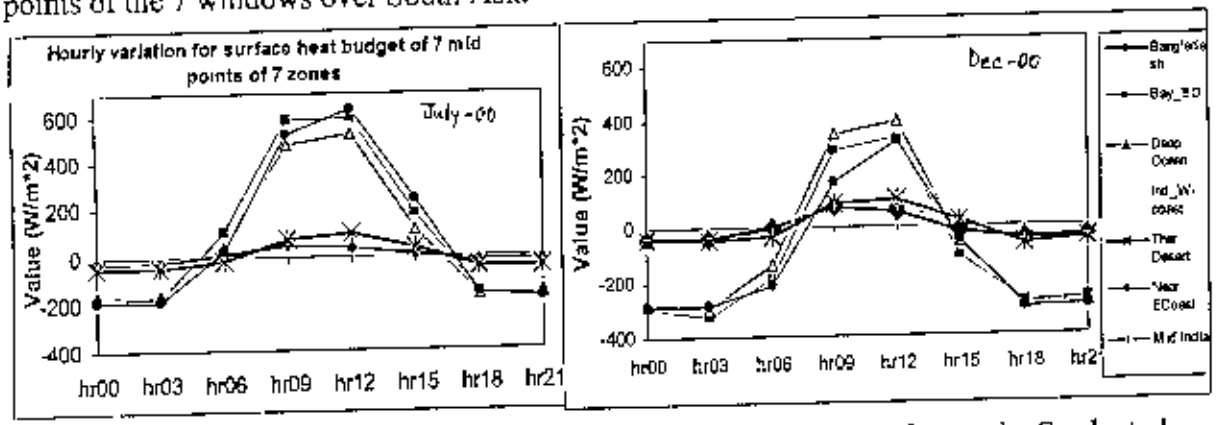

Fig.13 : Diurnal variations of SHB For GAS option in July & December at the 7 selected central points of the 7 windows over South Asia

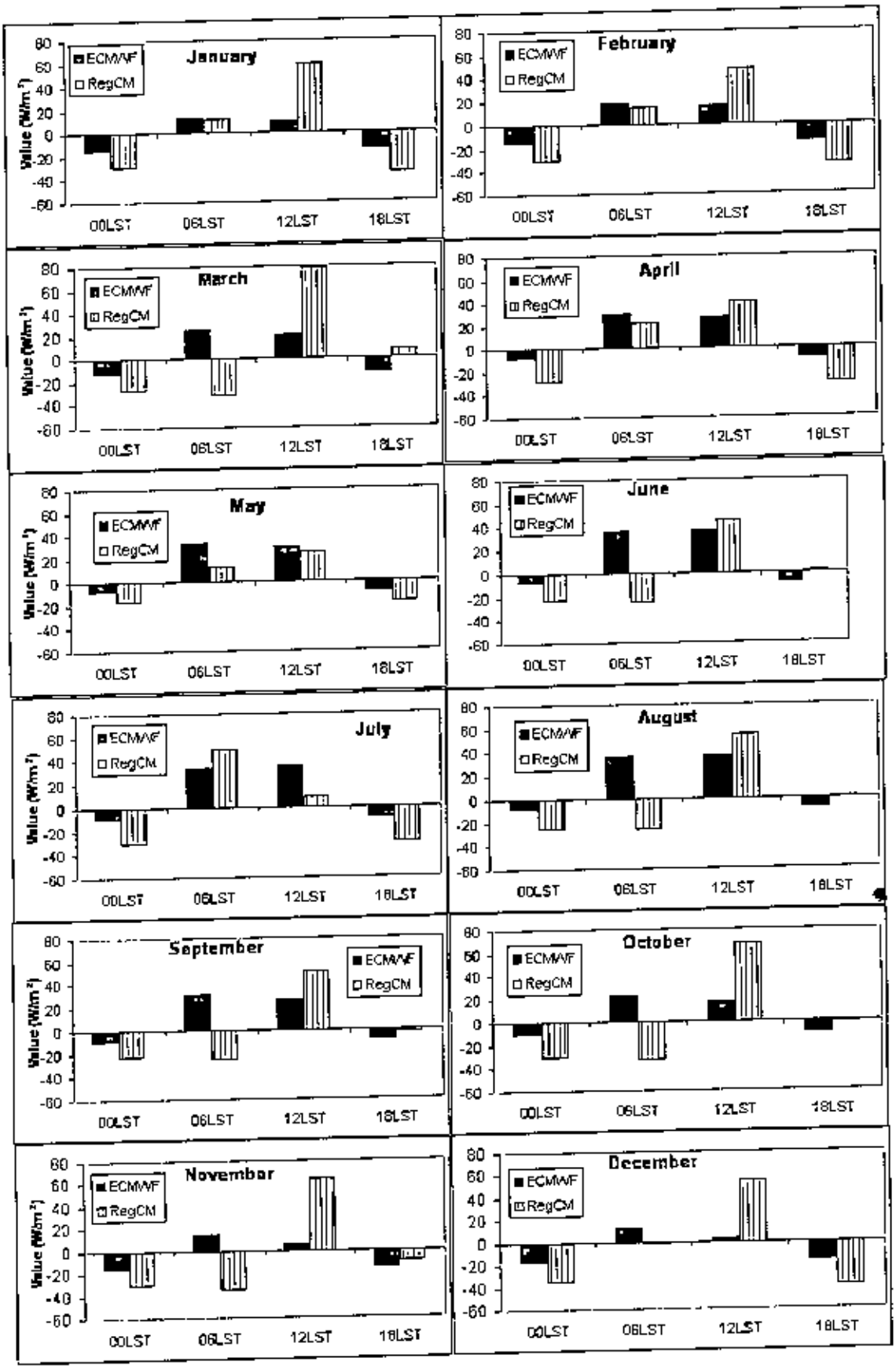

Fig.14: Hourly Variation of surface heat budget (SHB) for centre point (24.5°N, 90.5°E) of the selected area of Bangladesh for the year 2000

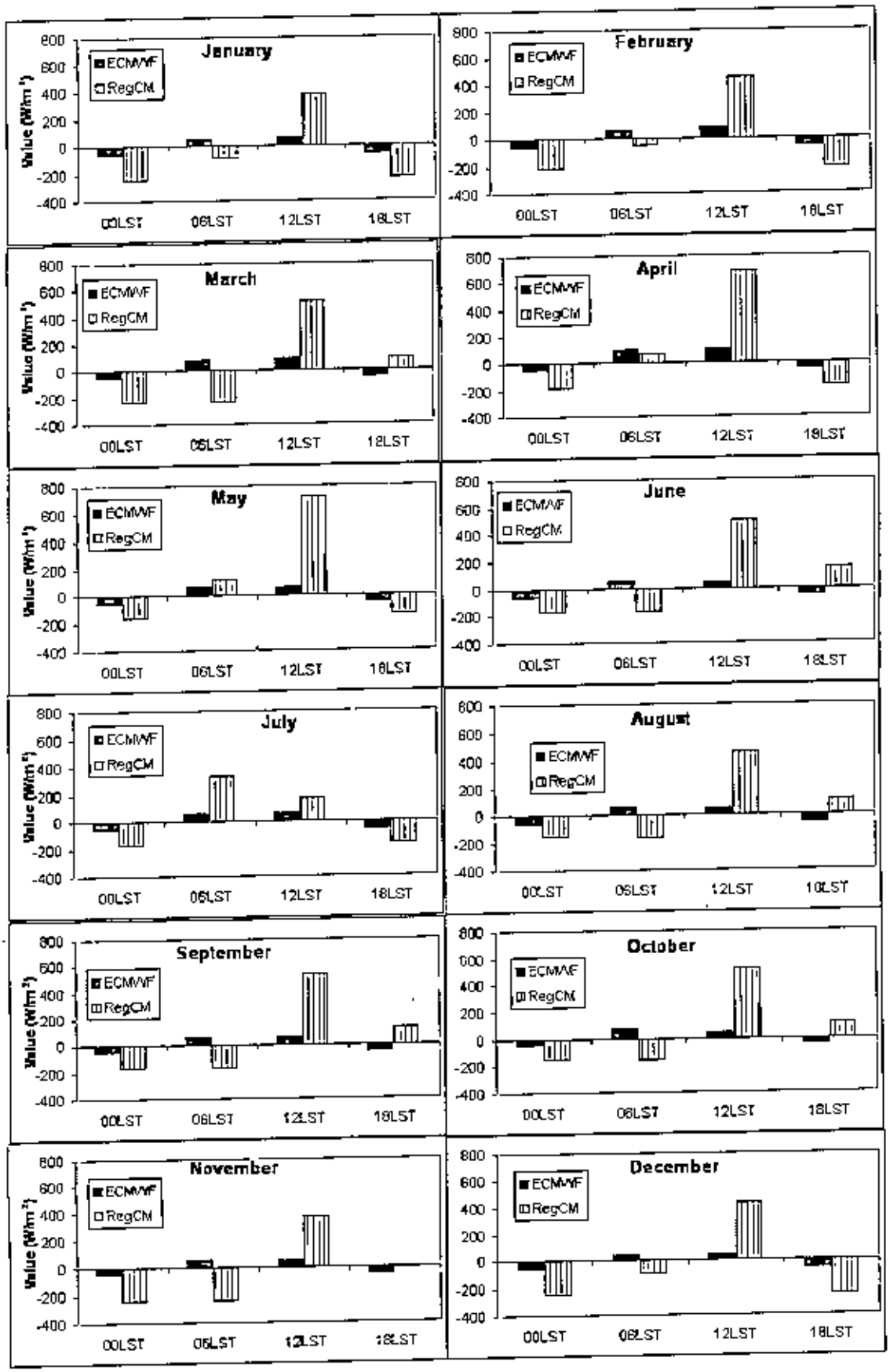

Fig.15: Hourly Variation of surface heat budget (SHB) for centre point (19.5^{0}N, 90.5^{0}E) of the selected area of Bay of Bengal for the year 2000

For ECMWF reanalysis data it has been observed in fig. 14, at the centre point (24.5^{0}N, 90.5^{0}E) of the selected area of Bangladesh that the value of SHB is always positive at 06, 12LST and is negative at 00, 18 LST. The value of SHB is increasing from January to August and decreasing from September to December. In June, July and August the value of SHB at 06, 12LST is high about 35W/m^2 and at 00, 18 LST the value of SHB is about -8 W/m^2.

For RegCM model data it is seen that at 12LST the value of SHB is always higher than the values at 00, 06 and 18LST for all months except July. In July the value of SHB at 6LST is higher (50W/m^2) than 00, 12 and 18LST. In January, February, April, May and July the value of SHB is positive at 06, 12LST and is negative at 00, 18 LST but for the remaining months only at 12 LST the value of SHB is positive. In March the value of SHB at 12LST is highest (78.7 W/m^2).

In fig. 15, for ECMWF reanalysis data it has been also observed at the centre point (19.5^{0}N, 90.5^{0}E) of the selected area of Bay of Bengal that the value of SHB is always positive at 06, 12LST and is negative at 00, 18 LST. The value of SHB is increasing from January to May and again decreasing from June to December. In March, April and May the value of SHB at 06, 12LST is high about 100W/m^2 and the value of SHB is about -35 W/m^2 at 00, 18 LST. In January, February, November and December the value of SHB is low about 35W/m^2 at 06, 12LST and is about -65 W/m^2 at 00, 18 LST than other months of the year 2000.

In April, May and July for RegCM model data the value of SHB is positive at 06, 12LST and is negative at 00, 18 LST but for the remaining months only at 12 LST the value of SHB is positive. The highest value (718.7 W/m^2) is observed at 12LST in April and the lowest value (-313.3 W/m^2) is in November.

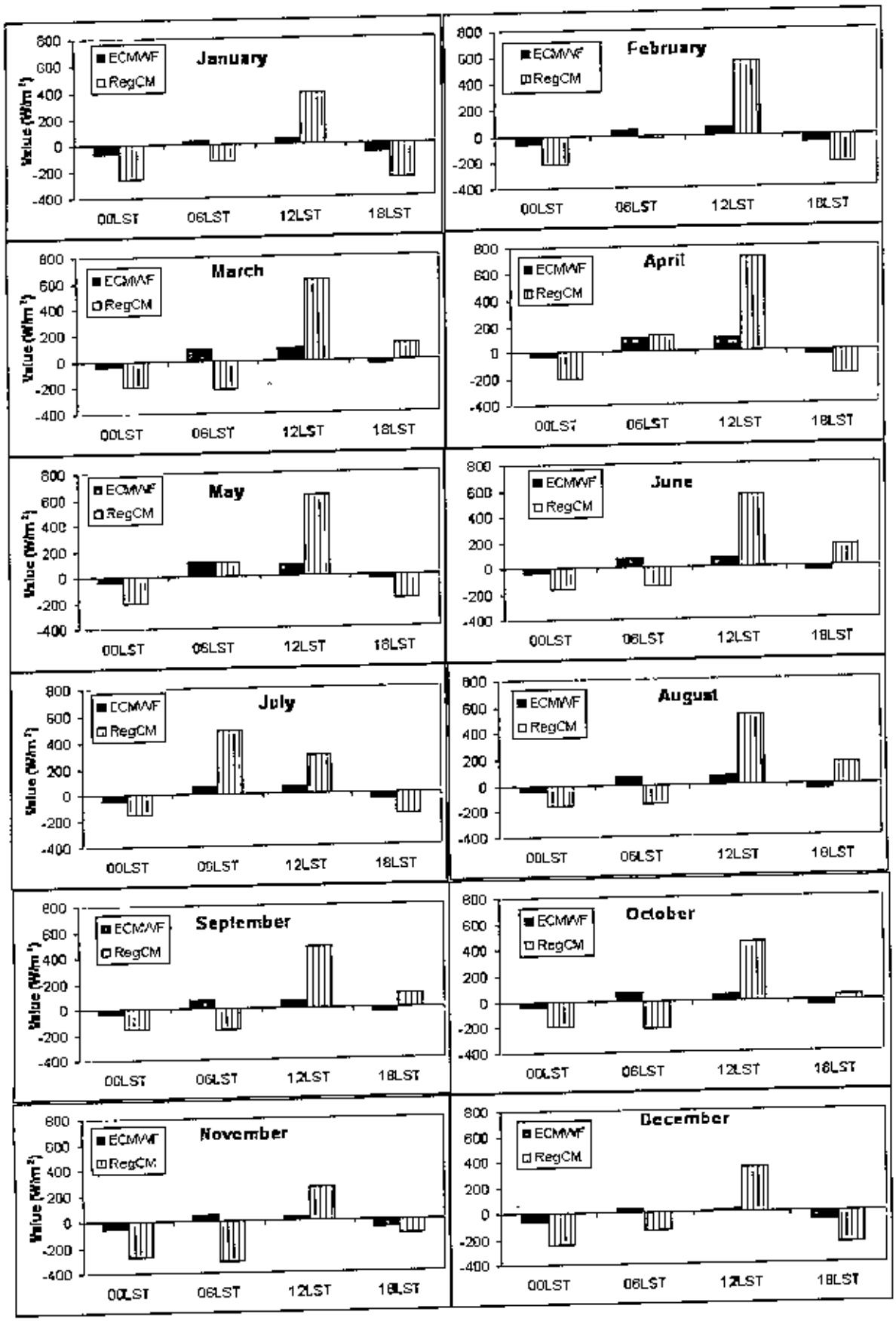

Fig.16: Hourly Variation of surface heat budget (SHB) for centre point (11.5^{0}N, 89.5^{0}E) of the selected area of Deep Ocean for the year 2000

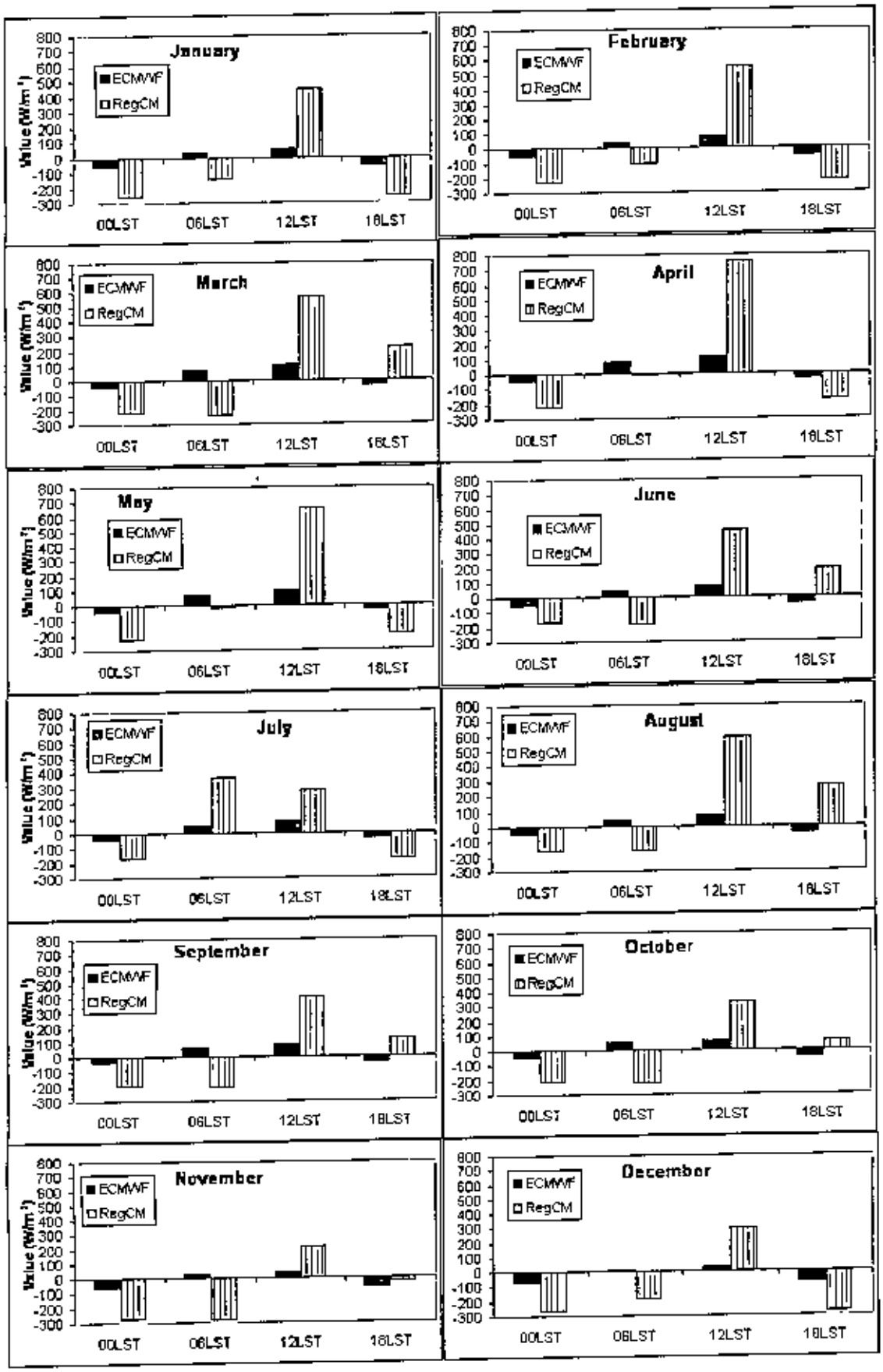

Fig.17: Hourly Variation of surface heat budget (SHB) for centre point (15.5°N, 83.5°E) of the selected area of Near East Coast of India for the year 2000

At the centre point (11.5^{0}N, 89.5^{0}E) of the selected area of deep ocean (far from the coast of Bay of Bengal) the highest value of SHB (97.7 W/m^2) is seen in fig 16 in April at 12 LST for ECMWF reanalysis data. The value of SHB is also positive at 06, 12LST and is negative at 00, 18 LST. The value of SHB is increasing from January to April and again decreasing from May to December. At 06, 12LST range of the value of SHB is from 41W/m^2 to 97.7W/m^2 and the range of the value of SHB is from -41W/m^2 to -56W/m^2 35 W/m^2 at 00, 18 LST. In December the value of SHB is low about 43W/m^2 and is about -53 W/m^2 at 00, 18 LST than other months of the year 2000.

In April, May and July for RegCM model data the value of SHB is positive at 06, 12LST and is negative at 00, 18 LST but for the remaining months only at 12 LST the value of SHB is positive. The highest value (723.46 W/m^2) is observed at 12LST in May which is very overestimate compare to ECMWF data and the lowest value (-247 W/m^2) is in December which is very underestimate compare to ECMWF data.

The result in fig. 17 shows at the point (15.5^{0}N, 83.5^{0}E) over ocean of the selected area of Near East Coast of India that the value of SHB is also positive at 06, 12LST and is negative at 00, 18 LST in all months for ECMWF data and in July for RegCM model data. For ECMWF data, the highest value (113.4 W/m^2) is observed in April at 12LST and the lowest value (-73 W/m^2) is observed in December at 18LST. The value of SHB is increasing from January to April and again decreasing from May to December. According to RegCM model data data, the highest value (756.38 W/m^2) is observed in April at 12LST which is about 7 times overrate compare to ECMWF data and the lowest value (-280.47 W/m^2) is observed in November at 06LST which is very underrate compare to ECMWF data..

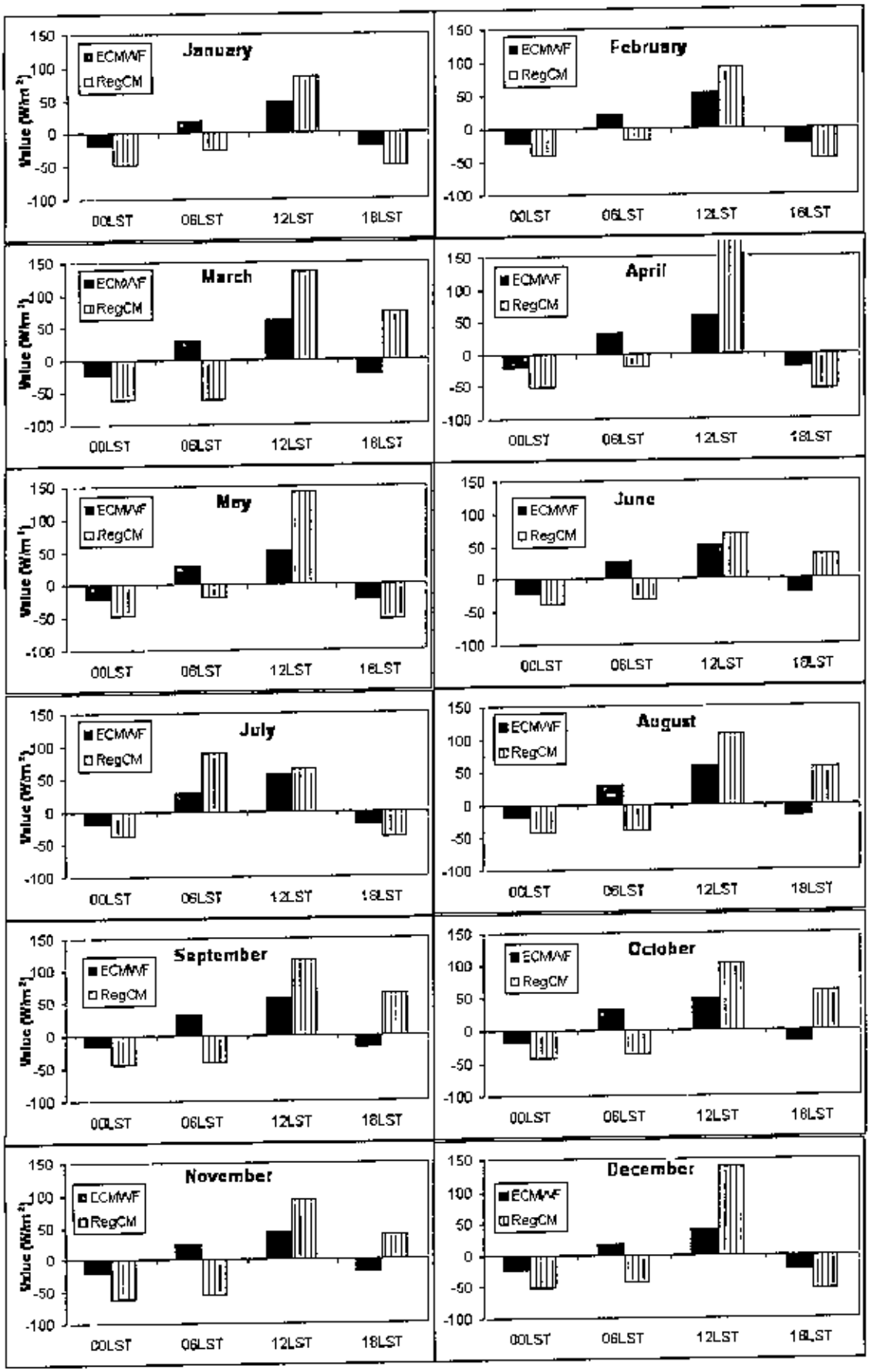

Fig.18: Hourly Variation of surface heat budget (SHB) for centre point (11.5^{0}N, 76.5^{0}E) over land of the selected area of West Coast of India for the year 2000

In fig. 18 at the point (11.5^{0}N, 76.5^{0}E) over land of the selected area of West Coast of India that the value of SHB is also positive at 06, 12LST and is negative at 00, 18 LST in all months for ECMWF data and in July for RegCM model data. For ECMWF data, the highest value (60.2 W/m^2) is seen in March at 12LST and the lowest value (-23.68 W/m^2) is observed in February at 18LST. The value of SHB is high from February to October at 12LST and low in December at 00, 18LST. According to RegCM model data data, the highest value (173 W/m^2) is observed in April at 12LST which is overrate compare to ECMWF data and the lowest value (-60 W/m^2) is observed in March at 00 and 06LST which is underrate compare to ECMWF data (-23 W/m^2).

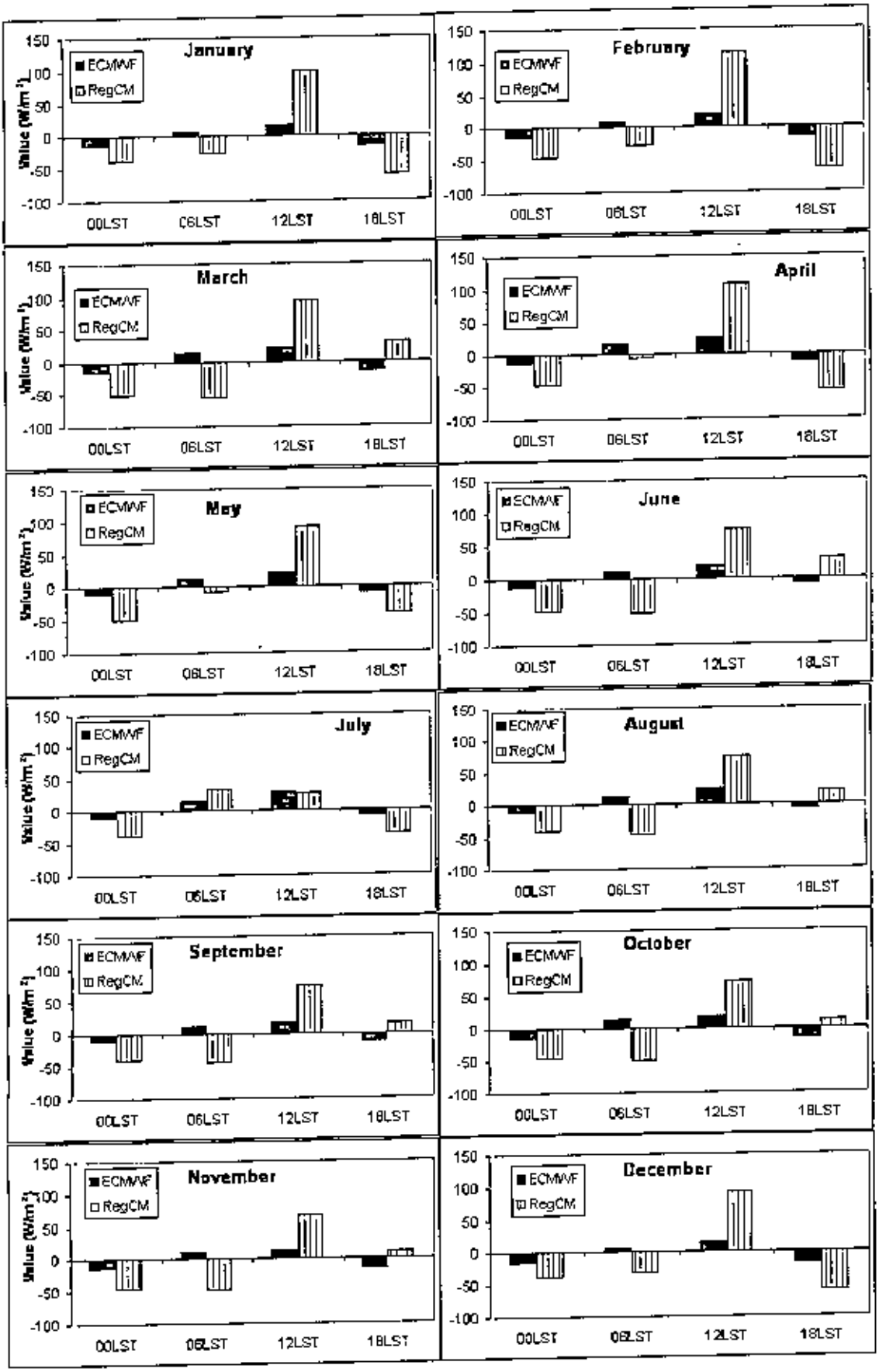

Fig.19: Hourly Variation of surface heat budget (SHB) for centre point (25.5^{0}N, 72.5^{0}E) of the selected Thar Desert area of India for the year 2000

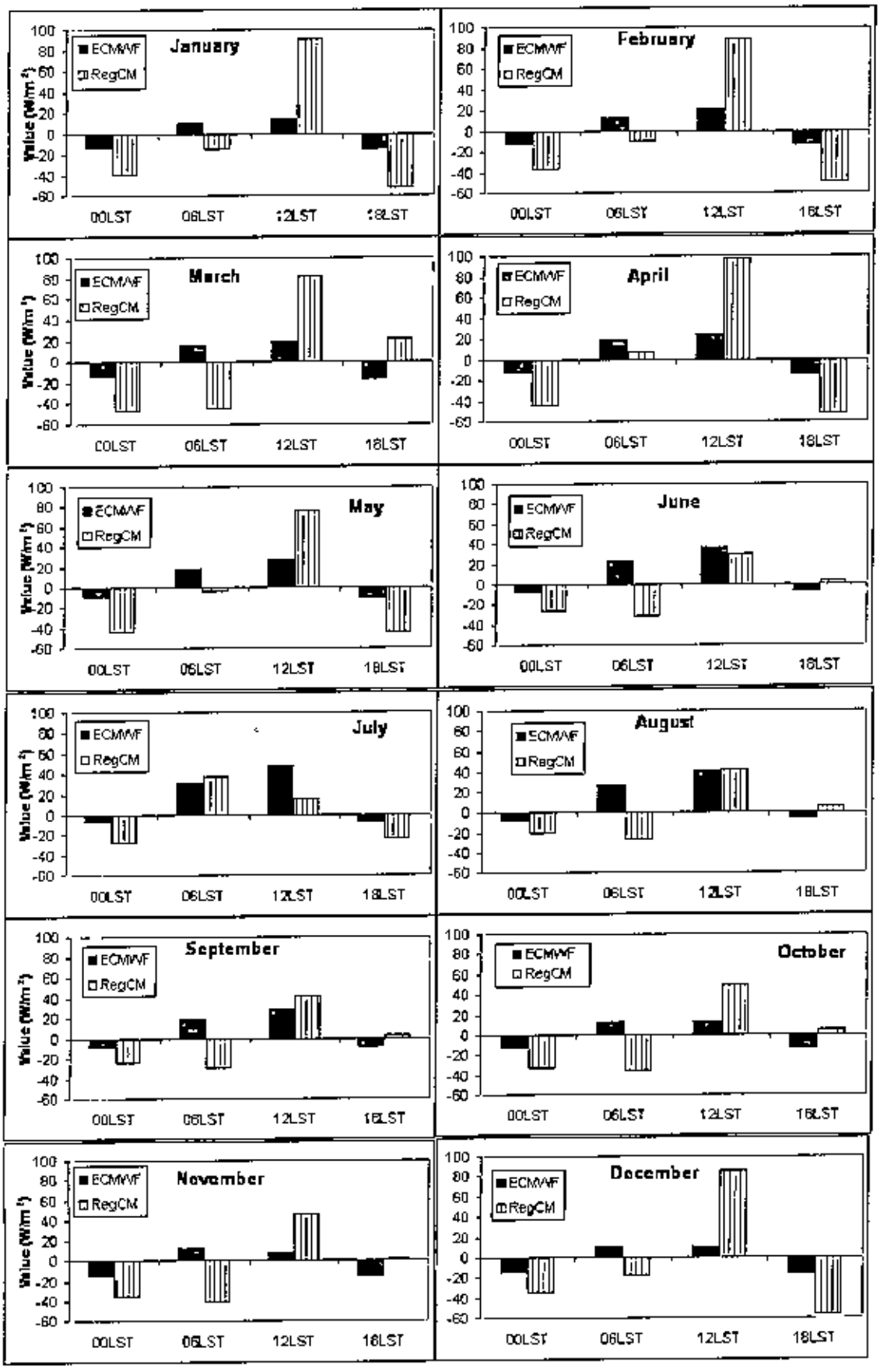

Fig.20: Hourly Variation of surface heat budget (SHB) for centre point (21.5^{0}N, 79.5^{0}E) of the selected area of Mid-India for the year 2000

For ECMWF reanalysis data in fig. 19 it has been also observed at centre point (25.5°N, 72.5°E) of the selected Thar Desert area of India that the value of SHB is always positive at 06, 12LST and is negative at 00, 18 LST. The value of SHB is high from March to August and low in November and December. In July the value of SHB at 12LST is the highest about 28.37W/m^2 and the value of SHB is the lowest -16W/m^2 at 18 LST in December.

For RegCM model data it has been seen the value of SHB is positive at 06, 12LST and is negative at 00, 18 LST in July and April. In April the value of SHB at 12LST is the highest (107 W/m^2) and the lowest (-60 W/m^2) at 18LST in December.

For ECMWF reanalysis data it has been also observed at centre point (21.5°N, 79.5°E) of the selected area of Mid-India in fig. 20 that the value of SHB is always positive at 06, 12LST and is negative at 00, 18 LST. The value of SHB is increasing from January to August and again decreasing from September to December. In July the value of SHB at 06LST is high about 48.48W/m^2 and the value of SHB is low -16W/m^2 at 18 LST in October, November and December.

For RegCM model data it has been seen the value of SHB is positive at 06, 12LST and is negative at 00, 18 LST in July and April. In April the value of SHB at 12LST is the highest (97.62 W/m^2) and the lowest (-66.25 W/m^2) at 18LST in December.

CHAPTER 5: SURFACE HEAT BUDGET FOR LATITUDE AND LONGITUDE VARIATION

A validation study on SHB has been conducted at 12N, 20N & 26N latitude along 70-94E longitude variations using RegCM model data with ECMWF data for the Pre-monsoon (March-May), Monsoon (June-September), Post-monsoon (October-November) periods and two months July and December for 1995-2000. In the following diagrams the deep line represent ECMWF data and light deep line shows RegCM GAS data.

At 12^0N latitude along 70-94^0E longitude

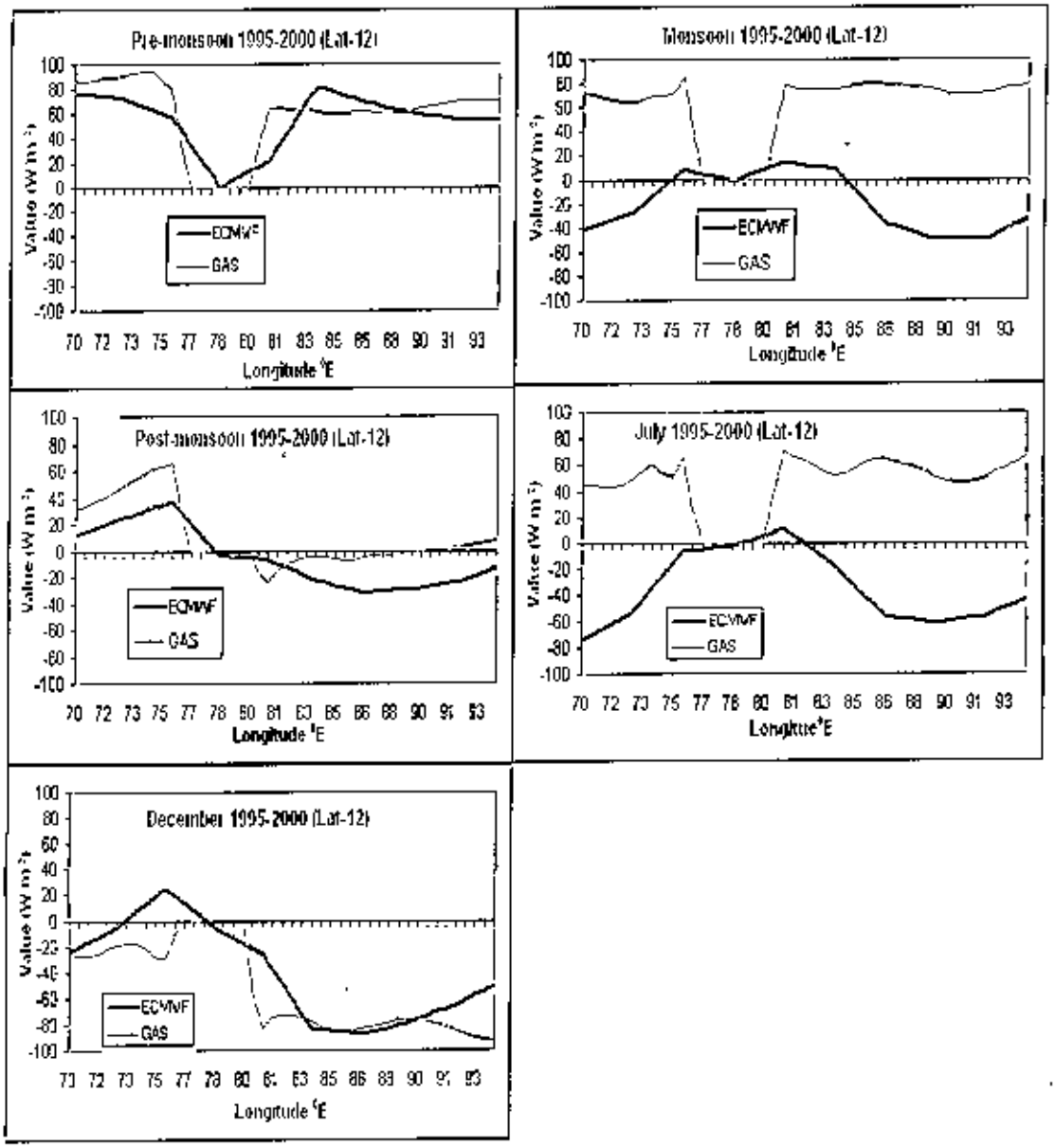

Fig.21: Seasonal variation of SHB at fixed 12^0N latitude along 70-94 ^{0}E Longitude variation for 6 years average (1995-2000):

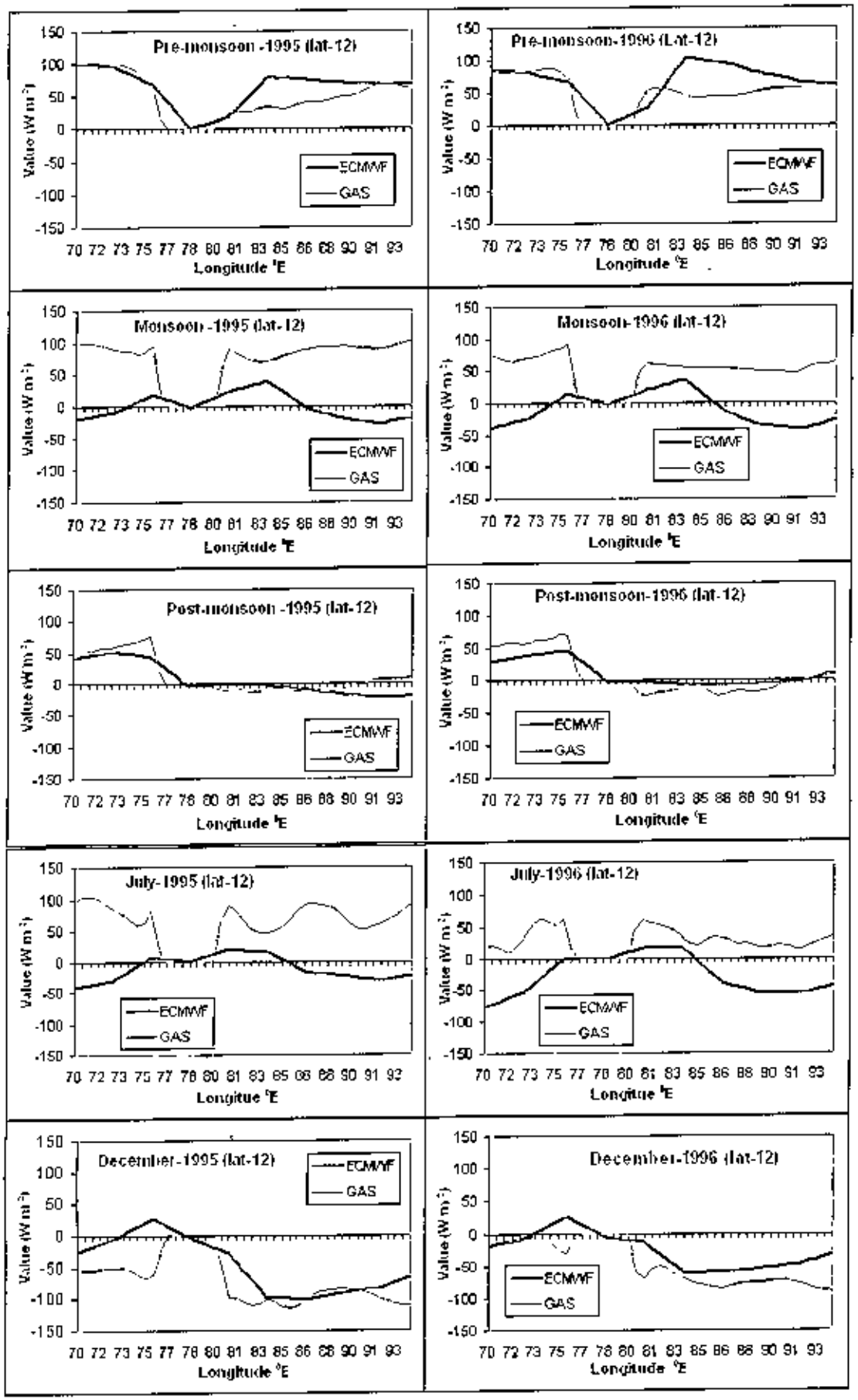

Fig.22: Seasonal variation of SHB at fixed 12^0N latitude along 70-94 ^{0}E Longitude variation for the years 1995 and 1996:

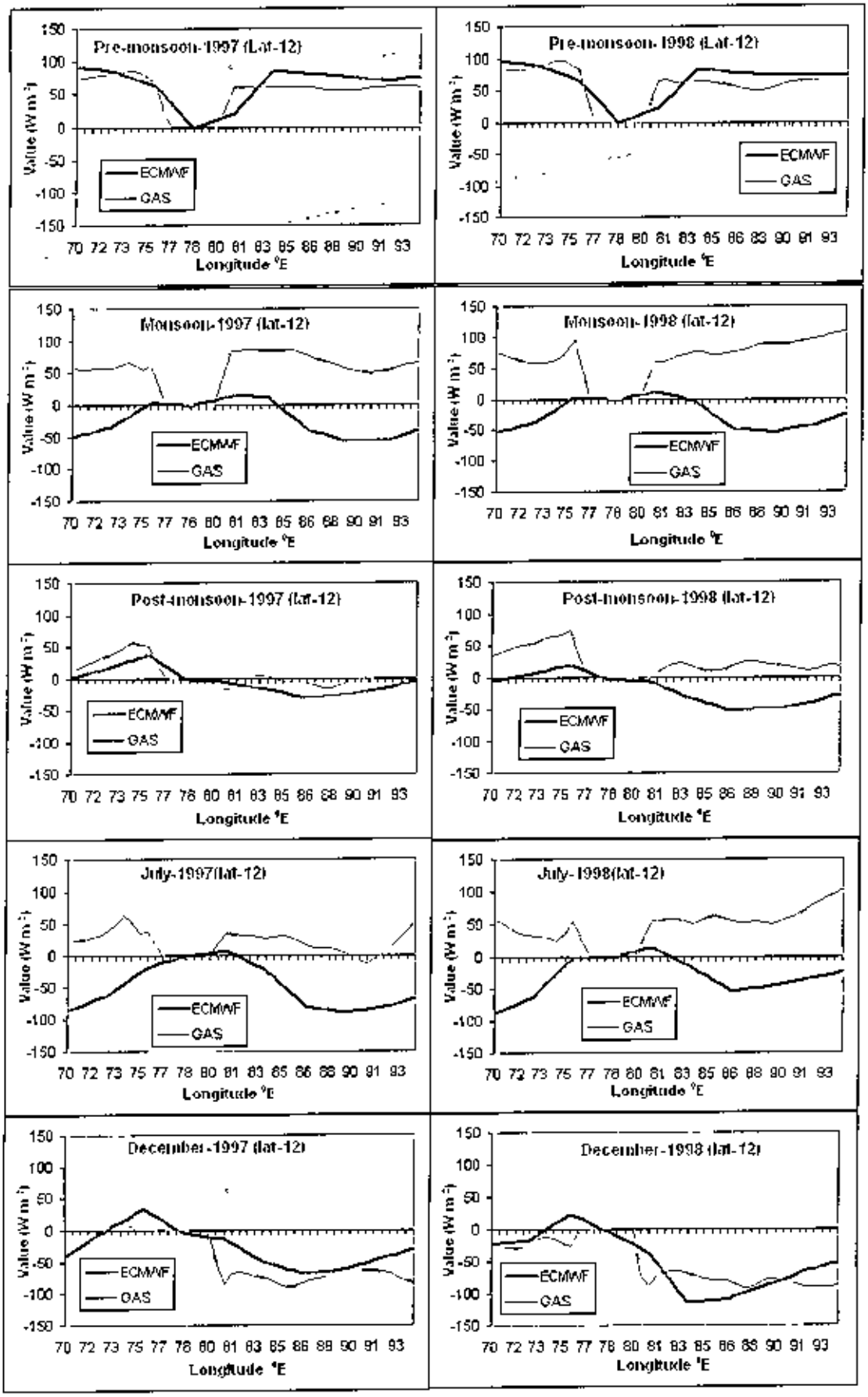

Fig.23: Seasonal variation of SHB at fixed 12^0N latitude along 70-94 ^{0}E Longitude variation for the years 1997 and 1998:

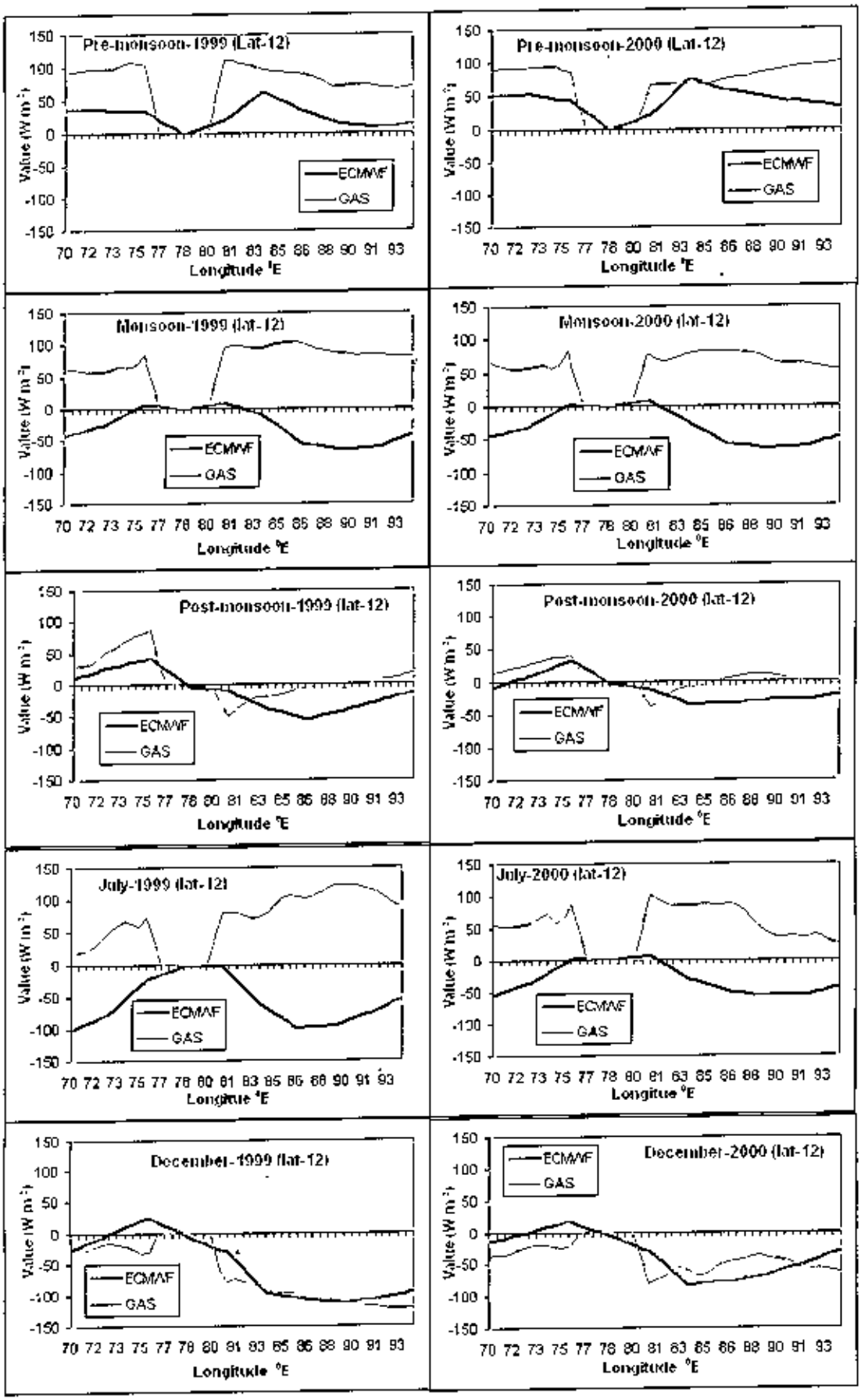

Fig.24: Seasonal variation of SHB at fixed 12^0N latitude along 70-94 ^{0}E Longitude variation for the years 1999 and 2000:

According to the figures 21-24, during Pre-monsoon season the RegCM GAS data and ECMWF data of SHB at 12^0N latitude shows similar value -0.6 W/m^2 at the point (12^0N, 78.2^0E). The RegCM GAS data are overestimate along 70-75.5^0E, 80.4-82.5^0E and 89.1-94^0E and along the remaining longitude variation are underestimate compare to the ECMWF data.

In monsoon season, the RegCM GAS data and ECMWF data of SHB at 12^0N latitude shows similar value -0.38 W/m^2 at the point (12^0N, 78.2^0E). The RegCM GAS data are overestimate along 70-76^0E and 80.4-94^0E. RegCM GAS data and ECMWF data of SHB differ very much about 100 W/m^2. GAS data are all positive along 70-94^0E longitude variation. The SHB of ECMWF data are negative along 70-74.4^0E and 84.2-94^0E and otherwise positive.

In post-monsoon season the RegCM GAS data and ECMWF data of SHB at 12^0N latitude are about same value -0.3 W/m^2 at the point (12^0N, 78.2^0E). The RegCM GAS data are overestimate along 70-75.5^0E, 82-94^0E and are underestimate compare to the ECMWF data along the remaining longitude variation. The SHB of ECMWF data are negative along 78.2-94^0E and positive along 70-77.6^0E.

The pattern of the line graph in Monsoon and in July is same.

In December the RegCM GAS data of SHB (-1.48 W/m^2) at the point (12^0N, 77.6^0E) is close to the ECMWF data (1.26 W/m^2) and also along 83.1-90.7^0E longitude variation (value about -80 W/m^2). The RegCM GAS data are overestimate along 78.2-79.8^0E and are underestimate compare to the ECMWF data along the remaining longitude variation.

At 20^{0}N latitude along 70-94^{0}E longitude

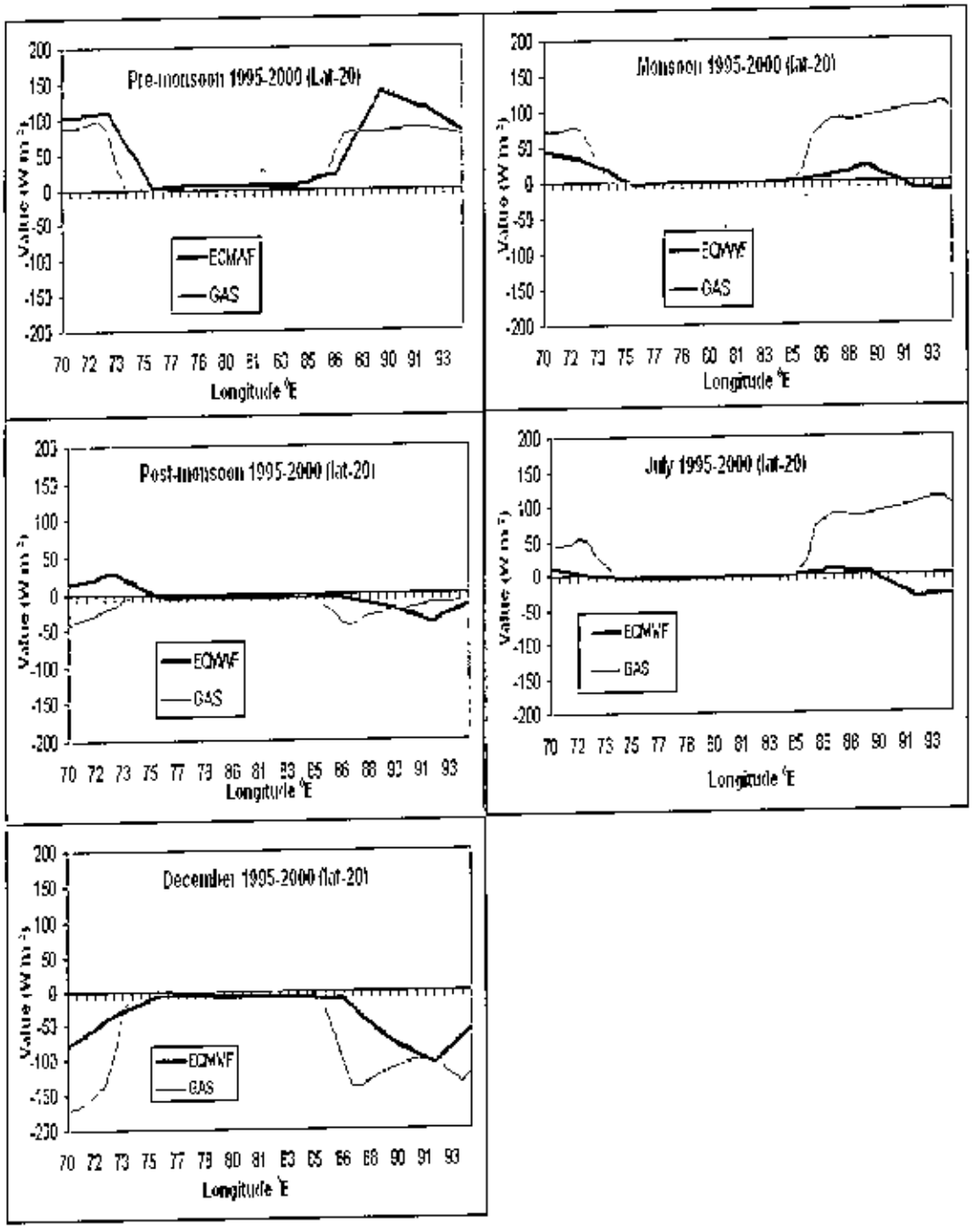

Fig.25: Seasonal variation of SHB at fixed 20^{0}N latitude along 70-94 ^{0}E Longitude variation for 6 years average (1995-2000):

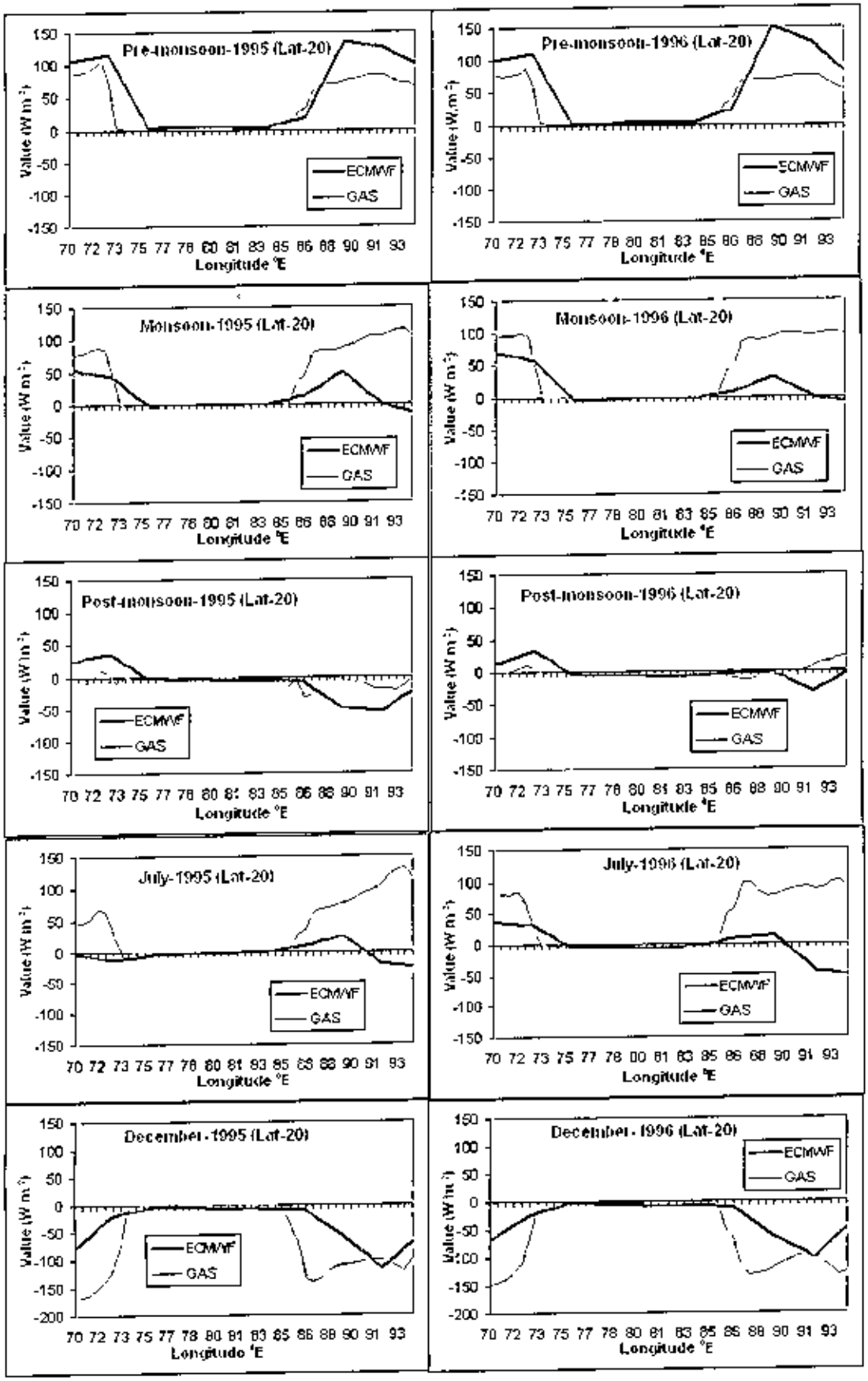

Fig.26: Seasonal variation of SHB at fixed 20^{0}N latitude along 70-94 ^{0}E Longitude variation for the years 1995 and 1996:

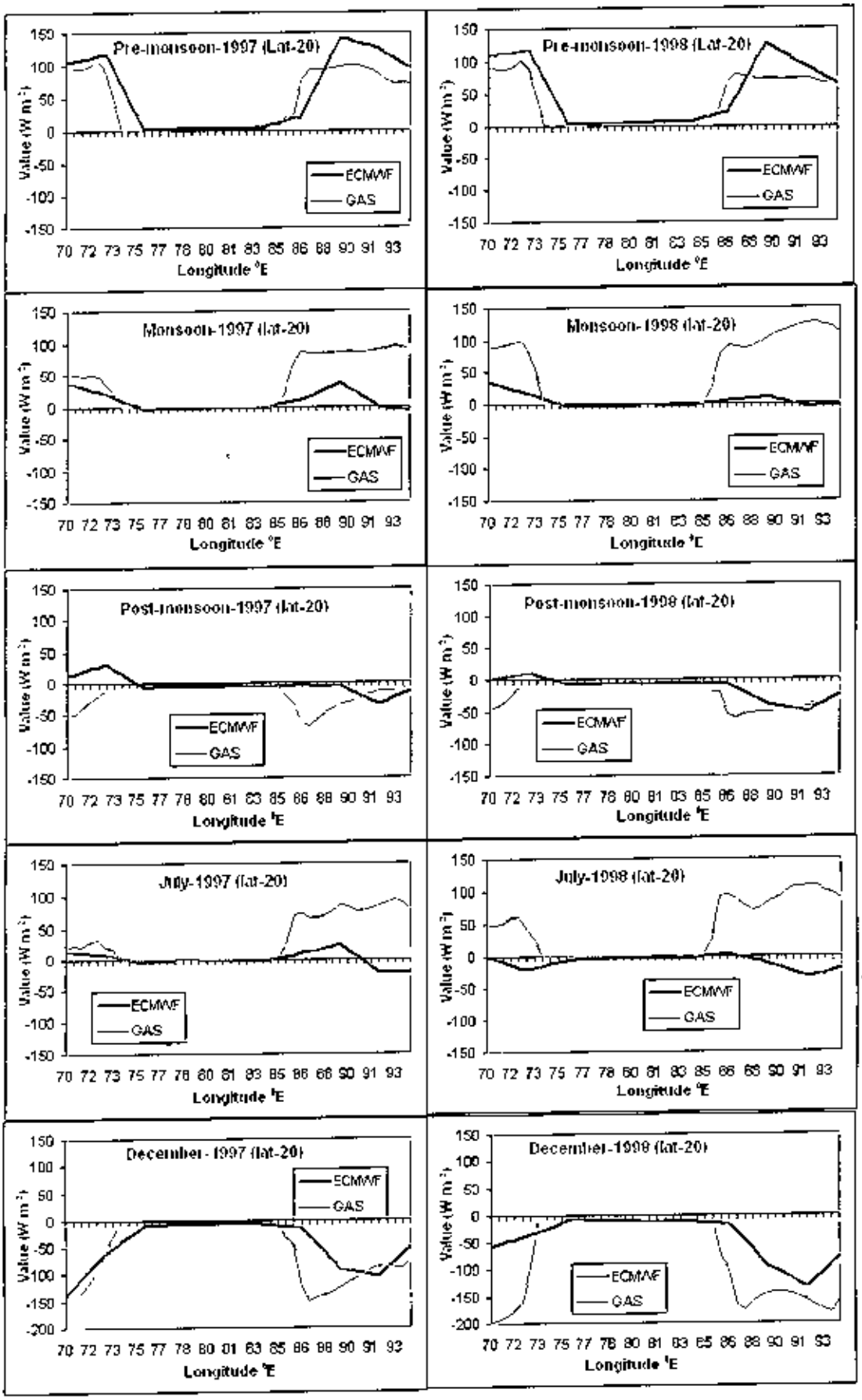

Fig.27: Seasonal variation of SHB at fixed 20^0N latitude along 70-94 ^{0}E Longitude variation for the years 1997 and 1998:

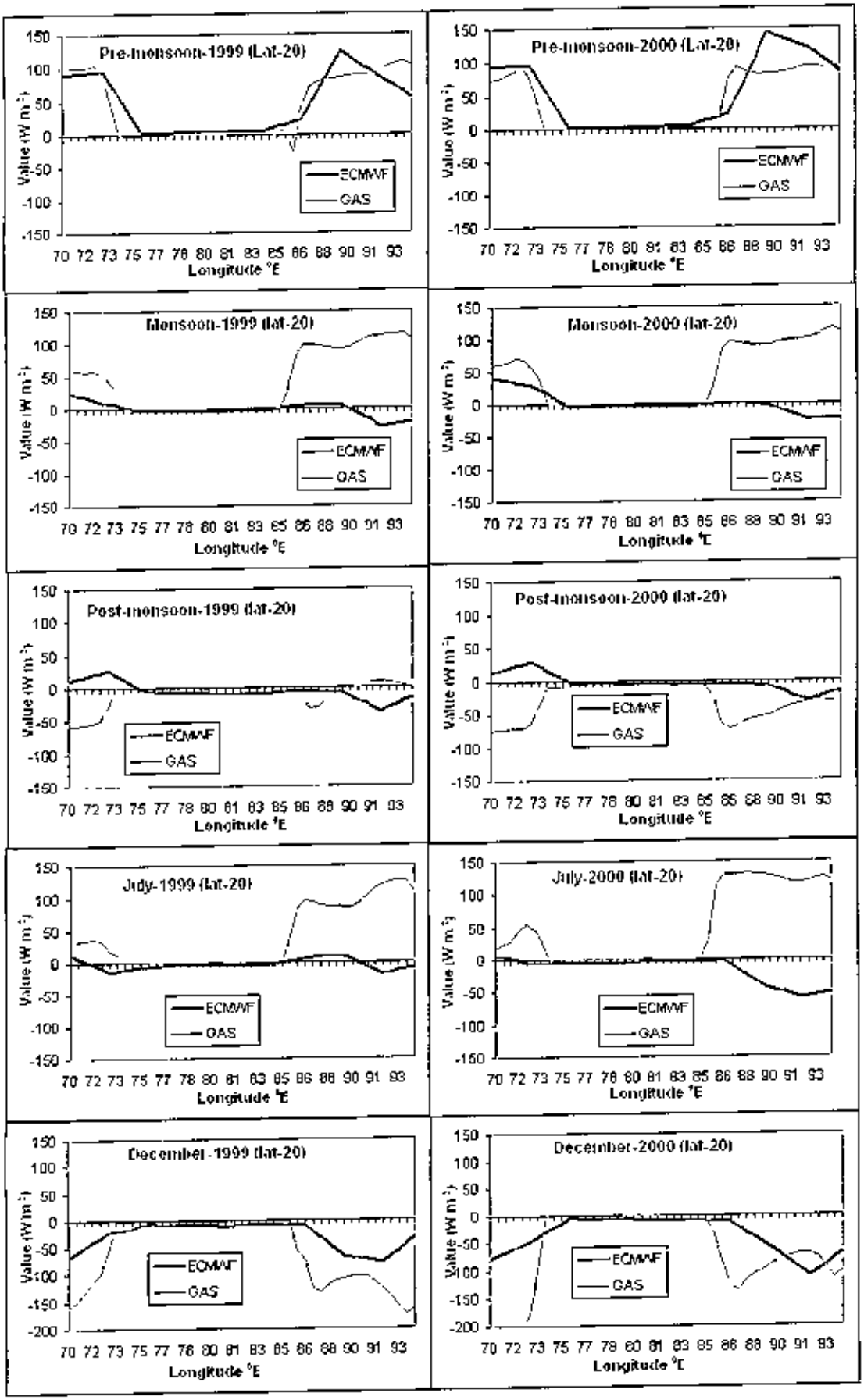

Fig.28: Seasonal variation of SHB at fixed 20^0N latitude along 70-94 ^{0}E Longitude variation for the years 1999 and 2000:

According to the figures 25-28, for the period of Pre-monsoon season the RegCM GAS data and ECMWF data of SHB at 20^0N latitude shows about similar value along 75.5-84.2^{0}E longitude variation, are overestimate along 86.4-87.5 and along the remaining longitude variation are underestimate compare to the ECMWF data. Along 75.5-84.2^{0}E longitude variation the range of SHB for both data is -0.32 W/m^2 to 3 W/m^2 and along the remaining longitude variation the range of SHB is 110 W/m^2 to 137 W/m^2.

In monsoon season, the RegCM GAS data and ECMWF data of SHB at 20^0N latitude demonstrates similar value -1.5 W/m^2 along 74.9-84.7^{0}E longitude variation, are underestimate at the point (20^0N, 73.8^{0}E) and along the remaining longitude variation are overestimate compare to the ECMWF data..

During post-monsoon season the RegCM GAS data and ECMWF data of SHB at 20^0N latitude are about same value -0.5 W/m^2 along 75.5-84.7^{0}E longitude variation. The RegCM GAS data are overestimate along 90.2-94^{0}E and are underestimate compare to the ECMWF data along the remaining longitude variation.

In July the RegCM GAS data and ECMWF data of SHB are about same along 73.8-84.7^{0}E longitude variation. The RegCM GAS data are overestimate along the remaining longitude variation.

In December the RegCM GAS data and ECMWF data of SHB are about same along 75.5-84.7^{0}E longitude variation. The GAS data for SHB are all negative along 70-94^{0}E and ECMWF data are also negative except along 73.3-77.6^{0}E

At 26^{0}N latitude along 70-94^{0}E longitude

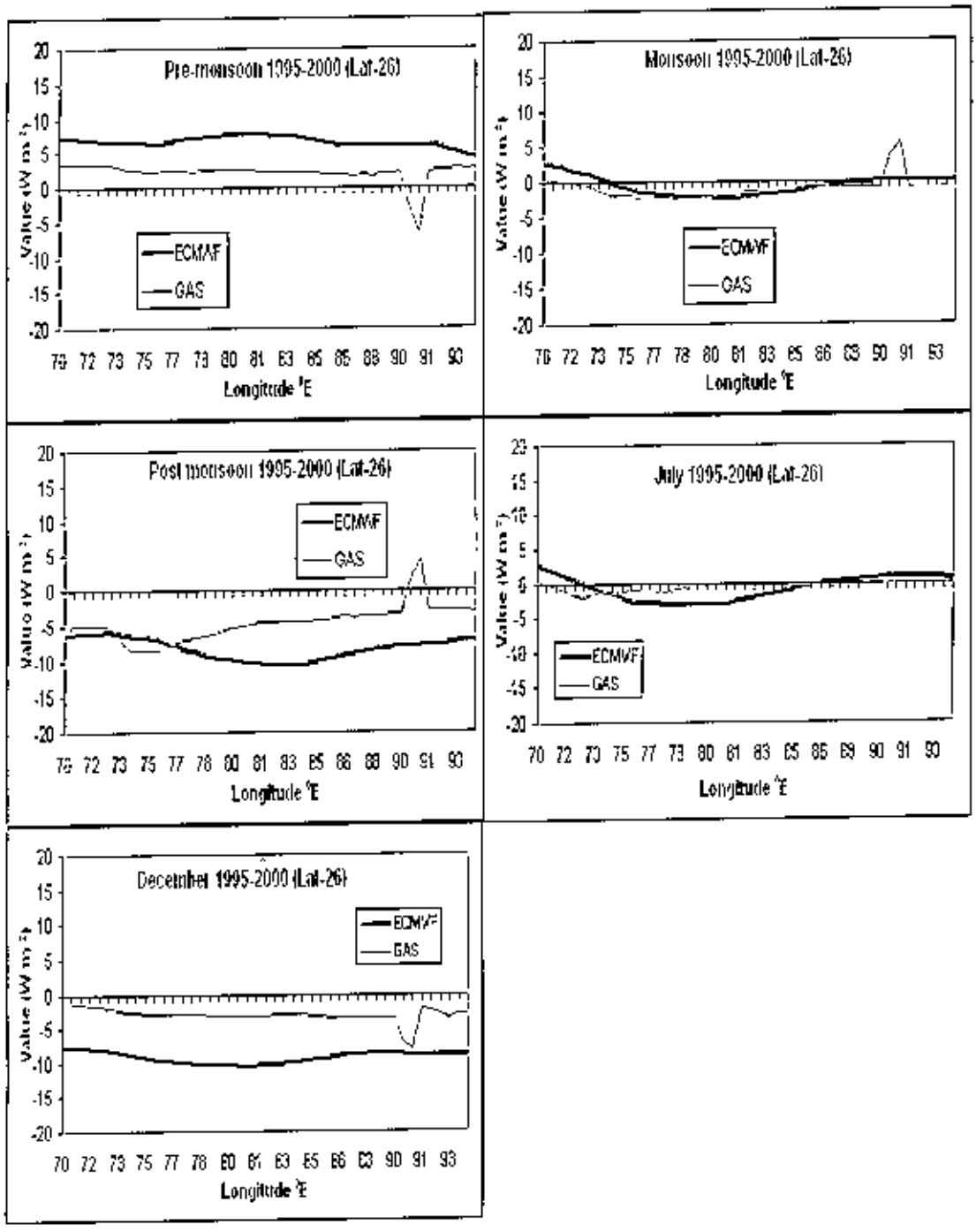

Fig.29: Seasonal variation of SHB at fixed 26^{0}N latitude along 70-94 ^{0}E Longitude variation for 6 years average (1995-2000):

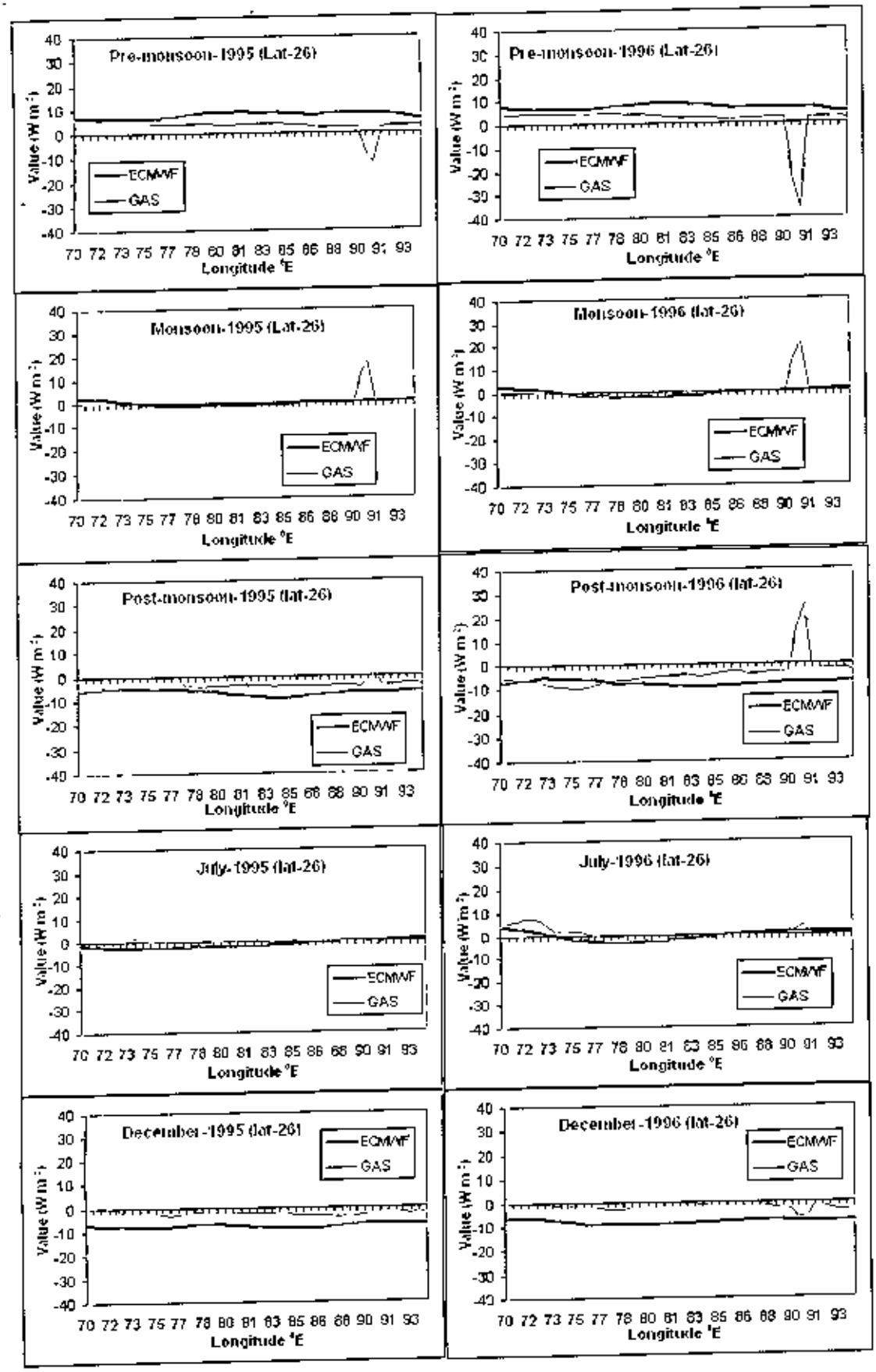

Fig.30: Seasonal variation of SHB at fixed 26^{0}N latitude along 70-94 ^{0}E Longitude variation for the years 1995 and 1996:

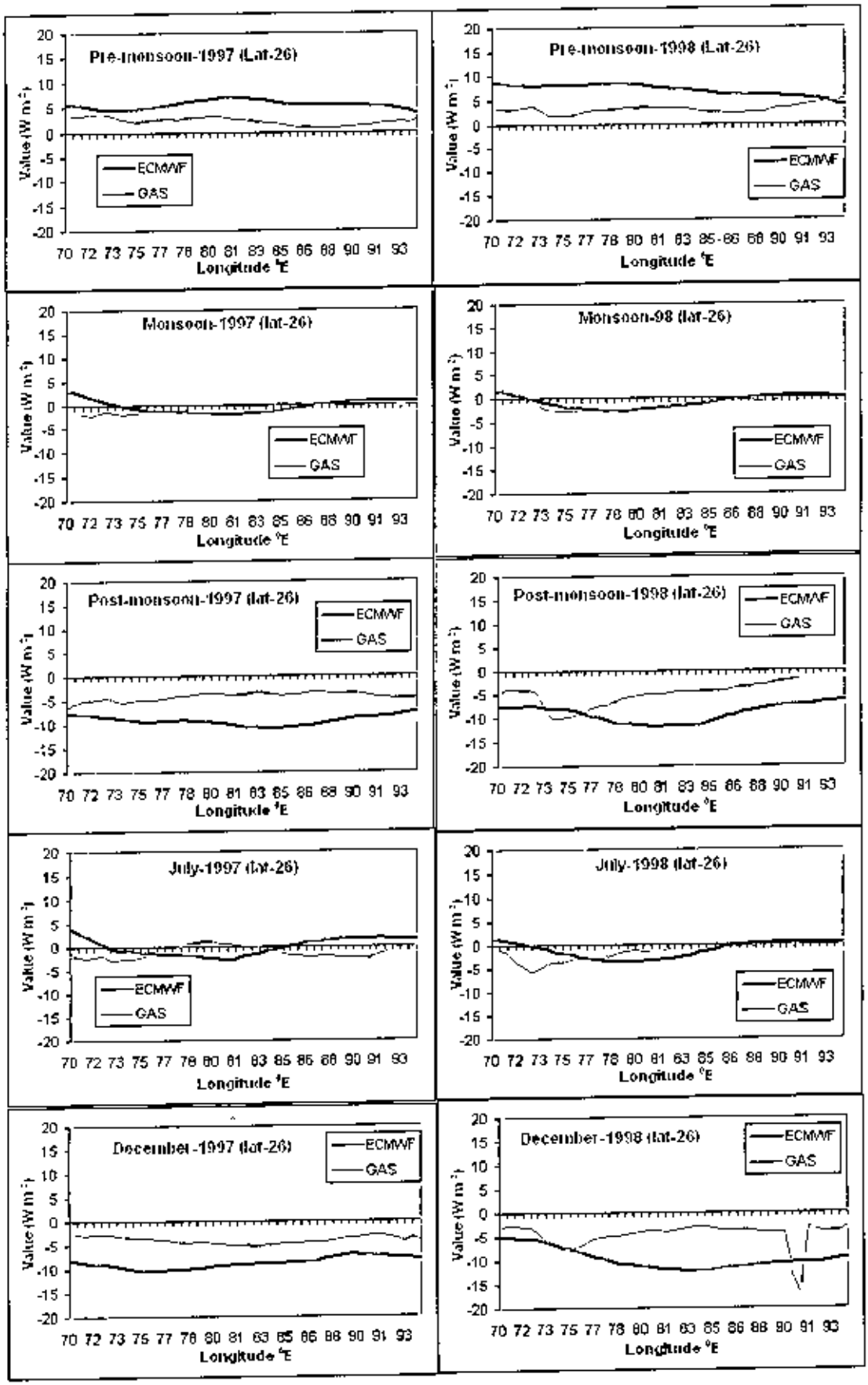

Fig.31:Seasonal variation of SHB at fixed 26^{0}N latitude along 70-94 ^{0}E Longitude variation for the years 1997 and 1998:

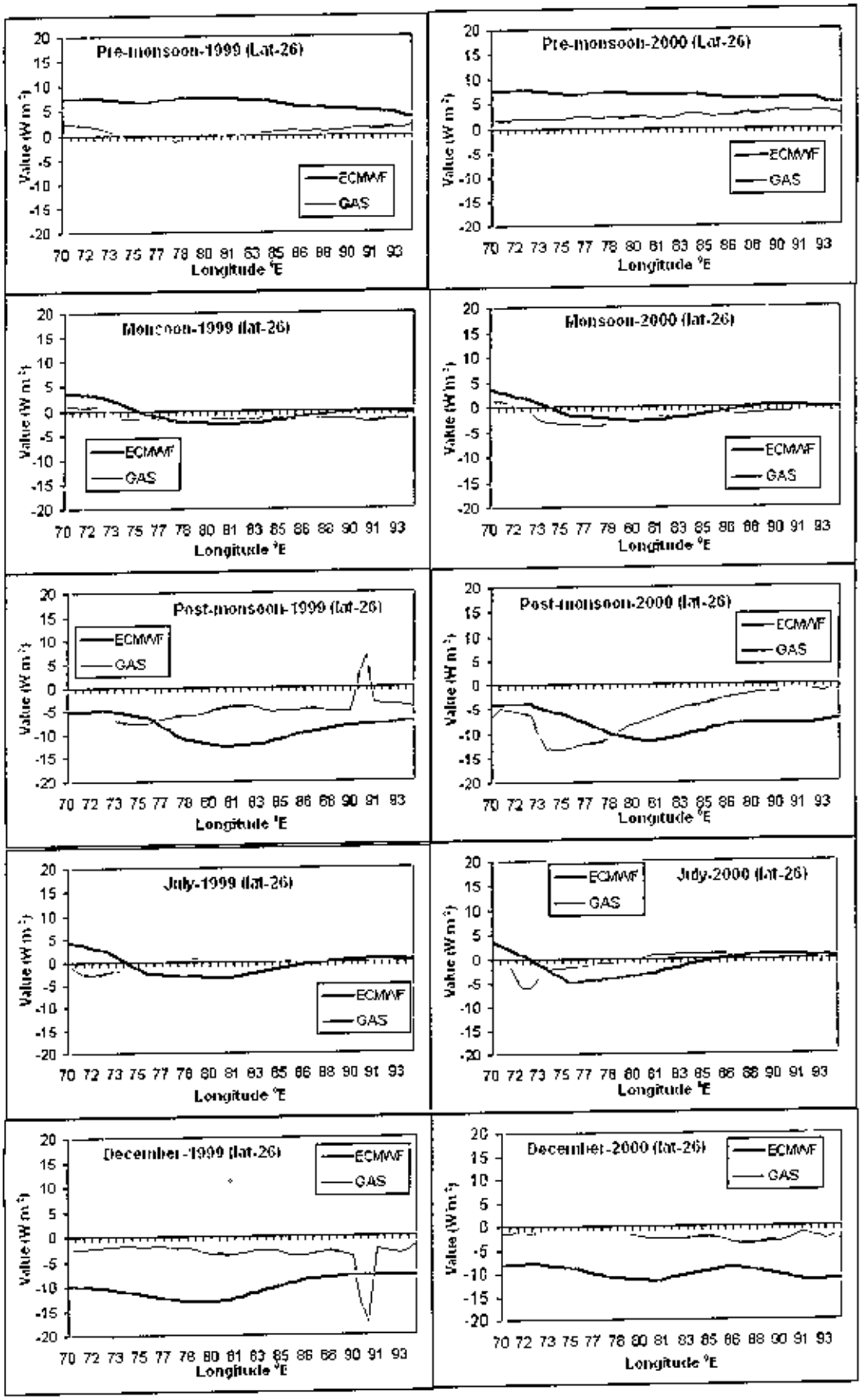

Fig. 32: Seasonal variation of SHB at fixed 26^{0}N latitude along 70-94 ^{0}E Longitude variation for the years 1999 and 2000:

As said by the figures 29-32, for the duration of Pre-monsoon season the RegCM GAS data and ECMWF data of SHB at 26^0N latitude are underrate along 70-94^0E longitude variation compare to the ECMWF data.

The RegCM GAS data are same about -2.2W/m^2 and ECMWF data of SHB are 6.5 W/m^2 - along 70-94^0E longitude variation except Gas data is -6.53W/m^2 at the point (26^0N, 90.7^0E).

In monsoon season the RegCM GAS data and ECMWF data of SHB at 26^0N latitude are about same along 70-94^0E longitude variation except at the point (26^0N, 90.7^0E) is overestimate compare to the ECMWF data. At the point (26^0N, 90.7^0E) the RegCM GAS data of SHB is 5.64W/ m^2. The best result has been seen for RegCM GAS data and ECMWF data of SHB (both data are same) in the year 1998.

During post-monsoon season the RegCM GAS data of SHB at 26^0N latitude are underestimate along 73.3-75.5^0E longitude variation and are overestimate compare to the ECMWF data along the remaining longitude variation. The RegCM GAS data and ECMWF data of SHB are all negative except at the point (26^0N, 90.7^0E) GAS data is 4.24W/ m^2.

In July the RegCM GAS data and ECMWF data of SHB are about similar. The range of the values for both data is from -3.2 to 2.2W/ m^2.

In December the RegCM GAS data of SHB are overestimate along 70-94^0E longitude variation compare to the ECMWF data except at the point (26^0N, 90.7^0E) both data is same, value is -8.0W/ m^2. The range of the values for ECMWF data is from -7W/ m^2 to -10W/ m^2 and for GAS data is from -6.7W/ m^2 to –1.76W/ m^2.

CHAPTER 6: DIFFERENT PARAMETERS OF SURFACE HEAT BUDGET FOR SEVEN SELECTED AREAS FOR THE YEAR 1995

Surface heat budget depends on four parameters which are net short wave radiation (Net downward - net upward ultraviolet energy flux), net long wave radiation (Net upward - net downward infrared energy flux), Sensible heat flux (upward) and Latent heat flux (upward). The values of these parameters are different for different areas due to the dissimilar characteristics of topography. ECMWF reanalysis data and RegCM3 (GAS) model data for 7 selected areas are taken for the year 1995 for analysis.

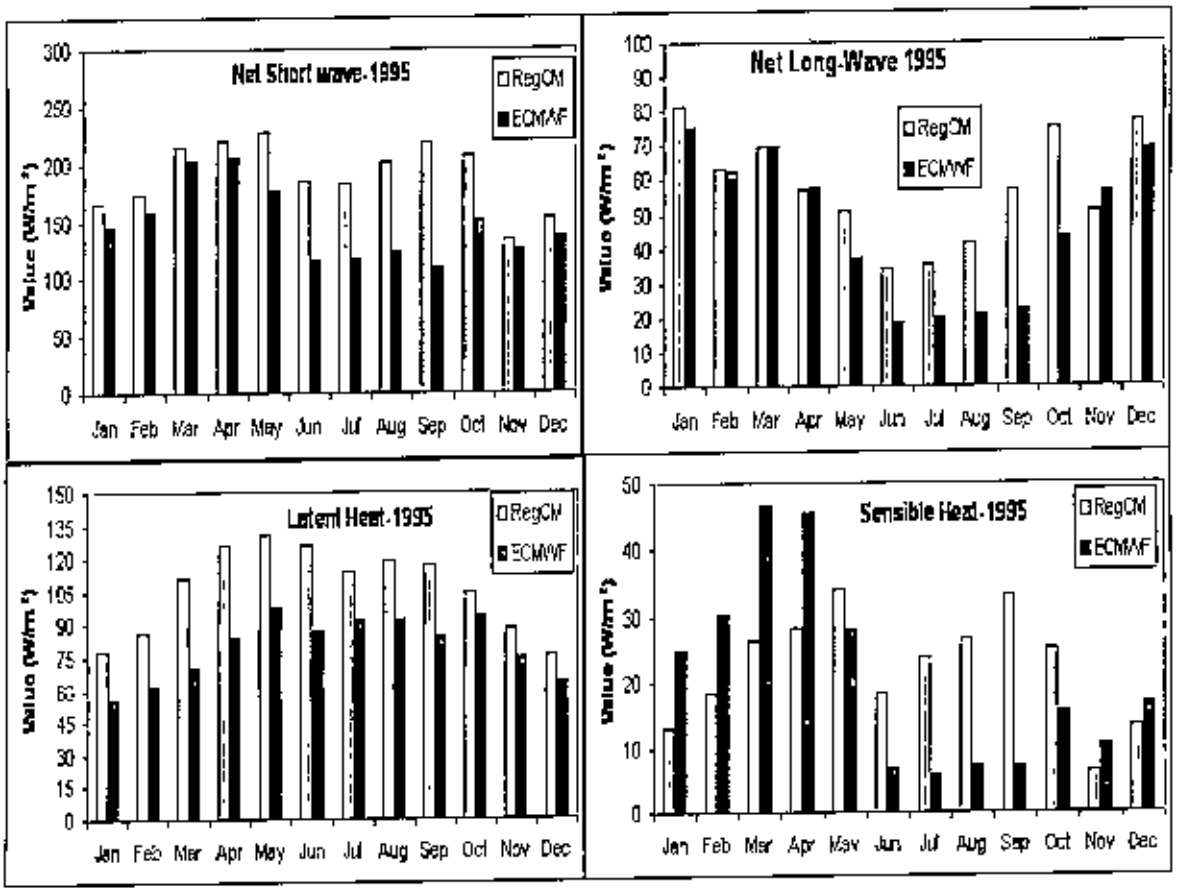

Fig. 33: Monthly variation of net short wave radiation (net solar energy), net long wave radiation, Sensible heat flux and Latent heat flux over Bangladesh

It has been observed in fig. 33 from January to April and in the month November, December for the selected area of Bangladesh that the values of net short wave of RegCM

model data are slightly overestimated about (15W/m^2) compared to ECMWF data but for the remaining months the values are more overestimate about more than 50W/ m^2. For both data the values of net short wave are high about 200W/ m^2. The data of RegCM model and ECMWF differs (107.8W/ m^2) very much in September. For both data the values of net short wave are low in monsoon season (June-September).

The values of net long wave of RegCM model data are about similar to ECMWF data from January to April and in the month November, December but for the remaining months the values are overestimate about on an average 20W/ m^2. The highest value is seen in January 81W/ m^2 for RegCM model data and 75W/ m^2 for ECMWF data and the lowest value is in June 34W/ m^2 for RegCM model data and 19W/ m^2 for ECMWF data. The values of net long wave of RegCM model data and ECMWF data in winter is high than the other seasons.

The RegCM model data of latent heat are overestimated about (33.7W/m^2) compared to ECMWF data in the Pre-monsoon and monsoon seasons. For sensible heat the RegCM model data are underestimated about (15W/m^2) in January-April and overestimate about (19W/m^2) in monsoon seasons compare to ECMWF data. For surface heat Budget over Bangladesh it has been seen that RegCM model data are underestimated in pre-monsoon season and overestimate in monsoon season due to the effect of the variation of sensible heat.

The value of all parameters of SHB for both data are low in monsoon season and in November-December the RegCM model data are similar to ECMWF data.

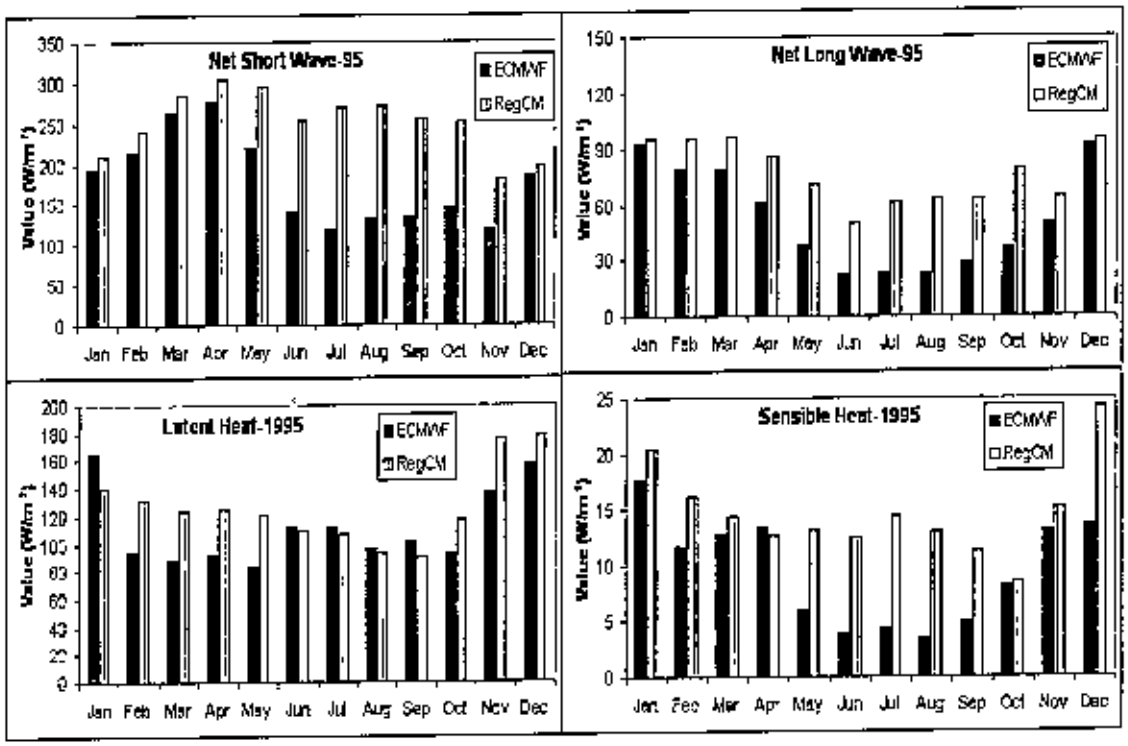

Fig. 34: Monthly variation of net short wave radiation (net solar energy), net long wave radiation, Sensible heat flux and Latent heat flux over Bay of Bengal

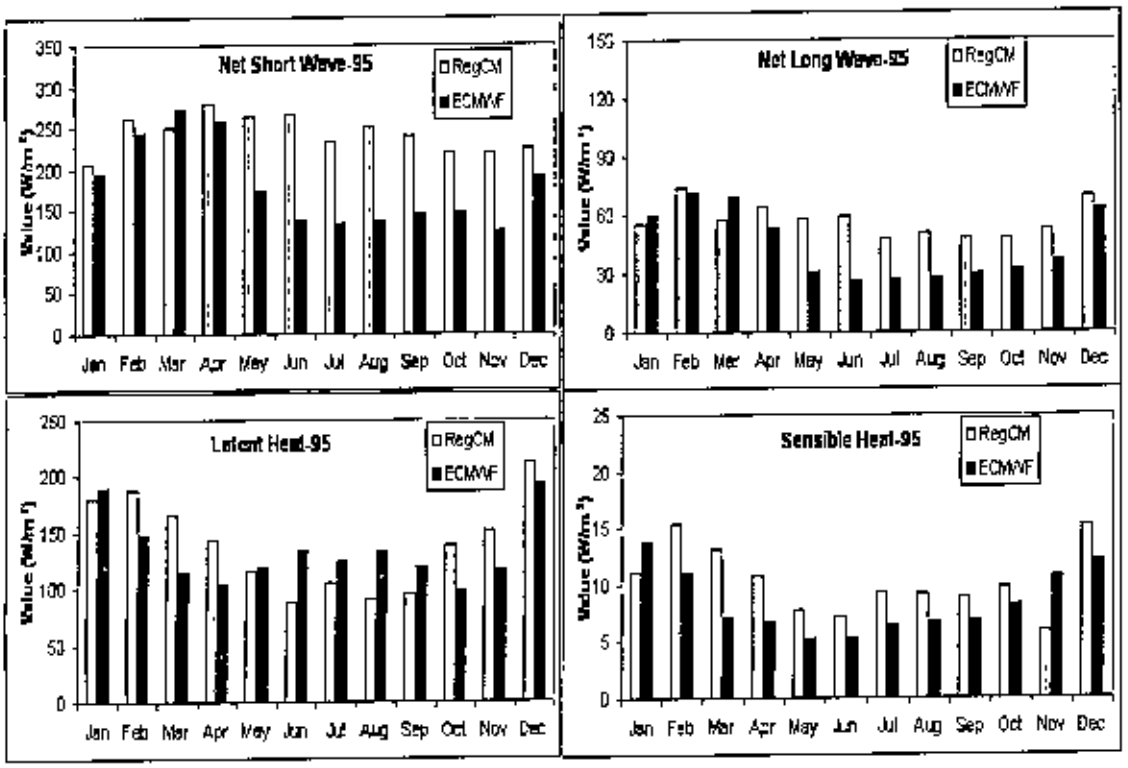

Fig. 35: Monthly variation of net short wave radiation (net solar energy), net long wave radiation, Sensible heat flux and Latent heat flux over Deep Ocean of Bay of Bengal

In fig. 34, Over Bay of Bengal near coastal region of Bangladesh the values of net short wave, net long wave and sensible heat are high in Pre-monsoon (March-May) and low in monsoon season due to cloud and precipitation. But for latent heat the value is high in monsoon season due to huge evaporation. So, the effect of latent heat is more on SHB. The values of net short wave, net long wave and sensible heat of RegCM model data are overestimated compares to ECMWF data in monsoon season. For latent heat the RegCM model data are similar to ECMWF data in monsoon season and overestimate in Pre-monsoon and monsoon season.

For RegCM model data and ECMWF data over Deep Ocean the patterns in fig.35 for net short wave, net long wave and sensible heat are same except for latent heat. Similar events occur for Bay of Bengal near coast and Deep Ocean (Bay of Bengal) far from Bangladesh coastal region. The value of all parameters of SHB of RegCM model data and ECMWF data for Deep Ocean is small compare to the values for Bay of Bengal.

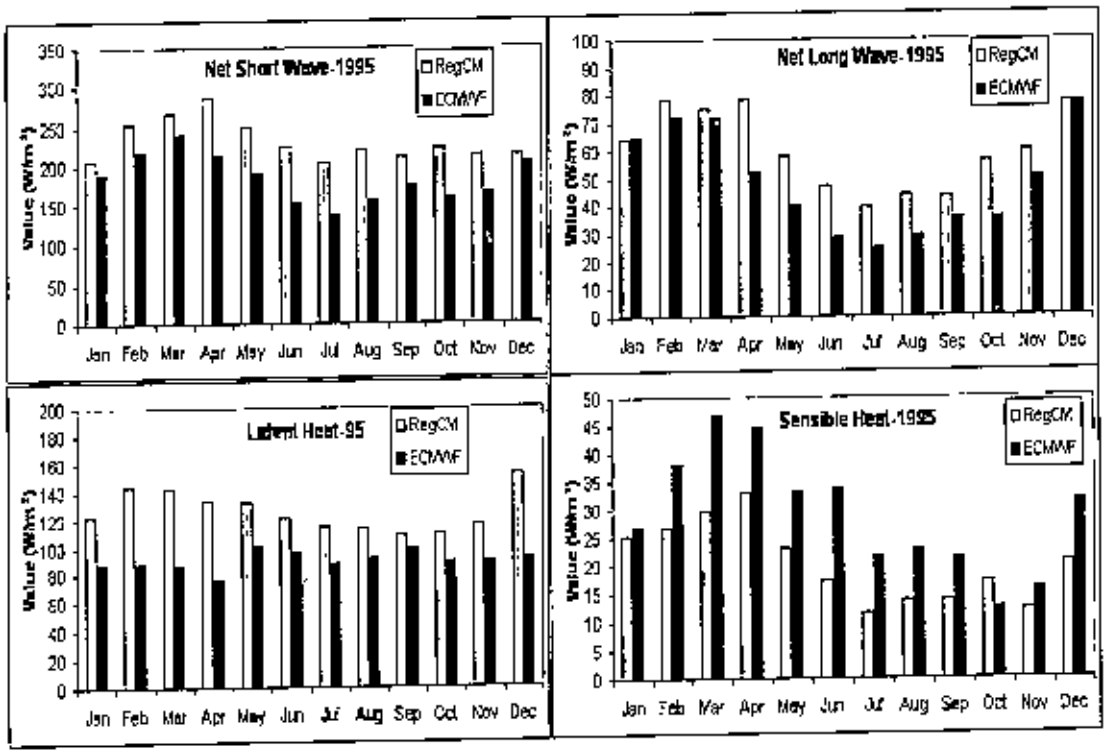

Fig. 36: Monthly variation of net short wave radiation (net solar energy), net long wave radiation, Sensible heat flux and Latent heat flux over West coast of India

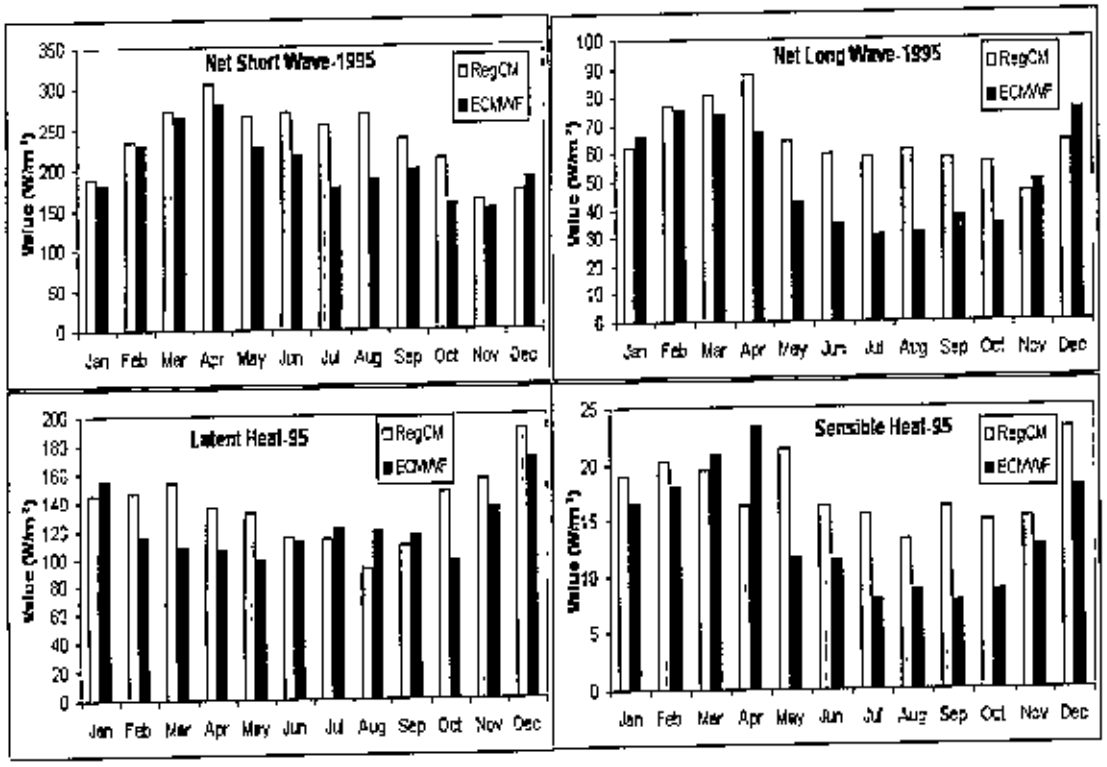

Fig. 37: Monthly variation of net short wave radiation (net solar energy), net long wave radiation, Sensible heat flux and Latent heat flux over near East Coast of India

For RegCM model data in fig.36 the values of net short wave radiation (net solar energy), net long wave radiation and Latent heat flux over West coast of India are overestimate for all months of the year 1995 compare to the ECMWF data. But for sensible heat RegCM model data shows underrate compare to the ECMWF data for all months except in October. The variation of SHB depends on the variant of Sensible heat.

In fig.37 for RegCM model data the values of net short wave radiation, net long wave radiation and Sensible heat flux over ocean and near East Coast of India are overestimate for monsoon season except for latent heat. The pattern of the values of net short wave radiation and net long wave radiation for RegCM model data and ECMWF data are similar and the pattern of the values of sensible heat and latent heat for RegCM model data and ECMWF data are different.

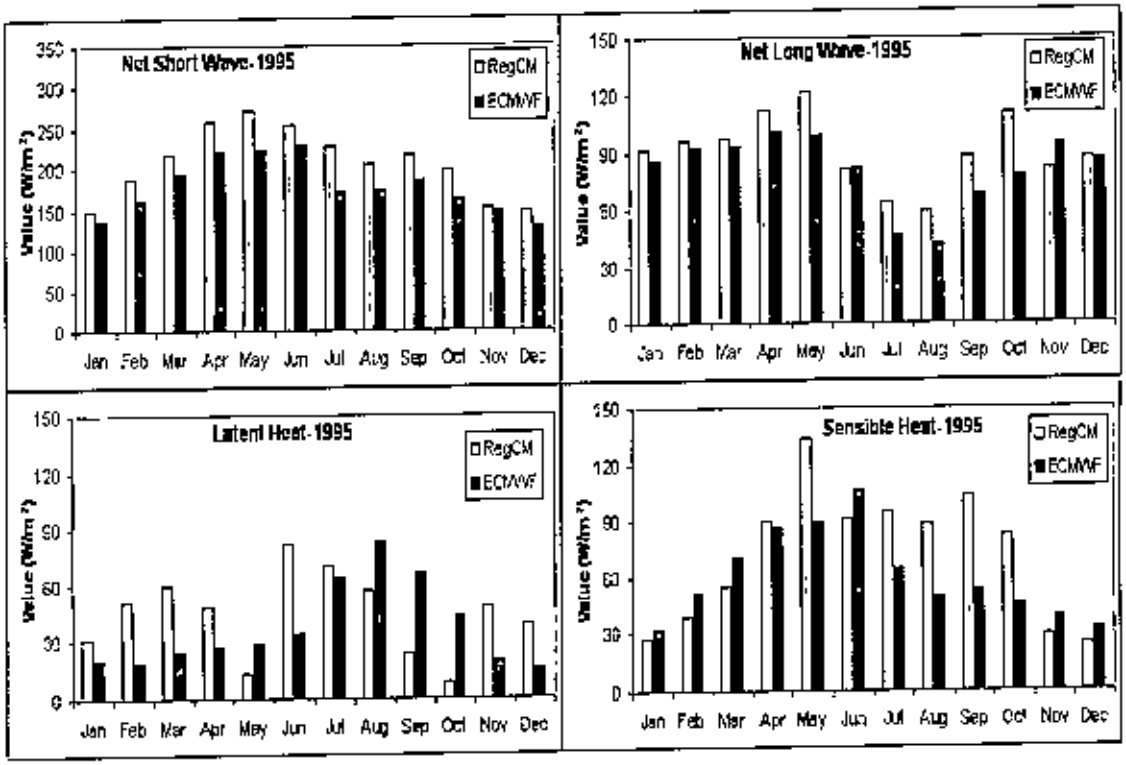

Fig. 38: Monthly variation of net short wave radiation (net solar energy), net long wave radiation, Sensible heat flux and Latent heat flux over Thar Desert of India

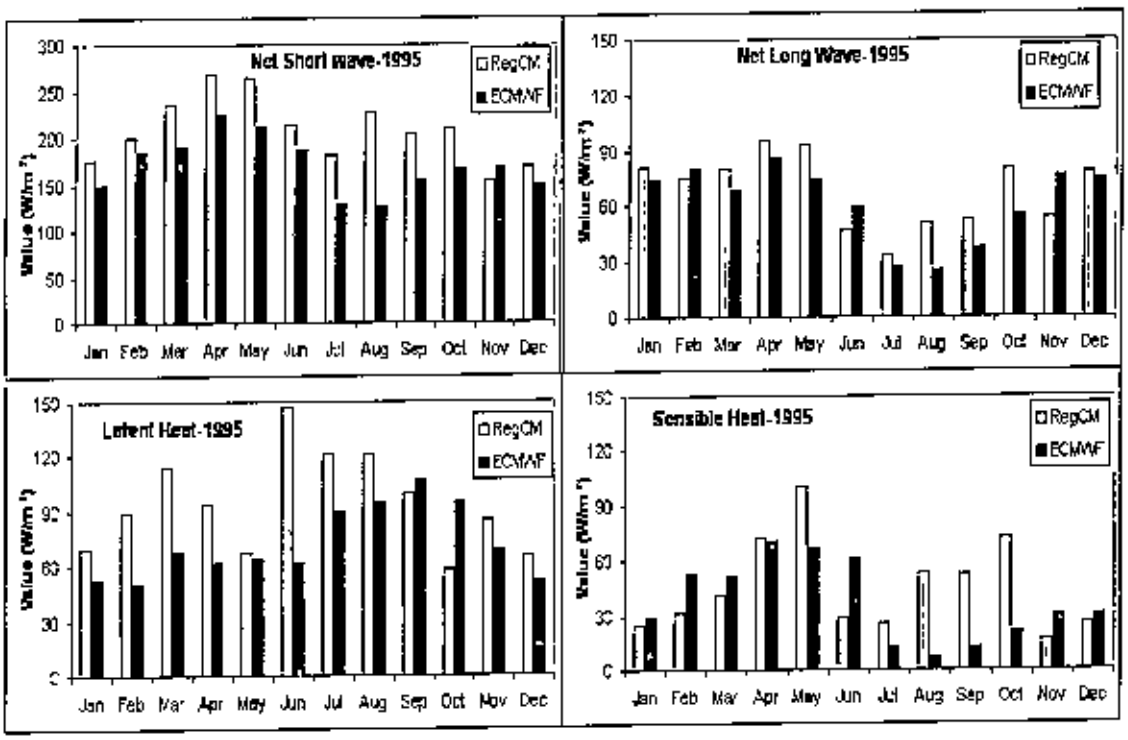

Fig. 39: Monthly variation of net short wave radiation (net solar energy), net long wave radiation, Sensible heat flux and Latent heat flux over Mid-India

As fig. 38 shows Over Thar Desert the values of net short wave and long wave for RegCM model data and ECMWF data are about similar. The values of net short wave are high in April-June about 250w/ m^2 and low in winter. The values of net long wave are high in April, May and low in July and August. For RegCM model data the values of latent heat are high in March, June and July and low in May and October about 10W/ m^2. For ECMWF data the values of latent heat are high in July-September and low in winter. For sensible heat the highest value is observed in May (133W/ m^2) for RegCM model data and in June (107W/ m^2) for ECMWF data. The value of sensible heat is low for both data in winter season.

About similar events are observed over Thar Desert and Mid-India according to the figures 38 and 39.

CHAPTER 7: SENSITIVITY TEST

Surface Heat Budget (SHB) for different schemes data of RegCM Model and ECMWF re-analysis data are taken for 1983 for analysis. The schemes of RegCM model are (1)Grell scheme with Arakawa-Schubert (GAS), (2) Grell scheme with Fritch-Chappell (GFC) assumptions. (3) Betts-Miller Scheme with Fritch-Chappell (BFC). (4) MIT-Emanuel scheme with Fritch-Chappell (EFC) and (5) Kuo Scheme with Fritch-Chappell (KFC). These schemes data of RegCM model are analyzed monthly to see the variation and which scheme data is suitable for the said 7 selected areas and also for fixed three latitudes 12^0N, 20^0N and 26^0N along 70-94^0E longitude variations for seasonally, July and December. The different schemes data of RegCM Model are also compared to the value of ECMWF re-analysis data.

For the selected area over Bangladesh the BFC, GAS, KFC and EFC schemes data show about similar to ECMWF data for all months except in March-June. Among these schemes data BFC data are more suitable than others. In March-June the BFC, GAS, KFC and EFC schemes data are underestimate compare to ECMWF data. Among the 5 schemes data GFC data are most underestimate compare to ECMWF data.

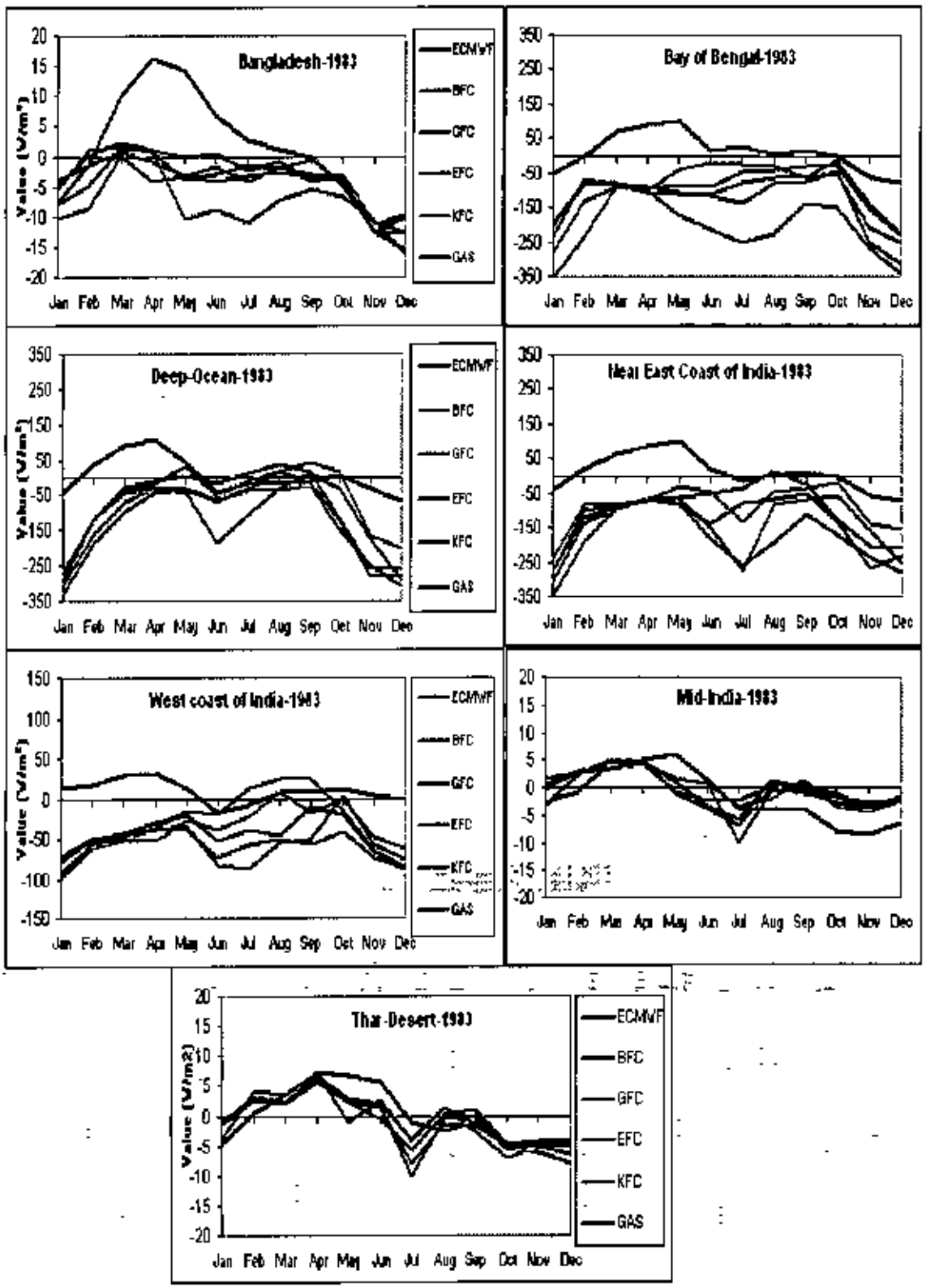

Fig.40: SHB for different scheme data of RegCM Model and ECMWF re-analysis data over selected 7 areas for the year 1983

Regarding to the fig. 40, for the selected area over Bay of Bengal beside Bangladesh coast BFC data are near to ECMWF data in June-October and underestimate in other months. The remaining schemes data are not suitable for this region.

For the selected area over Deep Ocean far from the coast of Bangladesh coast BFC data are near to ECMWF data in May-October and underestimate in other months. The remaining schemes data are not suitable for this region.

For the selected area of West coast of India all schemes data are underestimate for all months except the KFC scheme data are overestimate in monsoon (Jun-Sep) season compare to ECMWF data. Therefore no schemes data are suitable for this region.

For the selected area of Near East coast of India KFC data are near to ECMWF data from July to September and underestimate in other months. Other schemes data are suitable for this region. The pattern of BFC data is similar but underestimates for all months compare to ECMWF data.

For the selected area of Thar Desert in India the schemes BFC and GAS data are well than the other schemes evaluate to ECMWF data for all months. The GAS data are fluctuated slightly.

For the selected area of Mid-India all schemes data are near to ECMWF data except EFC data in July. Among these schemes BFC and GAS data are more accurate and slightly underestimates in Pre-monsoon and overestimate in monsoon season.

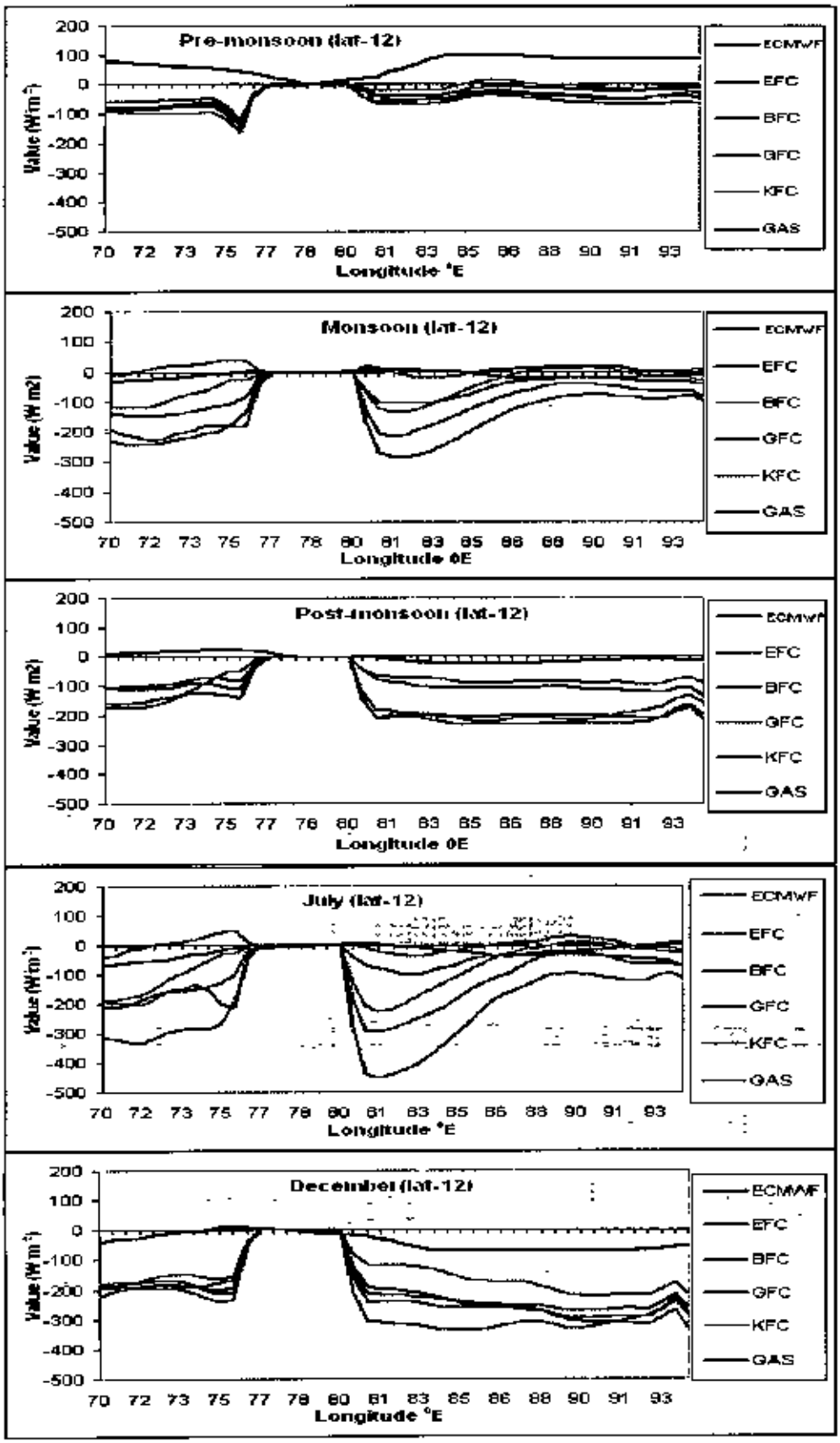

Fig.41: SHB for different schemes data of RegCM Model and ECMWF re-analysis data along 70-94^{0}E longitude variations at 12^{0}N latitude for the year 1983

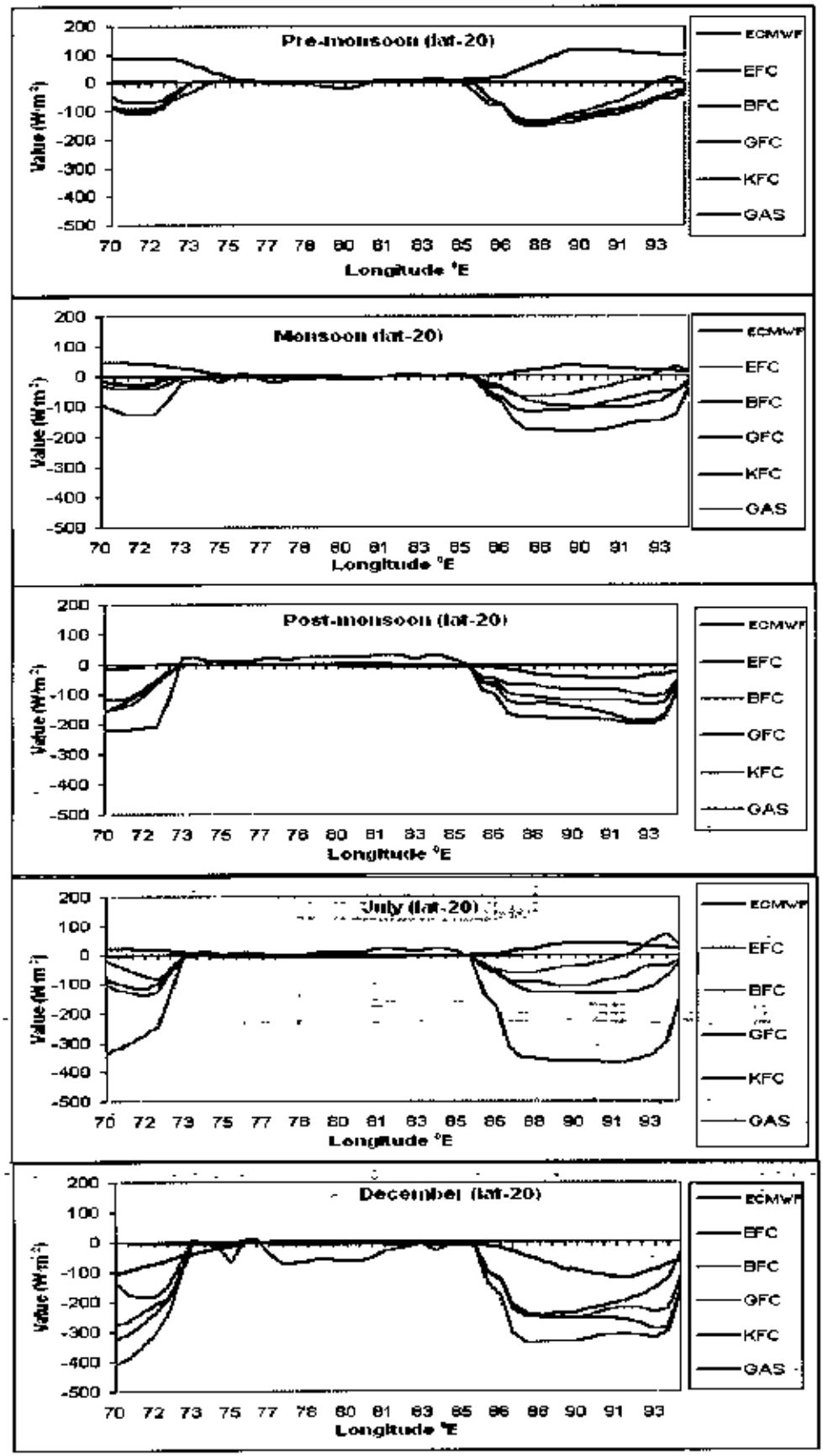

Fig.42: SHB for different schemes data of RegCM Model and ECMWF re-analysis data along 70-94^{0}E longitude variations at 20^{0}N latitude for the year 1983

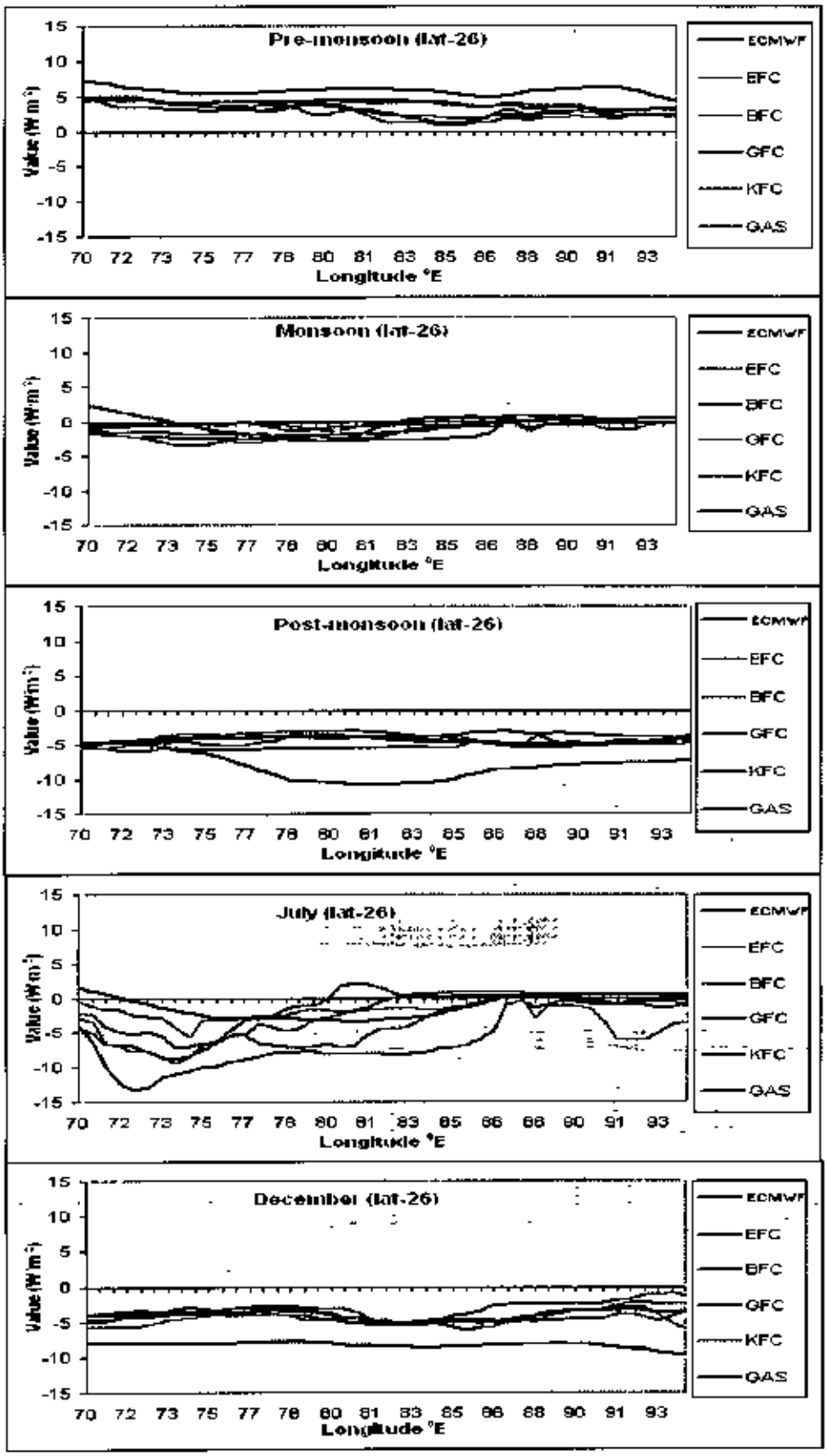

Fig.43: SHB for different schemes data of RegCM Model and ECMWF re-analysis data along 70-94^{0}E longitude variations at 26^{0}N latitude for the year 1983

It is observed that a lot of variations occur for different schemes data of RegCM Model compare to ECMWF data along longitude variations at different latitudes during different seasons and the months of July and December. The difference between all schemes data and ECMWF data are high over ocean and low over land.

At 12^0N latitude (as shown in fig. 41):

(a) During pre-monsoon season all schemes data and ECMWF data are abont same along 77-80^0E longitude and underrate along remaining longitude variation.

(b) In Monsoon season and in Jnly all schemes data and ECMWF data are close along 76-79.8^0E longitude. The KFC data is similar to ECMWF data along 76-94^0E longitude and slightly overrate along 70-75.9^0E. The BFC and GAS data are near to ECMWF data along 85.8-94^0E longitude and other schemes data are under estimate along 70-76^0E and 80-90^0E longitude variation.

(c) For the period of post-monsoon season all schemes data are underestimate along 70-77^0E and 79.8-90^0E compare to ECMWF data. All schemes data are comparable to ECMWF data along 77.1-79.8^0E longitude variant.

(d) All schemes data are more underestimate in December than post-monsoon.

At 20^0N latitude (as shown in fig. 42):

The KFC scheme data remain same about $3W/m^2$ along 70-94^0E longitude variation.

(a) In pre-monsoon season all schemes data and ECMWF data are about same along 74.9-85.3^0E longitude over land and underrate along remaining longitude variation.

(b) For monsoon season all schemes data and ECMWF data are also abont same along 74.9-85.3^0E longitude over land and nnderrate along remaining longitude variation except for BFC

data. The BFC data are similar to ECMWF data along 92.4-94^{0}E longitude. The pattern for all data in monsoon season is about same in July.

(c) During post-monsoon season all schemes data and ECMWF data are about equivalent along 73.3-85.3^{0}E longitude over land (except for GFC data which are overestimate) and underrate along remaining longitude variation (except for GFC data which are underestimate).

(d) In December all schemes data and ECMWF data are about close along 74.9-85.3^{0}E longitude except for GFC data. The GFC data are overestimate along 74.9-85.3^{0}E longitude and underestimate along remaining longitude variation.

At 26^{0}N latitude (as shown in fig. 43):

(a) During pre-monsoon season all schemes data show slightly underrate along 70-94^{0}E longitude variation over land compare to ECMWF data.

(b) For the period of monsoon season all schemes data are about to same along 73.3-94^{0}E and underestimate along 70-72.7^{0}E longitude compare to ECMWF data.

(c) In post-monsoon season all schemes data are overestimate along 73.3-94^{0}E longitude and same along left over longitude variation.

(d) In July the BFC data are well along 70-86.9^{0}E longitude and underestimate remaining longitude variation compare to ECMWF data. In December all schemes data are overestimate along 70-94^{0}E longitude variation compare to ECMWF data.

CONCLUSIONS

This analysis has been carried out to appraise the ability of RegCM model for simulation of surface heat budget (SHB) by comparing the model results with ECMWF reanalysis data in South Asian region. The SHB maintains the Earth's constant average temperature and GAS option of RegCM is able to simulate surface air temperature (only 2C cold bias). So, GAS option is taken for SHB study in 1995-2000.

- In respect to the thesis work of Mizanur Rahman on simulation of rainfall over Bangladesh by RegCM model, it was found that model overestimates in Pre-monsoon and underestimates in Monsoon for the period of 1995-2000. Opposite condition has been observed for SHB. Hence, SHB and precipitation are inversely related to each other and there is radiative impact on the development of convective system.
- It is found that over ocean the value of SHB is high during March-September and low during November-December. Over land the same condition is occurred except low in magnitude as the heat capacity of land is low than water. Over desert area and Mid-India the GAS option calculated values are close to ECMWF data.
- At different latitudes variations of SHB along longitudes are high over ocean and low over land during summer and opposite condition in winter because the input of solar energy is more in summer than winter. The best result is found for both data at 26^0N along 70^0E - 94^0E (over land) in monsoon season. The difference of SHB between RegCM and ECMWF data are also more over ocean than over land.
- For SHB (due to RegCM GAS option), the impact of the short wave radiation is more for water surface and both short wave radiation and sensible heat for land surface.
- According to hourly variation of SHB for both data positive phase has been observed at 12LST (local standard time) and negative phase at 00LST and 18LST. Both data have maintained the diurnal variation.

References

Anthes, R.,1977: A cumulus parameterization scheme utilizing a one-dimensional cloud model, *Monthly Weather Review*, vol. 105, 270-286.

Anthes, R. A., Kuo, Y.-H., Low-Nam, S., Hsie, E.-Y. and Bettge, T. M. 1989: Estimation of episodic and climatological skill and uncertainty in regional numerical models, *Quarterly Journal of the Royal Meteorological Society*, vol. 115, 11-137.

Anthes, R., Hsie, E. and Kuo, Y.-H., 1987: Description of the penn state / ncar mesoscale model version 4 (mm4), ncar tech. note. ncar/tn-282, Technical report, *National Centre for Atmospheric Research*.

Anthes, R. T. W., 1978: Development of hydrodynamic models suitable for air pollution and other mesometeorological studies, *Monthly Wearther Review*, vol. 106, 1045-1078.

Anthes, R.A., N.L. Seaman and T.T. Warner, 1980: Comparisons of numerical simulations of the planetary boundary layer by a mixed-layer and multi-level model. *Mon. Wea. Rev.*, vol. 108, 365-376.

Anthes, R., 1977. A cumulus parameterization scheme utilizing a one-dimensional cloud model, *Monthly Weather Review*, vol. **105**, 270-286.

Beheng, K., 1994: A parameterization of Warm cloud microphysical conversion processes, *Atmospheric Research*, vol. 51, 2722-2732.

Bates, G., Giorgi, F. and Hostetler, S., 1993: Towards the simulation of the effects of the great lakes on regional climate, *Monthly Weather Review*, vol. 121, 1373-1387.

Bates, G.T., 1990: A case study of the effects of topography on cyclone development in the western United States. *Monthly Weather Review*, vol. 118, 1808-1825.

Betts, A., 1982: Cloud thermodynamic models in saturation point coordinates, vol. 39, 2182-2191.

Betts, A., 1986: A new convective adjustment scheme. Part I: *Observational and theoretical basis*, vol. 112, 667-691.

Betts, A., 1997: The parameterization of deep convection, in R. Smith (ed.), The physics and parameterization of moist atmospheric convection, *Kluwer Academic Publishers* 255-279.

Bates, G., Hostetler, S. and Giorgi, F., 1995. Two-year simulation of the great lakes region with a coupled modeling system, *Monthly Weather Review*, vol. 123, 1505-1522.

Betts, A. and Harshavardhan, 1987. Thermodynamic constraint on the cloud liquid water feedback in climate models, *Atmospheric Research*, vol. 92, 8483-8485.

Betts, A. and Harshavardhan, 1987: Thermodynamic constraint on the cloud liquid water feedback in climate models, vol. 92, 8483-8485.

Betts, A. K. and Miller, M., 1993: The Betts-Miller scheme, Chapter 9, The representation of cumulus convection in numerical models of the atmosphere, (Eds.K.A. Emanuel and D.J. Raymond),Meteo. *Mon., American Meteorological Society*, 107-121.

Itaru Okada, Takashi Yamanouchi, 2004. Seasonal Change of the Atmospheric Heat Budget over the Southern Ocean from ECMWF and ERBE data, Journal of Climate: Vol. 15, No.17, 2527-2536.

Leung, L. R., Ghan.S. J., Wang, W.-C., Wei, H.-L., Zhao. Z.-C. and Luo, Y., 1998b. Intercomparison of t he reanalyzed East Asian monsoon climate and regional climate simulations driven by the reanalyses. In *Proceedings of the First WCRP International Conference on Reanalyses*, WMO/TD-No. 876, 179-182.

McGregor, J. L., Walsh, K. J. and Katzfey, J. J., 1993. Nested modelling for regional climate studies. In Jakeman, A. J., Beck M. B. and McAleer, M. J. (edited), Modelling Change in Environmental Systems, Wiley and Sons, 367-386.

Trenberth, K. E., Caron, J. M., Stepaniak, D. P.,2001. The atmospheric energy budget and implicatios for surface fluxes and ocean heat transports, Climate Dynamics, vol. 17, 259-276.